

**Climate Change Scenario Simulations over
Eritrea by Using a Fine Resolution Limited
Area Climate Model:
Temperature and Moisture Sensitivity**

by

Asmerom Fissehatsion Beraki

Submitted in partial fulfillment of the requirements
for the degree of

MASTER IN SCIENCE

in the

Faculty of Natural and Agricultural Sciences
University of Pretoria

July 2005

Climate Change Scenario Simulations over Eritrea by Using a Fine Resolution Limited Area Climate Model: Temperature and Moisture Sensitivity

Asmerom Fissehatsion Beraki

Promoter: Prof. C.J. de W. Rautenbach
Department: Department of Geography, Geoinformatics and Meteorology
Faculty: Faculty of Natural and Agricultural Sciences
University: University of Pretoria
Degree: Master of Science

Summary

The climate of the eastern section of the Sahelian latitude, especially over the Eritrean subdomain, is often associated with long drought episodes from which the atmospheric mechanisms are poorly understood. In an effort to improve our knowledge of weather and climate systems over this region, the PRECIS Regional Climate Model (RCM) from the United Kingdom (UK) was obtained and implemented. Such a climate model that is based upon the physical laws of nature has the ability to simulate regional-scale atmospheric patterns, and therefore, may significantly contribute to our understanding of local atmospheric processes. In this dissertation the assessment of past regional climate trends from both observations and model simulations, and the simulation of scenarios for possible future climate change were regarded as important. To investigate this, the PRECIS RCM was first nested over the Eritrean domain into the “atmosphere only” HadAM3H global General Circulation Model (GCM) and forced at its lateral boundaries by a 30-year present-day (1961-1990) integration of the same global model. Secondly, the PRECIS RCM was constrained at its lateral boundary by the “fully coupled” HadCM3 GCM (for Sea Surface Temperatures (SSTs) and sea-ice) and its improved atmospheric component (HadAM3H GCM). The latter simulations provided boundary conditions for the A2 and B2 future emission scenarios (Special Report on Emission Scenarios (SRES)) to simulate a 20-year (2070-2090) projection of future climate. These experiments allowed for verification of both spatial and temporal present-day climate simulations, as well as possible future climate trends as simulated by the PRECIS RCM over the Eritrean domain, with specific emphasis on temperature and moisture related variables.

The study indicates that PRECIS RCM climate simulations are mostly in harmony with observed spatial patterns. This skill may be attributed to the full representation of the climatic system (land surface, sea, ice, atmosphere and atmospheric chemistry such as sulphur and greenhouse gasses) in the model configuration. However, when comparing PRECIS RCM results with the much coarser resolution ($2.5^{\circ} \times 2.5^{\circ}$) National Centre for Environmental Prediction (NCEP) reanalysis data, obvious differences do occur. These differences are not necessarily the result of poor model performance, but may be attributed to more detailed simulations over the finer RCM grid ($0.44^{\circ} \times 0.44^{\circ}$).

Future climate scenario simulation with the PRECIS RCM over Eritrea produce increased surface temperature in both the A2 and B2 SRES scenario integrations, relative to the present climatology. This temperature increase also appears in the driving GCM (HadCM3) as well as in other GCM results from the Inter Governmental Panel for Climate Change (IPCC) initiative. There are, however, mixed signals in rainfall projections. According to PRECIS RCM results, rainfall is expected to increase in most of the Eritrean region.

ACKNOWLEDGEMENTS

The author is gratified to express his appreciation to the following persons and institutions for their assistance and contribution to make this work possible:

- The *British Met Office (Hadley Centre for Climate Prediction and Research, UK)* and in particular Dr. Richard Jones, Ruth Taylor and David Hein for supplying the PRECIS RCM and its driving boundary conditions.
- Prof. C.J. de W. Rautenbach for his advice and for creating a suitable working environment at the University of Pretoria.
- Francois Engelbrecht and Human Buirski, for their technical assistance during the course of this work.
- Dr. Nebo Jovanovic Benade and Prof. Julia Maxster for their support during the proposal development phase of this dissertation.
- Karin Marais from the South African Weather Service (SAWS) library for her genuine help in compiling most of the references used in this work.
- Tekle Yemane for supplying the available national (Eritrean) database and his technical assistance in GIS.
- NOAA National Centre for Environmental Prediction (NCEP) for making their reanalysis data freely available, which have been intensively utilized in my research.
- Dr Fourie Joubert for providing additional computing facilities which reduced the time of model simulations significantly.
- Last but not least, my gratitude goes to my family and friends for their persistent encouragements and almighty God for giving me the strength to challenge this complicated and unexpected but interesting profession.

TABLE OF CONTENTS

CHAPTER 1	Introduction	
1.1	Background	1
1.2	Driving forces of the climate and atmospheric modelling	3
1.3	The need for research over Eritrea	4
1.4	Objectives of the research	5
1.5	Organization of the report	7
CHAPTER 2	General profile of Eritrea	
2.1	Geographical location	9
2.2	Historical background	9
2.3	Population	10
2.4	Climate	10
2.5	Landform and drainage system	12
2.6	Soils and geology	14
2.7	Land use and vegetation cover	15
2.8	Agro-ecological zones	17
2.9	Agricultural activities	18
CHAPTER 3	Climate modelling on regional spatial scales	
3.1	Introduction	21
3.2	Global general Circulation models	22
3.3	The need for down-scaling	23
3.4	Down-Scaling approach	24
3.5	Nested climate models	24
3.5.1	Types of nesting	25
3.5.1.1	One-way nesting	25
3.5.1.2	Two-way nesting	26
3.5.1.3	Multiple nesting	26
3.6	Numerical integration of climate Models	27
3.7	Physical parameterization in climate models	28
3.8	Model simulations on longer time-scales	30

CHAPTER 4 Characteristics of the past and present climate of Eritrea

4.1	Introduction	31
4.2	Observed climate patterns	32
4.2.1	Atmospheric circulation	32
4.2.1.1	Mean sea level pressure and near-surface wind patterns	32
4.2.1.2	Moisture advection and rainfall patterns	36
4.3	Observed climate trends and variability	39
4.3.1	Rainfall	40
4.3.2	Near surface air temperature	41
4.3.3	Mean sea level pressure	43
4.4	Drought events	44
4.4.1	Background	44
4.4.2	The proposed mechanisms	45

**CHAPTER 5 Future climate projections for Eritrea from GCM
simulations**

5.1	Introduction	47
5.2	Global future climate scenarios simulations	47
5.3	Greenhouse gases and aerosols emission scenarios	49
5.4	IPCC GCM climate projections for Eritrea	51
5.4.1	IPCC simulated climate change scenarios for July	52
5.4.1.1	Average surface temperature projections	52
5.4.1.2	Average rainfall projections	54
5.4.2	IPCC simulated climate change scenarios for January	57
5.4.2.1	Average surface temperature projections	57
5.4.2.2	Average rainfall projections	60

**CHAPTER 6 Climate change simulations using the PRECIS regional
climate model system**

6.1	Introduction	64
6.2	Model description	64
6.3	Experimental design	66
6.3.1	Model domain and configuration	66
6.3.2	Present climate simulations	68

6.3.3	Future climate simulations	68
6.4	Verification methods	69
6.5	Results and discussions	70
6.5.1	Mean sea level pressure	70
6.5.2	Near surface wind patterns	73
6.5.3	Precipitation rate	76
6.5.4	Surface temperature	79
6.6	Model evaluation	82
6.7	Climate change scenario projections with the PRECIS RCM system	86
6.7.1	Surface temperature	86
6.7.1.1	July projections	86
6.7.1.2	January projections	87
6.7.2	Precipitation rate	89
6.7.2.1	July projections	89
6.7.2.2	January projections	89
CHAPTER 7	Conclusions	93
APPENDEIX A	Model verification techniques	
A.1	Introduction	96
A.3	Taylor diagram	96
A.3.1	Theoretical basis	96
APPENDEIX B	Python code for model output manipulation	99
REFERENCES		102

LIST OF SYMBOLS

E	:	RMS difference
\bar{E}	:	Bias
E'	:	Pattern RMS difference
f_n	:	Model variable
N	:	Discrete points (in time and/or space)
R	:	Correlation coefficient
r_n	:	Observed variable
α	:	Positive constant
σ	:	Vertical (sigma) coordinate
σ_f, σ_r	:	standard deviation (for model and observed fields)

LIST OF FIGURES

- Figure 2.1:** Geographical location of Eritrea in north-east Africa, with Sudan to the west and Ethiopia to the South (Adapted from: United Nations, 2000).
- Figure 2.2:** Mean annual rainfall totals over Eritrea (left) and rainfall regions of Eritrea (right) based upon rainfall systems and annual distribution as obtained from GIS database of WRD (1997)
- Figure 2.3:** Annual average temperature distribution over Eritrea as derived from Advanced High Resolution Radiometer data (from AVHRR channel 5) and correlated with station data (RMSE 1 °C - 3°C)
(Source: <http://www.punchdown.org/rvb/temps/mapindex.html>, 2004/12/20)
- Figure 2.4:** Map of Eritrea's surface water resource and drainage patterns as obtained from GIS database of WRD (1997)
- Figure 2.5:** A map that exhibits major soil types in Eritrea as obtained from GIS database of FAO (1994)
- Figure 2.6:** The map illustrates major land use zones of Eritrea. It was obtained and digitized from National Center for Earth Resources Observation and Science (EROS) (originally derived from thematic maps and other source material).
<http://edcintl.cr.usgs.gov/archives.shtml>, 2003/09/10.
- Figure 2.7:** A typical vegetation map of Eritrea with 12 vegetation types. (Source: FAO/MOA, 1997)
- Figure 2.9:** A typical agro-ecological map of Eritrea indicating six agro-ecological zones as obtained from GIS database of WRD (1997)
- Figure 2.10:** Spatial distribution of production zones of the main crops in Eritrea. Major cultivated crops include barely, wheat, African finger millet, taff and maize (Source: FAO, 1997)
- Figure 4.1:** Observed seasonal Mean Sea Level Pressure (MSLP) in hPa and averaged near-surface winds ($\times 10 \text{ ms}^{-1}$) over the period (1948-2003) as obtained from NCEP reanalysis data. The maps represent the four Boreal seasons namely, (a) September to November (SON), (b) March to May (MAM), (c) June to August (JJA) and (d) December to February (DJF).
- Figure 4.2:** Observed (a) precipitation rate in mm per day, (b) precipitable water in kg m^{-2} , (c) zonal moisture flux and (d) meridional moisture flux in $\text{kg m}^{-1}\text{s}^{-1}$ averaged over the months June to August (JJA) and period 1948-2003. The climatology was calculated from the NCEP reanalysis data set.
- Figure 4.3:** Observed mean monthly rainfall in mm for Filfil (1928-63) and Faghena (1947 to 1962) as obtained from the Department of Water Resources (DWR) of Eritrea. These two stations are found along the eastern escarpment of the Eritrea Highlands that is covered with remnants of the tropical rain forest and referred to as Green Belt.

- Figure 4.4:** The domain that will be considered in PRECIS nested climate model (NCM) simulations. Eritrea is indicated in gray. In the following sections NCEP reanalysis data are spatially averaged over the box **A**.
- Figure 4.5:** Annual rainfall anomalies (black line) and 5-years moving averages (gray line) over the period 1900-1990 for Asmara that is located on the central Highlands of Eritrea as obtained from the Department of Water Resources (DWR).
- Figure 4.6:** Weighted average time series (1950 to 2000) of near-surface temperature anomalies ($^{\circ}\text{C}$) as calculated from NCEP reanalysis data for the seasons (a) JJA, (b) DJF, (c) MAM and (d) SON and the entire domain of figure 4.4. Gray lines denote five-year moving averages.
- Figure 4.7:** As figure 4.6 but averaged over box-area **A**.
- Figure 4.8:** Weighted average time series (1950 to 2000) of Mean Sea Level Pressure (MSLP) anomalies (hPa) as calculated from NCEP reanalysis data for the seasons (a) JJA, (b) DJF, (c) MAM and (d) SON and the entire domain of figure 4.4. Gray lines denote five-year moving averages.
- Figure 4.9:** As figure 4.8 but averaged over box-area **A**.
- Figure 5.1:** Anthropogenic emission projections of CO_2 for the six SRES scenarios, A1B, A2, B1 and B2, A1FI and A1T plus the updated and replaced well known the IS92a scenario as obtained from the IPCC Special Report on Emissions Scenarios (SRES) dataset (appendix II).
- Figure 5.2:** July near-surface temperature ($^{\circ}\text{C}$) projections for the 2080s relative to 1961-90 for the six IPCC GCMs (indicated in the right bottom of each plot) for the A2 SRES scenario. Eritrea is indicated in letter "A".
- Figure 5.3:** As figure 5.2 but for B2 SRES scenario.
- Figure 5.4:** Spatially averaged near-surface temperature ($^{\circ}\text{C}$) projections for July 2080s for the A2 and B2 SRES scenarios over the Eritrea domain. The graphs denote (a) spatial averages, (b) minimum, (c) maximum and (d) spatial coverage (%) of positive anomalies of near-surface temperatures.
- Figure 5.5:** July rainfall ($\text{mm}\cdot\text{day}^{-1}$) projections for the 2080s relative to 1961-91 for the six IPCC GCMs (indicated in the right bottom of each plot) for A2 SRES scenario. Eritrea is indicated in letter "A".
- Figure 5.6:** As figure 5.2 but for B2 SRES scenario.
- Figure 5.7:** Spatially averaged rainfall ($\text{mm}\cdot\text{day}^{-1}$) projections for July 2080s for the A2 and B2 SRES scenarios over the Eritrean domain. The graphs denote spatial (a) averages, (b) minimum, (c) maximum and (d) aerial coverage (%) of positive anomalies of rainfall.
- Figure 5.8:** January near-surface temperature ($^{\circ}\text{C}$) projections for the 2080s relative to 1961-90 for the six IPCC GCMs (indicated in the right bottom of each plot) for the A2 SRES scenario. Eritrea is indicated in letter "A".
- Figure 5.9:** As figure 5.2 but for B2 SRES scenario.

- Figure 5.10:** Spatially averaged near-surface temperature ($^{\circ}\text{C}$) projections for January 2080s for the A2 and B2 SRES scenarios over the Eritrea domain. The graphs denote spatial (a) averages, (b) minimum, (c) maximum and (d) aerial coverage (%) of positive anomalies of near-surface temperatures.
- Figure 5.11:** January rainfall ($\text{mm}\cdot\text{day}^{-1}$) projections for the 2080s relative to 1961-91 for the six IPCC GCMs (indicated in the right bottom of each plot) for A2 SRES scenario. Eritrea is indicated in letter "A".
- Figure 5.12:** As figure 5.10 but for B2 SRES scenario.
- Figure 5.13:** Spatially averaged rainfall ($\text{mm}\cdot\text{day}^{-1}$) projections for January 2080s for the A2 and B2 SRES scenarios over the Eritrean domain. The graphs denote spatial (a) averages, (b) minimum, (c) maximum and (d) aerial coverage (%) of positive anomalies of rainfall.
- Figure 6.1:** The figures illustrate the PRECIS RSM system model topography (a) in meters and model domain (b) with the grid resolution of $0.44^{\circ} \times 0.44^{\circ}$.
- Figure 6.2:** Average of Mean Sea Level Pressure (MSLP) for July (1961-1990) as obtained from (a) the NCEP reanalysis data and (b) the baseline integration of the PRECIS RCM system. The contour interval is 1 hPa.
- Figure 6.3:** Average of Mean Sea Level Pressure (MSLP) for January (1961-1990) as obtained from (a) the NCEP reanalysis data and (b) the baseline integration of the PRECIS RCM system. The contour interval is 1 hPa.
- Figure 6.4:** Near-surface wind streamlines for July (1961-1990) as obtained from (a) the NCEP reanalysis data and (b) the baseline integration of the PRECIS RCM system.
- Figure 6.5:** Near-surface wind streamlines for January (1961-1990) as obtained from (a) the NCEP reanalysis data and (b) the baseline integration of the PRECIS RCM system.
- Figure 6.6:** Precipitation rate (mm/day) for July (1961-1990) as obtained from (a) the NCEP reanalysis data and (b) the baseline integration of the PRECIS RCM system.
- Figure 6.7:** Precipitation rate (mm/day) for January (1961-1990) as obtained from (a) the NCEP reanalysis data and (b) the baseline integration of the PRECIS RCM system.
- Figure 6.8:** Surface temperature ($^{\circ}\text{C}$) for July (1961-1990) as obtained from (a) the NCEP reanalysis data and (b) the baseline integration of the PRECIS RCM system.
- Figure 6.9:** Surface temperature ($^{\circ}\text{C}$) for January (1961-1990) as obtained from (a) the NCEP reanalysis data and (b) the baseline integration of the PRECIS RCM system.
- Figure 6.10:** Model evaluation diagram for all considered variables for July (+) and January (\diamond). The top panel (a) shows when the NCEP fields are interpolated to the PRECIS resolution while (b) shows the reverse. The Root Mean Square (RMS) difference values and standard deviations were normalized with observation to suite the analysis. The RMS difference is the proportional distance between NCEP

(reference) and PRECIS RCM fields. The radial distance is the standard deviation and the angular coordinate is the pattern correlation. See figure A.1 for the geometric relationship among these three measures of standard skill) (after Taylor, 2000)

- Figure 6.11:** Surface temperature ($^{\circ}\text{C}$) climate change anomalies as generated by the PRECIS RCM system for July in the 2080s relative to the baseline climate of 1961 to 1990. Simulations are for the (a) A2 and (b) B2 SRES scenarios and the isotherm interval is 0.5°C .
- Figure 6.12:** Surface temperature ($^{\circ}\text{C}$) climate change anomalies as generated by the PRECIS RCM system for January in the 2080s relative to the baseline climate of 1961 to 1990. Simulations are for the (a) A2 and (b) B2 SRES scenarios and the isotherm interval is 0.5°C .
- Figure 6.13:** Precipitation rate ($\text{mm}\cdot\text{day}^{-1}$) climate change anomalies as generated by the PRECIS RCM system for July in the 2080s relative to the baseline climate of 1961 to 1990. Simulations are for the (a) A2 and (b) B2 SRES scenarios and contour intervals are 1.5mm .
- Figure 6.14:** Precipitation rate ($\text{mm}\cdot\text{day}^{-1}$) climate change anomalies as generated by the PRECIS RCM system for January in the 2080s relative to the baseline climate of 1961 to 1990. Simulations are for the (a) A2 and (b) B2 SRES scenarios and contour intervals are 1.5mm .
- Figure A.1:** Geometric relationship between the correlation coefficient, R , the pattern RMS difference, E' and the standard deviations, σ_f and σ_r , of the test and reference fields, respectively.

LIST OF TABLES

Table 6.1: Model performance over all grid points (91x51) covering the PRECIS RCM system domain as compared to the corresponding NCEP reanalysis fields for January and July. Variables are surface temperature (°C), MSLP (hPa), precipitation rate (mm.day⁻¹) and the horizontal wind components (m.s⁻¹) on different temporal scales.

LIST OF ABBREVIATIONS

AGCM	Atmospheric General Circulation model
AOGCM	Atmosphere-Ocean General Circulation model
BMO	United Kingdom Meteorological Office
CCSR/NIES99	Japanese Centre for climate system Research fully coupled GCM
CGCM1/CCCma	Canadian Centre for Climate modelling and analysis
CSIRO	Commonwealth Scientific and Industrial Research Organization (Australia).
CSIRO-Mk2b	CSIRO fully coupled GCM
ECHAM4	German Climate Research Centre fully coupled GCM
ECMWF	European Centre for Medium-Range Weather Forecasts
ENSO	El Niño Southern Oscillation
EROS	National Center for Earth Resources Observation and Science
GCM	Global Climate Model
GFDL	Geophysical Fluid Dynamics Laboratory
GFDL99-R30	GFDL fully coupled GCM
GISS	Goddard Institute for Space Studies
HadAM3H	The Hadley Centre Atmosphere only GCM
HadCM3	The Hadley Centre Fully Coupled GCM
HadISST	Hadley Centre Observed Sea Surface Temperature
HadRM3	The Hadley Centre Regional Climate Model
IPCC	Intergovernmental Panel for Climate Change
ITCZ	Intertropical Convergence Zone
LAM	Limited Area Atmospheric Model
MLWE	Ministry of Land, Water and Environment
MM5	Regional Climate Model of Pennsylvania State University (PSU) – National Centre for Atmospheric Research (NCAR) version 5
NCEP	National Centre for Environmental Prediction
NCM	Nested Climate Model
NWP	Numerical Weather Prediction
RCM	Regional Climate Model
PRECIS	Providing Regional Climates and Impacts Studies
SRES	Special Report on Emission Scenarios
SST	Sea Surface Temperature
UKMO	UK Met Office
UNFCCC	The United Nations Framework Convention on Climate Change.
WRD	Water Resources Department

CHAPTER 1

INTRODUCTION

1.1 BACKGROUND

Anthropogenic (human-induced) forcing and its effect on the climate recently became a global concern. Man's impact on the Earth's climate began during ancient civilizations where forests were burned and cleared for agricultural purposes. However, these interferences were insignificant in comparison to the magnitude of natural fluctuations in climate. It is believed that the impact of the modern human population on climate is much more severe, as outlined by the recent report of the United Nations Framework Convention on Climate Change (UNFCCC) (UNFCCC; 2003), and scientists believe that anthropogenic forcing may have a significant impact on human life and biodiversity.

Since the start of the industrial revolution (1860), and especially over the previous half-century, it is increasingly recognized that the magnitude of human influence on Earth's environment persistently intensified. Henderson-Seller and McGuffee (2001) suggested that for the first time in the history of our planet emissions of trace gasses from human activities equal, or even exceed, emissions from natural sources. Human influences, as Jones *et al.* (2003) infers, will continue to change the atmospheric composition throughout the 21st century. Anxieties are now plausibly felt, and extensively uttered about the possible immense of impact on the global climate owing to the enhanced levels of greenhouse gases concentrations on the atmosphere (Fischer *et al.*, 2002). Society adapted according to the conditions of a given climate, and changes in that climate may place significant stress on society (Hewitson, 2004).

Anthropogenic greenhouse warming and possible climate change might result in the shift of climatic zones, the rise in sea levels, more frequent storms, droughts and floods as well as other unprecedented environmental changes. These phenomena might pose challenges to society and might even undermine the

existing sustainable utilization of natural resources. They have the potential to influence every sphere of life, as we know it today, if neglected.

Despite their contribution to anthropogenic gas releases are insignificant, developing countries are found to have the most vulnerable populations. Vulnerable populations have limited capacity to protect themselves against and to recover from environmental hazards, and in particular against extreme events such as drought and floods. Those countries that dependent on localized rural agriculture activities as a source for food supply might be most severely affected.

Recognizing that the problem of greenhouse warming is global, the UNFCCC entered into force in 1994. The Kyoto Protocol, which sets out more specific, bindings commitments, followed in 1997. The objective of the Convention (Article 2) is the “stabilization of greenhouse gas concentrations in the atmosphere to a level that would prevent potentially dangerous anthropogenic interference with the climate system”. Such a level should be achieved within a timeframe sufficient to allow for ecosystems to adapt naturally to climate change, to ensure that food production is not threatened and to enable economic development to proceed in a sustainable manner (UNFCCC, 2003).

Assessment of vulnerability to greenhouse warming induced climate change is mostly based upon scenarios of future climate. These scenarios are generally derived from projections of climate change undertaken by General Circulation Models (GCMs). Data from present global GCM climate projection simulations are available in fairly coarse spatial resolutions (hundreds of kilometers), and local or regional detail that is needed for impact assessments at a national level is often not captured. A widely applicable approach for adding this detail to global projections is to nest a Regional Climate Model (RCM) with a finer grid resolution within the simulated fields of a global GCM (Jones *et al.*, 2003). This approach is also known as nested climate modelling, and the RCM used is often referred to as a Nested Climate Model (NCM). Knowledge of climate variability on a local or regional spatial scale is important for assessing the impacts of potential future climate change on society. For this reason much attention has been given in recent years to climate simulations using RCMs (see Chapter 3 for details) driven by output from coarser resolution GCMs.

1.2 DRIVING FORCES OF THE CLIMATE AND ATMOSPHERIC MODELLING

The primary processes that drives Earth's climate are the planetary radiation balance between the incidence and emitted solar radiation that governs the difference in energy between low and high latitudes and the effect of Earth's rotational rate on atmospheric and oceanic circulation (Henderson-Seller and McGuffeie, 2001). External (e.g. Milankovitch variations, solar activities and others) and internal (e.g. tectonic, geothermal and anthropogenic) perturbations tend to alter the climate system either positively or negatively (from a human and biodiversity perspective). These perturbations might lead to the warming or cooling of the Earth's surface and atmosphere. It is a known fact that both natural and anthropogenic perturbations caused by variations in the chemical composition of the atmosphere contribute to climate variability and even consistent change. According to present radiation properties and the solar constant the average near-surface temperature of an Earth without an atmosphere would have been in the order of -17°C . In reality an average temperature of approximately $+15^{\circ}\text{C}$ is measured today, meaning that natural greenhouse gasses is responsible for an increase of more than 30°C . Greenhouse gases in the atmosphere, such as carbon dioxide (CO_2) and water vapor, lead to positive radiative forcing or warming of the atmosphere, whilst most atmospheric aerosols lead to a negative radiative forcing or cooling of the atmosphere (Henderson-Seller and McGuffeie, 1987).

Any anthropogenic disturbance in climate will be embedded into the more extensive background of natural climate variability that occurs over a wide range in time and space. The ocean-atmosphere El Niño-Southern Oscillation (ENSO) phenomenon is a typical example of such natural climate variability.

To distinguish between anthropogenic and natural climate variability, it is required that the anthropogenic signal be identified against the background noise of natural climate variability (IPCC WGI, 2001). GCMs are the only tools that can distinguish between the two types of climate variability, meaning that long-term simulations of climate change may be of great value (Bash, 1988). Nevertheless, GCM climate change experiments should not be regarded as future predictions, but should rather be seen as a possible realization of how global climate may evolve in the future when subjected to imposed greenhouse gas forcing (Viner, *et al.*, 1995)

Over the past decades there have been a proliferation of interest at many institutions in modelling the climatic response to increased greenhouse gas concentrations (e.g., Geophysical Fluid Dynamics Laboratory (GFDL), the National Center for Atmospheric Research (NCAR), Goddard Institute for Space Studies (GISS), the United Kingdom Meteorological Office (BMO), Commonwealth Scientific and Industrial Research Organization (CSIRO), Canadian Center for Climate modelling and analysis (CCCMA) and others). All these institutions develop and run sophisticated GCMs, which allowed for an ensemble of climate change scenario simulations that were recently investigated under the umbrella of the IPCC.

Most of these models produced results that agree upon the cooling of the stratosphere, the warming of the troposphere and a global water cycle enhancement under conditions of a doubling in CO₂ concentrations.

1.3 THE NEED FOR RESEARCH OVER ERITREA

The potential of global climate change as a consequence of increased anthropogenic greenhouse gas emission has been recognized as a potential threat to society (Hewitson, 2001). Although Africa, of all the major world regions, has contributed the least to this threat because of its low per capital fossil energy use and hence low greenhouse gas emissions, it is the most vulnerable continent to climate change because widespread poverty and limited capabilities to adapt (Awosika *et al.*, 2001).

In the context of the present debate around international agreements, it is important that uniform assessments be carried out to compare and evaluate national, regional and global impacts of climate change on every vulnerable realm, in general, and on food and agricultural production, in particular. Such quantified impacts of climate change and spatial adaptive policies are the prime drives to mitigate the consequences of climate change (Fischer *et al.*, 2002). As a result, extensive resources are being invested in climate change research by many nations in an effort to understand the potential regional manifestation and impact of such change (Hewitson, 2001).

Eritrea is a relatively young country that gained independence in 1991. It is also regarded as one of the developing African nations that appear to be most

vulnerable to climate change and variability because of widespread poverty - presumably as a result of a prolonged war, poor management practices and a lack of expertise. Previous studies have indicated that countries in the Sahelian latitudes are noticeably affected by climate variability (especially droughts) related to the ENSO phenomena. Eritrea is located in the eastern part of the Sahelian latitudes, and is in general regarded as a semi-arid country. Future changes in the climate of this region might influence temperature and moisture prone activities, especially those related to agriculture.

These circumstances have prompted the need to improve current knowledge of the climate of Eritrea. Together with this is a need to assess the future response of climate to a growing change in the chemical composition of the atmosphere as a result of human interferences, and the probable consequences on regional and national scale. This emphasizes the need for more detailed RCM simulations in comparison to the coarse resolution of current GCM simulations (including GCMs used in the IPCC initiative). So far no regional scale climate or climate change scenario simulations have been carried out over the Eritrean region. Even if this could be done, climate model verification will be difficult to perform as a result of a lack of well-documented observations. The research in this dissertation attempts to fill these gaps by introducing simulations of present day as well as possible future climates with a high-resolution RCM over the Eritrean domain.

1.4 OBJECTIVES OF THE RESEARCH

The core objective of the research in this dissertation is to introduce a RCM facility that will facilitate the simulation of present and possible future climate patterns over Eritrea. This is achieved through the following sub-objectives:

OBJECTIVE 1

To develop a regional climate modelling facility for performing climate simulations over Eritrea by implementing the PRECIS RCM system from the Hadley Center of the BMO.

Climate and climate change scenarios simulations are particularly vital for developing countries where economic stresses are likely to increase if significant changes in climate appear. In order to address this need the Hadley Center of the BMO had developed the Providing Regional Climates for Impacts Studies

(PRECIS - pronounced “pray-sea” as in French) RCM system that can run on an affordable, easily available personal computer (PC). The model is an atmospheric and land surface model of limited area and high resolution, which can be run over any part of the globe. Atmospheric dynamics, the atmospheric sulphur cycle, clouds and precipitation, radiative processes, the land surface and deep soil characteristics are all included. The model equations are solved in spherical polar coordinates, and the latitude-longitude grid is rotated so that the equator lies inside the region of interest in order to obtain a quasi-uniform grid box area throughout the region. Objective 1 intends to introduce the PRECIS RCM to develop a climate simulation facility for Eritrea.

OBJECTIVE 2

To use the PRECIS RCM system in order to perform present day climate model simulations over Eritrea and to verify the simulated climate against the best observational data available.

In an effort to validate model simulations of the standard meteorological variables, i.e., rainfall, temperature, wind patterns and pressure fields, a baseline climate simulation of 30 years (1961-1990) is compared with observational data obtained from the National Center for Environmental Prediction (NCEP) reanalysis dataset, which is available for the period 1948 to 2003. NCEP data with its coarse resolution of $2.5^{\circ} \times 2.5^{\circ}$, is probably not the best to use for RCM-scale verification, but as a result of the war and political instability over the past few decades, observational station data over Eritrea is not reliable, and good continuous records do not exist. PRECIS RCM results, with the verification analysis in mind, will be used to explain the major driving mechanisms of climate over Eritrea.

OBJECTIVE 3

To determine possible future climate response to different future emission scenarios over the Eritrean region.

Since the industrial revolution that started in 1860, and in particular during the last half-century, it is increasingly recognized that anthropogenic influences on Earth's environment may be significant. The interference may cause that the current atmospheric composition be altered. Objective 3 intend to determine possible future climate responses to the A2 and B2 future emission scenarios (also known

as the A2 and B2 Special Report on Emission Scenarios (SRES) scenarios) over the Eritrean region.

1.8 ORGANIZATION OF THE REPORT

Eritrea has experienced intermittent drought, coupled with land degradation and intensifying desertification, provoked by mismanagement practices. These problems pose an additional burden in the strategy to achieve food security and sustainable development. CHAPTER 2 provides a general profile of Eritrea by appraising briefly on the natural geography and the associated resource foundations that include:

- (1) climate
- (2) landform and drainage systems
- (3) soils and geological settings
- (4) land use and vegetation cover
- (5) agro-ecological zone
- (6) the status of agricultural activities.

CHAPTER 3 outlines the fundamentals of atmospheric modelling by putting particular emphasis on RCMs and their capabilities. It also highlights the ultimate driving force beyond RCMs development, and how RCM simulations add value to GCMs fields.

The climate of the eastern section of the Sahelian latitudes is poorly documented and understood. Previous studies mainly concentrated on the western and central parts of these latitudes. CHAPTER 4 describes key features of the observed climate. It offers a full coverage on how recent and present climate system of the region did evolved by focusing on observational patterns and trends. This is done in the context of climate change and variability. CHAPTER 4 also intends to address the mechanisms responsible for, and the origin of persistent droughts that often occur in the sub-Saran latitudes. It appears as if these droughts worsened over the past two decades.

CHAPTER 5 demonstrates possible future climate responses to enhanced greenhouse gases and aerosols over Eritrea. GCM simulations from the most recent Intergovernmental Panel for Climate Change (IPCC) are used to

supplement PRECIS RCM climate projections. Both the A2 and B2 SRES scenarios are considered. Inter-model consistency in simulated atmospheric variables is regarded as an important feature in future climate scenario simulations.

At the synoptic scale, modern GCMs can simulate the many processes of the atmosphere to a great degree of accuracy, and are reliable tools. However, computational constraints prevent them from performing detailed climate simulations at the mesoscale. RCM were developed as a computationally feasible alternative to obtain high-resolution climate simulations. Over the past decade many RCM simulations have been performed over various regions of the Earth. Climate simulations by the newly introduced PRECIS RCM system over the Eritrean Sub-Saharan Africa domain are presented in CHAPTER 6. The chapter attempts to offer a comprehensive model description and experimental design. Subsequently, the model's performance in capturing present-day (baseline) climate is both qualitatively and quantitatively verified against observations. Future climate projections by the PRECIS RCM under A2 and B2 SRES scenarios are also discussed.

CHAPTER 7 contains a number of conclusions. The chapter underpins the performance of the PRECIS RCM in simulating present-day and future climates. Opportunities and possibilities of utilizing the latter as input for impact models are also discussed.

The objective measures of skill that have been used to verify the PRECIS RCM performance (CHAPTER 6) are elaborated upon in APPENDIX A. The python code that was developed to manipulate PRECIS RCM output results is presented in APPENDIX B.

CHAPTER 2

GENERAL PROFILE OF ERITREA

2.1 GEOGRAPHICAL LOCATION

Eritrea is located between latitudes 12° 42' N to 18° 2' N and longitudes 36° 30' E to 43° 20' E, in the northeastern part of Africa (Kayouli *et al.*, 2002). Being part of the sub-Saharan Africa, it fits in between Sudan to the north and west, Ethiopia and Djibouti to the south and the Red Sea to the east and northeast (figure. 2.1). The country covers an area of about 124,000 km² and has over 350 tiny islands in the Red Sea, over half of which make up the Dahlak Archipelago (America on line service, 2002).



Figure 2.1: Geographical location of Eritrea in north-east Africa, with Sudan to the west and Ethiopia to the South (Adapted from: United Nations, 2000).

2.2 HISTORICAL BACKGROUND

Eritrea's strategic location attracted several expansionist powers (UA and MOA, 1998). Starting from the 16th century, Eritrea had fallen under the control of

influence of different foreign powers, including the Turks, Egyptians and in modern history by Italy, Britain and Ethiopia (MLWE, 2001). The fall of Eritrea under the full control of Ethiopia in 1962 provoked a long war of liberation that culminated in Eritrean independence in 1991 (CIA, 2002), but left the country in wreck. After seven years of peace and relief, however, the country was again forced to engage in border-war (1998-2001) with its long-time rival, Ethiopia. This imposed war did, by far, cause its reviving economy to collapse again.

2.3 POPULATION

As MLWE (2001) detailed, Eritrea has an estimated population of 3.5 million, growing at a rate of about 3.0 % annually, with an average density of about 28 persons per km². More than 80 % of Eritrea's populations live in rural areas. Mainly due to suitability of climate, about two thirds of the population lives in the highlands which has an altitude of higher than 1500 meters Above Mean Sea Level (AMSL). Despite the fact that Eritrea is small in land coverage it hosts diverse ethnic groups. These ethnic groups are divided into nine nationalities namely the Afar, Bilen, Hedarb, Kunama, Nara, Rashaida, Saho, Tigre and Tigrigna. The Tigrigna and Tigre nationalities constitute the majority of the population. Within these nationalities Tigrigna, Tigre and Arabic are widely spoken languages.

2.4 CLIMATE

Eritrea is located in the sub-Saharan latitudes where the Sahelian climate dominates. The eastern boundary of the Sahara desert covers the north-western part of Eritrea where the minimum average annual rainfall is less than 100 mm (figure 2.2). Rainfall gradually increases towards the south-east. There is a concern about the gradual infringement of the Saharan desert from the northwest, which is aggravated by persistent longer drought episodes. From previous studies, different views have been proposed for the possible mechanisms and causes of these dry episodes (see Chapter 4 for details).

In general rainfall is low over Eritrea and significantly varies from year to year (Hurni and Koller, 2002). The central highland receives most rain, but owing to the rugged terrain and thin soil formations that is largely deforested, most of the rain

water is channeled away by flash floods. Soil-water infiltration is therefore extremely low. Over lower altitudes infiltration of soil-water is also low because of high evaporation and lower rainfall (GoE, 1995).

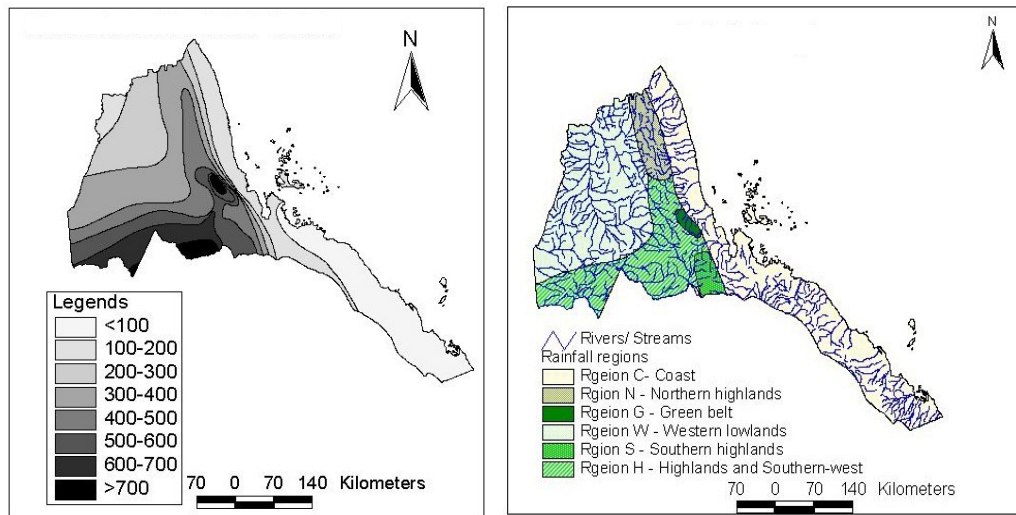


Figure 2.2: Mean annual rainfall totals over Eritrea (left) and rainfall regions of Eritrea (right) based upon rainfall systems and annual distribution as obtained from GIS database of WRD (1997)

Eritrea experiences high temperatures since it is located in the sub-tropical latitudes of the Northern Hemisphere. However, temperatures are highly influenced by local topography that leads to noticeable differences in spatial temperature ranging from a mean annual temperature of 10°C to 34°C (figure 2.3). Temperatures increase toward the eastern and western lowlands, and decreases to a minimum over the central highlands that bisects across the country meridionally.

The wind patterns in Eritrea results from both synoptic and local forcings, but are largely modified by local thermal forcing interacting with atmospheric stratification and topography. Pressure systems due to differential heating and cooling of Asia, Africa and the Indian Ocean are the main forces behind air movement in the Red Sea region (Garbesi *et al.*, 1996). While seasonal wind patterns over Eritrea are caused by the North-east and South-west monsoon, diurnal wind patterns are significantly influenced by local land-sea breezes. When the land mass south and west of Eritrea warms during daytime surface air rises, while cooler, denser air from the Red Sea flows towards Eritrea to replace it. The result is a cyclic diurnal

wind speed pattern, with wind speeds peaking during and after the hottest parts of the day and then dying down during the nighttime (Karen, 1998).

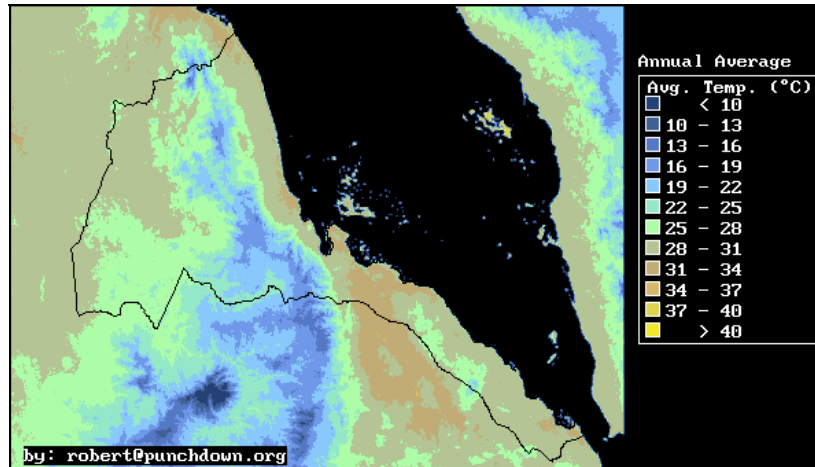


Figure 2.3: Annual average temperature distribution over Eritrea as derived from Advanced High Resolution Radiometer data (from AVHRR channel 5) and correlated with station data (RMSE 1 °C - 3°C)
(Source:<http://www.punchdown.org/rvb/temps/mapindex.html>, 2004/12/20)

2.5 LANDFORM AND DRAINAGE SYSTEM

Topographically, Eritrea is characterized by central highlands that divide the country between its eastern and western low lands (Kayouli *et al.*, 2002). According to MLWE (1997b) the Eritrean landmass is the product of the combined effect of geological and subsequent modification of geomorphologic processes. These processes are responsible for the formation of major physiographic regions:

- The Highland or plateau that is sub-divided into the Central and Southern Plateaus, Upper Anseba, Halhal, Northern, and Eastern Highlands and Mereb Trough.
- The Slopes and Escarpment that includes the Western and Eastern Slopes and Escarpments.
- The Lowlands that includes the Western and Eastern Lowlands.

The drainage system of the country is, more or less the manifestation of its physiographic settings. The genesis and flow direction of the system, apart from its geologic evolution, lies within the circle of these settings. The highlands that divides Eritrea into its Western and Eastern lowlands, defines the flow direction of the rivers. Eritrea, as shown in figure 2.4, has six catchments.

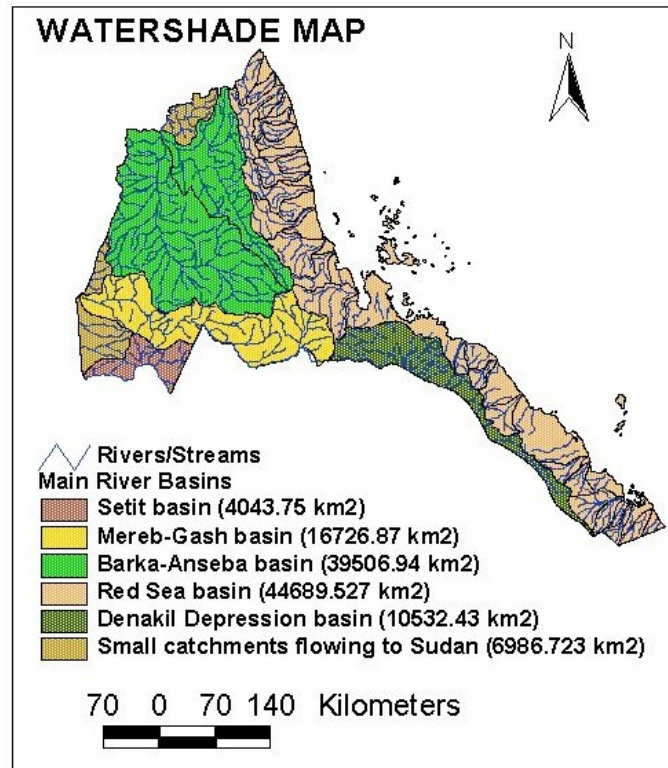


Figure 2.4: Map of Eritrea's surface water resource and drainage patterns as obtained from GIS database of WRD (1997)

On the basis of flow direction and destination FAO (1994) classified Eritrean rivers into three main drainage systems:

- The Mereb-Gash and Tekeze-Setit river systems, draining into the Nile.
- The eastern escarpment and the Barka-Anseba river systems, draining into the Red Sea.

- The river systems of a narrow strip of land along the southeastern border with Ethiopia, draining into the closed Denakil Basin.

The Mereb (upper course of Gash) and Tekezze rivers are found on the border with Ethiopia. As GoE (1995) states, except for the Tekezze Setit, which has a perennial flow, all the other Eritrean river systems are intermittent.

A preliminary assessment indicates that Eritrea is not gifted with appreciable amounts of both surface and ground water resources. The scant rainfall over the Highlands disappears as runoff because of rugged and denuded topographic features and the impermeable nature of the geological formations. Hydrological, climatological, topographical and geological factors, together with human actions of deforestation and war created a chronic shortage of water for human consumption and industrial uses (GoE, 1994).

2.6 SOIL AND GEOLOGY

Soils of Eritrea vary from region to region in terms of texture, fertility and other natural characteristics (Kayouli et al., 2002). So far no known reliable and detailed soil survey has been conducted. Available soil maps are estimated downscaled products from global soil maps or were produced during the colonial time. Diverse soil maps and descriptions are commonly found in literatures. In many cases they lack consistency and are not suitable for application purposes.

As indicated in figure 2.5 leptosols appear to be the most dominant soil type in Eritrea and covers the Highlands and southern extension of eastern part of the country. Other soil types found in the Highlands are chromic, eutric, calcic cambisols that have a distinctive red-brown color, lithosols, xerosols and fluvisols. In the northern and southern parts of the Red Sea coastal plains, sandy desert soils are most common. In other parts of the country ortho-solonchaks, regosols, and andosols are observed. Soils in the western parts include vertisols and fluvisols.

The geology of Eritrea formed through a process of continuous uplifting and faulting. Eritrean geology is divided into two distinctive regions: (a) the central and northern Highlands and (2) the coastal and low altitude areas. The central and northern Highlands consist of the Pre-Cambrian Basement complex and is known

to be one of the oldest formations found in Africa. The western highlands with their typical flat-topped mountains are mostly covered by tertiary basaltic flows. In western Eritrea, the basement complex was covered at a later stage by young quaternary sediments, although local rocky outcrops of the basement complex also occur (Mohr, 1970; Drury et al., 1994 cited in Ogbasighi, 2001:7). The formations along the Red Sea coasts line and the southern Danakil plains are younger and consist of tertiary and quaternary sediments with volcanic rocks. The latter are associated with the Red Sea and the Afar rift system, which cuts through the area from south to north accompanied by many fault lines. During the Tertiary, sandstone and limestone were formed along the eastern coast, where at present lagoons and salt plains are found (Mohr 1961,1987 cited in Ogbasighi, 2001:7).

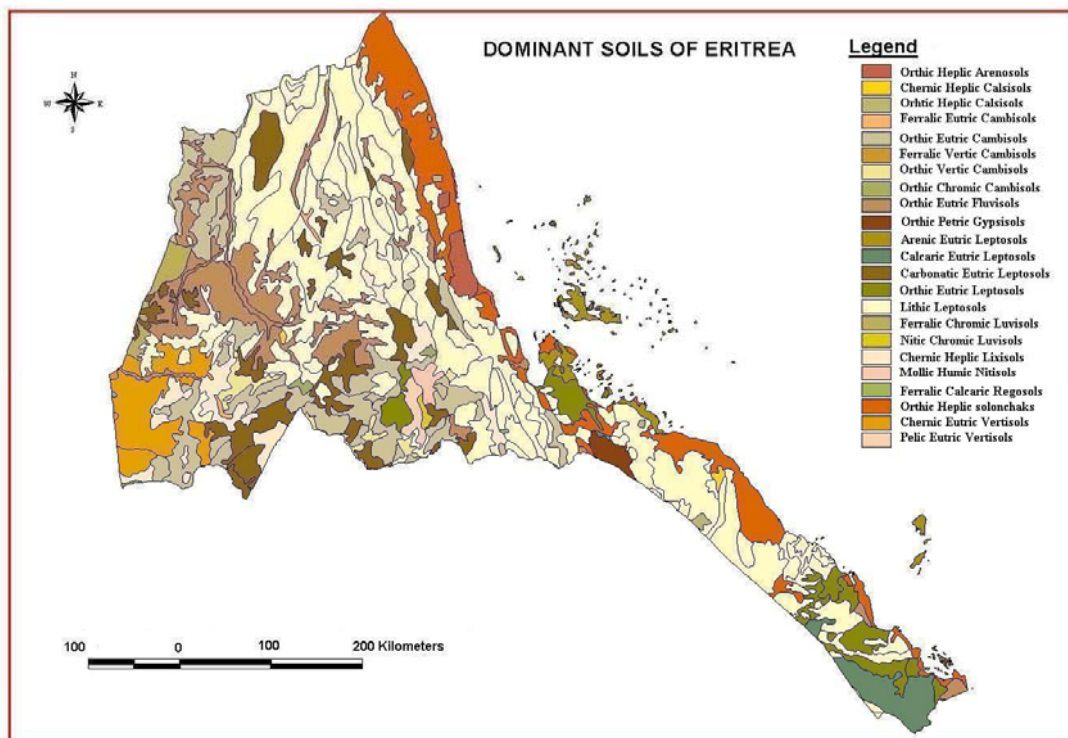


Figure 2.5: A map that exhibits major soil types in Eritrea as obtained from GIS database of FAO (1994)

2.7 LAND USE AND VEGETATION COVER

Since detailed land use studies have not yet been completed in Eritrea, no standard land use classification system exists. As indicated in figure 2.6, the

northwestern low altitude region and costal plains are arid zones that are populated by nomadic populations. These areas could also be categorized under pasture zones since they are supporting animal rising activities upon which the nomadic populations depend. Crop zones and pasturelands are mainly found in the central and southern high lands, and southwestern low altitude region.

Vegetation in Eritrea has been subjected to long time mismanagement and over exploitation. Its depletion was associated with the removal of natural vegetation for the expansion of farming, fuel wood, grazing, etc (GoE, 1995). In 1952, Eritrea's forest resources covered an area of 12,525 km², i.e., about 11% of Eritrea's surface. This resource has been reduced to a figure of less than one percent at present (MLWE, 1998). Following an international convention (MoA, 2002) the natural forest cover of Eritrea has been classified into six major vegetation types by aggregating the details presented in figure 2.7. These vegetation types include Highland forest, mixed woodlands of acacia and associated species, bush or shrub vegetation, grasslands to wooded grasslands, riverine forest and mangrove.

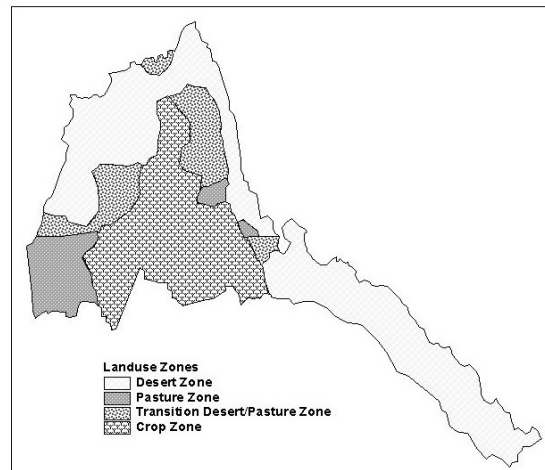


Figure 2.6: The map illustrates major land use zones of Eritrea. It was obtained and digitized from National Center for Earth Resources Observation and Science (EROS) (originally derived from thematic maps and other source material).
<http://edcintl.cr.usgs.gov/archives.shtml>, 2003/09/10.

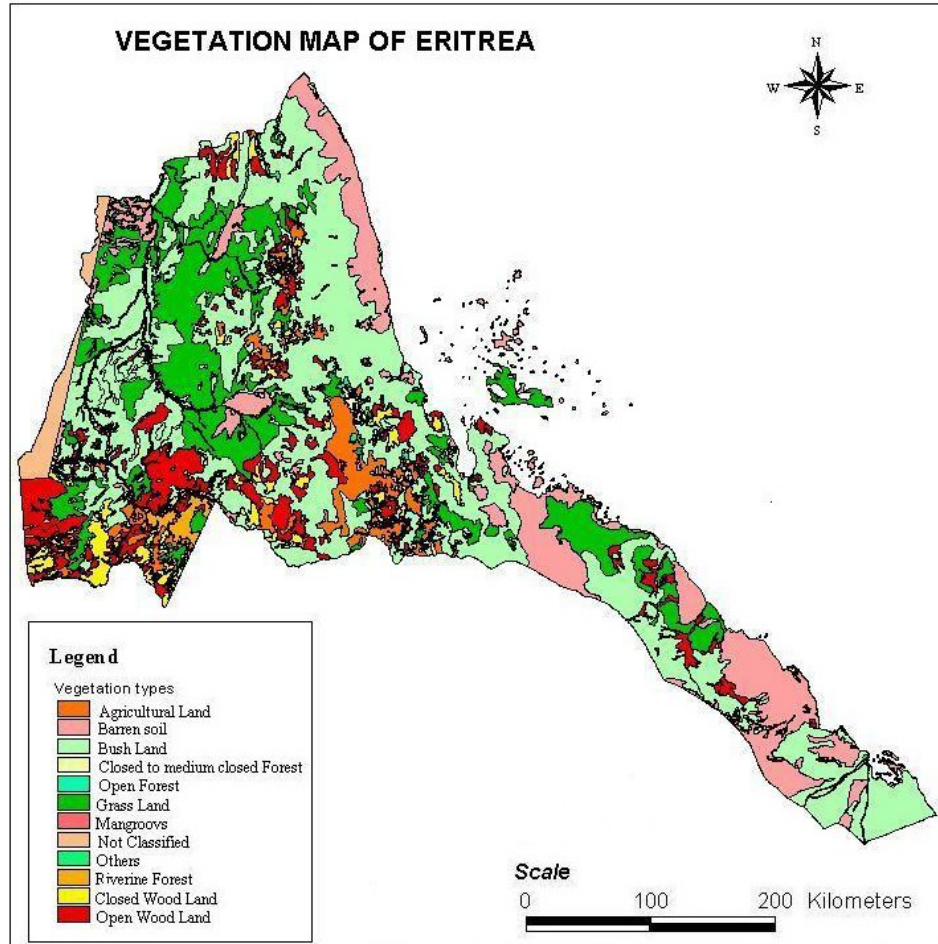


Figure 2.7: A typical vegetation map of Eritrea with 12 vegetation types. (Source: FAO/MOA, 1997)

2.8 AGRO-ECOLOGICAL ZONES

As indicated before, Eritrea is a country with complex landscapes and a variable climate, which result in a wide variety of agro-ecological conditions. As in most other land resource disciplines, no detailed assessment of agro-ecological zones has been completed. Available information was derived from work done in the early 1980s by the Ministry of Agriculture of Ethiopia (e.g., MLWE, 1997a). Although this inventory is not free from limitations (developed from outdated Landsat imagery and aerial photography and without considering inter-annual climate variability) the methodology adopted for its development proved to be sound. The study identified six zones (figure 2.8) on the basis of broad similarities of moisture and temperature regime, natural vegetation cover, soils and land use.

The major zones were each sub-divided into a number of Agro-Ecological Units (AEU) based upon more specific differences of landform, soil type, land cover or land use. Accordingly, 55 AEU were recognized and defined (see MLWE, 1997a).

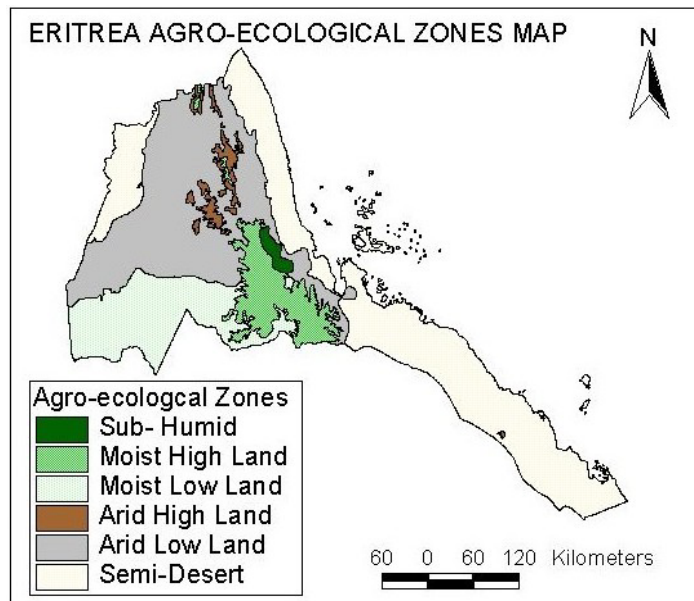


Figure 2.9: A typical agro-ecological map of Eritrea indicating six agro-ecological zones as obtained from GIS database of WRD (1997)

2.9 AGRICULTURAL ACTIVITIES

A large part of Eritrea is unsuitable for agriculture due to climate, soil characteristics or other constraints. There are about 3.2 million hectares of arable land in Eritrea, of which less than 15 percent is normally cultivated. More than 95 percent of the cultivated area is rain-fed (FAO, 2002). Rain-fed agriculture is characterized by low productivity, greatly subsistence and traditional in nature. Modern agricultural inputs such as fertilizers, agro-chemicals and systematic management schemes are often non-existent. This makes Eritrea's agriculture particularly vulnerable for changes in the climate or climate variability.

Eritrean climate, as noted earlier, is characterized by intra-seasonal and inter-annual variability with a high frequency of drought events. Rainfall variability in both magnitude and spatial distribution are the main constraints against the development of rain-fed agricultural activities. What makes the situation

particularly venerable is the fact that the majority of the population depends on rain-fed agricultural activities for their livelihood.

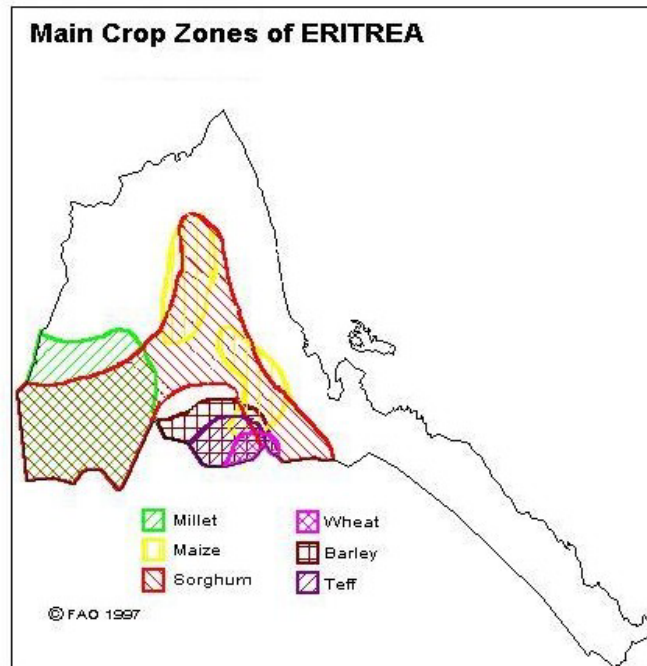


Figure 2.10: Spatial distribution of production zones of the main crops in Eritrea. Major cultivated crops include barley, wheat, African finger millet, taff and maize (Source: FAO, 1997)

The higher rainfall summer season of June-July-August (JJA) is the most suitable for rain-fed agricultural activities. It is during this season that most of the national food production takes place. There is a potential to improve productivity and to minimize risks associated with rain-fed activity by introducing inter-seasonal rainfall predictions, although longer-term changes in climate and climate variability might have a devastating effect on the country's current agriculture activities if more dry spells is anticipated. The major cultivated crops include barley, wheat, African finger millet, taff and maize (figure 2.10).

Potential exists to increase crop production through the expansion of irrigated land (MLWE, 1997b). Proper management of the existing land and water resource creates additional flexibility to boost agricultural land productivity and sustainability. Currently, irrigation potential is not fully exploited and is still in its early stage. The south-western and north-western regions along major riverbanks,

eastern low altitude regions and valley bottoms of the highlands are expected to niche extensive irrigation schemes. Apart from climate awareness, raising agricultural productivity through the use of modern technology and the establishment of irrigation-based commercial farms is a critical component for sustainable future food security.

CHAPTER 3

CLIMATE MODELLING ON REGIONAL SPATIAL SCALES

3.1 INTRODUCTION

In an effort to improve our understanding of the many aspects that govern atmospheric circulation, scientists expressed the flow in the atmosphere in terms of the primitive equations of flow dynamics (Rautenbach, 1999). At the end of the nineteenth century Bjerknes (1904) significantly contributed to the science of Numerical Weather Predictions (NWP). He was a pioneer by suggesting that, given prescribed observed initial fields, it was possible to determine the prognoses of atmospheric flow at any future time by numerically solving the hydro-dynamical equations. In essence, NWP is an initial value problem since the accuracy of short-term forecasts rely upon the accuracy of the initial field used in the forecast simulation.

The British scientist Lewis Fry Richardson (1922) was the first to initiate routine weather prediction by means of numerical integration. Although his procedures were basically sound, there were some flows that resulted in large errors with respect to the observed fields. The enormous computing time required to solve the equations in the general form he used discouraged any immediate further attempts of NWP. However, theoretical research continued and led to some direct applications to practical problems. Carl-Gustaf Rossby (1939), for example, demonstrated the importance of linearized perturbation of the equations of motion in NWP (Haltiner and Williams, 1980).

It was another invention in the late 1940s, namely the electronic computer that led to a new breakthrough. This enabled Charney *et al.* (1950) to produce the first successful NWP in 1951 where after he wrote a scientific paper about anticipated future development in the discipline of NWP. Following this development, Lorenz (1963) proposed that prediction of the atmospheric state was not possible, unless present atmospheric conditions were precisely known. Owing to the inevitable

inaccuracy and incompleteness of weather observation in some areas of the globe, it is still not possible to produce the ideal initial field. Lorenz also discovered that the chaotic (or non-linear) nature of the atmosphere imposed a finite limit of about two weeks to NWP. At that time his fundamental discovery was “only of academic interest” and not actually relevant to operational NWP since the accuracy of even a 2-day forecast was rather poor. Since these discoveries computer-based NWP have improved to such an extent that Lorenz’s limit of predictability started to become nearly attainable in practice, especially with ensemble forecasting. Scientists also start to explore the predictability of longer-range atmospheric propagation, such as predictions of the El Niño (Kalnay *et al.*, 1998) or simulations of the Earth’s climate. These efforts, however, required energy conservation in the formulation of the atmospheric equations (Haltiner and Williams, 1980).

Climate modelling is young but fast developing science. Both ocean and land surface processes as simulated by climate models had developed from simple specified surfaces to highly parameterised processes in present GCM codes. According to Henderson-Seller and McGuffee (2001) the development of computational power and the capability for forecast have been exponential. The computational capability currently available still lags behind, and to a large extent inhibits the resolution of GCMs to resolve local or regional scale process. Nested Climate Models (NCMs) were introduced to achieve regional climate simulations. GCMs and NCMs have reached a high level of sophistication. GCMs are currently widely employed to produce climate simulations on a global scale, while NCMs are nested within these models to produce more detailed regional simulations.

This chapter explores the fundamentals of atmospheric modelling by putting particular emphasis on NCMs and their capabilities. It also highlights the ultimate reasons that led to the formulation of NCMs, and how NCMs simulations added value to GCMs results.

3.2 GLOBAL GENERAL CIRCULATION MODELS

The fundamental process driving the global climate system is heating by incoming short-wave solar radiation and the subsequent cooling by outgoing long-wave infrared radiation into space (Cubasch and Cess, 1990). This heat flux exchange keeps the global temperature of the Earth close to constant, and to a

great extent modulate the global atmospheric circulation, which in turn, influences complex smaller scale flow patterns found in the atmosphere. A climate model simulation is therefore an attempt to simulate these complex atmospheric processes that govern Earth's climate. Many aspects of the climate are not yet well understood, and a significant number of the uncertainties when modelling the atmosphere, ocean and cryosphere are still directly related to the lack of knowledge (Henderson-Seller and McGuffeie, 1987). GCM simulations therefore strive to calculate the full three-dimensional character of the climate comprising at least the global atmosphere and the oceans (Henderson-Seller and McGuffeie, 2001). In GCMs the major Earth system components that affects climate are normally represented in sub-models (atmosphere, ocean, land surface, cryosphere and biosphere), accompanied by specific physical formulations that link these components in order to produce a balanced climate simulation (IPCC WGI, 2001).

GCM dynamics are represented by the governing atmospheric equation that include the equation of motion (Newton's second law), the first law of thermodynamics, the law of conservation of mass or continuity equation, the equation of state (ideal gas law) and the conservation equation of the water substances such as moisture (Haltiner, 1971). Those processes not explicitly governed by the atmospheric equations in the model dynamics are integrated into the model by means of physical parameterisations (see section 3.7).

3.3 THE NEED FOR DOWN-SCALING

On the synoptic scale, present global GCMs succeed to adequately simulate the main characteristics of the atmospheric circulation (Engelbrecht *et al.*, 2002). However, most GCMs employed for climate variability and climate change studies have a coarse resolution owing to computational requirements (McGregor, 1993). Finer grid resolutions require smaller time steps that lead to more numerical equations to solve for a specific simulation to be completed.

For this reason, most current GCMs do not have a resolution fine enough to resolve meso-scale processes, which are often necessary for local or regional scale impact assessment modelling. As an alternative regional NCMs were introduced to obtain more detailed climate simulations for selected regions on the globe. These models are nested within global GCMs, and are fed across its lateral

boundaries by information produced by the GCM. It should, however, be emphasised that NCMs are not formulated to replace GCMs, but rather to supplement GCMs by adding downscaled detail to the coarser resolution of GCMs (Jones *et al.*, 2003).

3.4 DOWNSCALING APPROACH

The essence of climate modelling is to produce applicable detailed (high-resolution) atmospheric pattern data over the largest-possible area for the longest period of time. Observational data introduced through a process of data assimilation yields improved initial conditions, and reliable boundary conditions such as topography and surface energy forcing (vegetation, soil type and ocean temperatures) ensures that the model (either a GCM or NCM) receives adequate information across its boundaries. Vegetation forcing, land-water contrast urban effects (heat islands) may cause significant climate signals such as topographical precipitation, sea breezes and lake and heat island circulation. To include all these detail on a global fine resolution grid demands a high level of computational capability. The process of downscaling, where simulated results from a GCM is fed into either a NCM or statistical package, becomes an attractive alternative to produce detailed results over an area of interest.

When NCM research started in the late 1980s, GCMs had a horizontal grid resolution of approximately 300-500 km. These models were not suitable for regional or local scale climate change or climate variability studies. The process of downscaling was introduced and both statistical and dynamical models were developed for this purpose (Leung *et al.*, 2003). These two basic methods of downscaling may also be combined into a hybrid downscaling process if used simultaneously. Downscaling is a process of refining GCM output spatially and/or temporally to produce more detailed information on a local or regional scale.

3.5 NESTED CLIMATE MODELS

In recent years, much attention has been given to the understanding of climate variability on the sub-continental or regional spatial scales. This was mostly done through the application of NCMs or other Regional Climate Models (RCMs) (Engelbrecht *et al.*, 2002; McGregor *et al.*, 1993). The nested climate modelling approach allows for a finer resolution model (defined over a limited area) to be

nested within simulations results produced by a GCM. More detailed simulations are produced over the region of interest, which includes detailed topography, vegetation types, soil types and smaller scale meteorological phenomenon that might occur in the NCM domain. NCMs are therefore sound alternatives for performing high-resolution climate simulations over any area of interest on the globe.

During model simulations information is supplied by the GCM that is fed across the lateral boundaries of the NCM. When GCM fields are interpolated in time and space to fit the NCM resolution on its boundaries, a buffer zone is introduced over the boundaries of the NCM domain. This allow for a smooth transfer of information across the boundaries. Four and eight NCM grid points, starting from the boundary towards the centre of the NCM domain, are usually considered for the buffer zone.

No matter which type of nesting procedure is employed, it seems to be important to account for consistency between the model physics of the GCM and NCM as the model resolution gets finer. When the model resolution becomes fine enough to resolve processes such as convection, the convection parameterisation needs to be excluded from the NCM. It is, however, still an unresolved problem to diagnose the exact border where the parameterisation physics needs to be withdrawn (Leung *et al.*, 2003).

3.5.1 TYPES OF NESTING

3.5.1.1 ONE-WAY NESTING

Nested climate modelling requires that boundary information propagate from the GCM into the NCM domain. One-way nesting only permits disturbances in the coarse grid to enter the fine grid of the NCM while tow-way nesting (see next section) allows disturbances to enter and leave the fine nested grid mesh. However, many NCMs developed to date employ the so-called "relaxation" method to generate meteorological lateral boundary conditions for one-way nesting (Engelbrecht, 2000). The purpose is to force the NCM resolution towards the coarser resolution field over a lateral boundary zone. An alternative one-way nesting technique is spectral nesting. In this scheme, the GCM forces the low

wavenumber component of fields in the regional domain while the NCM calculates the high wavenumber components (Houghton *et al.*, 1995).

One-way nesting, as explained by McGregor *et al.* (1993), is a widely used approach where the flow of information occurs only from the GCM grid to the NCM grid. Nested modelling requires that boundary information to propagate freely into the nested domain and that the nested model does not suffer excessive reflection of its generated flows. A commonly used scheme is that of the relaxation method first suggested by Davies (1976). In this scheme, several (typically five) boundary rows form a buffer zone at each time step with full incorporation of the outer solution at the outermost rows, tapering off over the inner rows to the internal solution of the NCM. A slightly different one-way nesting scheme is that of Perkely and Kreizberg (1974). In this scheme there are four buffer rows over which the tendencies of the models variables are weighted. In a three-dimensional atmospheric model, the disturbances are more complicated and travel from many directions, so full attenuation of the reflections is not achieved. The residual reflections are mainly manifested near the horizontal boundaries in the divergence field, which may lead to some noise in vertical velocity and related precipitation patterns. Although the precipitation patterns may appear somewhat noisy near the boundaries, it should be noted that this noise does not ordinarily lead to contamination of the interior fields. This is because the GCM moisture and temperature fields strongly override the modifications made to the heating and drying of the NCM in the boundary zone.

3.5.1.2 TWO-WAY NESTING

In one-way nesting approach the circulation produced by the NCM does not feed back into the GCM (Engelbrecht, 2000). It would be most appropriate if boundary information could propagate freely into and out of the NCM (two-way flow of information). This is actually more difficult to achieve than one-way nesting if the GCM and NCM have different architectures (McGregor, *et al.* 1997). Norris and Doty (1998) have reported the inclusion of two-way nesting scheme in MM5 nested regional model.

3.5.2.3 MULTIPLE NESTING

Multiple nesting is similar to one-way nesting, where one NCM is forced at its lateral boundaries by a second coarser resolution NCM, instead of by GCM. This approach is applied to yield high-resolution meteorological fields to capture small-scale processes such as thunderstorms.

3.6 NUMERICAL INTEGRATION OF CLIMATE MODELS

The formulation of atmospheric dynamics, parameterisation schemes and numerical integration techniques applied in both NCMs and GCMs are essentially similar. The major difference is that a NCM covers a limited area within a global GCM, and that atmospheric mass and temperature fluxes continuously crossing the boundaries of the NCM domain. As the NCM does not consider any atmospheric circulation features outside its domain, it needs to receive far field global information across its boundaries.

For large-scale atmospheric motion, the atmosphere is normally assumed to be in hydrostatic equilibrium, i.e., the vertical acceleration may be neglected (Haltiner, 1971). This assumption, known as the hydrostatic assumption, is currently widely applied in climate GCMs. The hydrostatic approximation is found to be valid for grid resolutions greater than approximately 10km. Inaccuracies may arise over steep terrain or during deep convection when finer grid resolutions are considered (McGregor *et al.*, 1993).

Generally, the accuracy of global weather and climate GCMs depends on many factors, including the accuracy of the knowledge of the state of the atmosphere at the initial time of model simulation, the numerical methods applied, and the horizontal grid and vertical layer resolution (Layton, 2003). Most GCMs use a sigma or hybrid- sigma vertical coordinate which is terrain following at the surface of the Earth, while the upper air coordinate gradually changes to follow a surface of constant pressure or potential temperature. On the horizontal plane most global GCMs consider a spherical coordinate that follows longitudes and latitude to solve the advection equations. A well-known disadvantage of spherical coordinates is the convergence of the meridians of the latitude-longitude grid toward the poles. This is often controlled by the use of Fourier filtering along latitude lines for grid point models to avoid time step restrictions (McGregor, 1995 b). However, for computational reasons, accuracy and uniform applicability of physical parameterisation more uniform regular horizontal grids are used in

NCMs. For example, the Lambert Conformal, Gnomonic Cubic (Sadourny, 1972) and Conformal Cubic coordinates (Rančić *et al.*, 1995) may be mentioned. The latter is engaged in stretch grid models (McGregor, 1995a). It implies that the horizontal grid projection of a global GCM does not always fit the projection of the NCM grid. This might give rise to interpolation instabilities at the lateral boundaries of NCMs.

As detailed by Layton (2003), GCM and NCM integrations require calculations that are known to be very time-consuming on even modern computers. In particular, a long-standing problem in the integration of NWP models is related to Eulerian time discretization where the maximum permissible time step is restricted by stability rather than accuracy. This implied that for an integration to be stable, the time step has to be small enough for the time truncation error to be much smaller than the spatial truncation error. Smaller time steps obviously require more computer time. Early models used an explicit Leapfrog method in numerical integration, where the time step was limited by both the Courant–Friedrichs–Lewy (CFL) criteria and propagation of gravity waves. Discretization schemes based upon the semi-Lagrangian treatment of advection offer the promise of larger time steps, with relatively no loss in accuracy compared to Eulerian-based advection schemes (Robert, 1981; Staniforth & Côté, 1991). Since gravity terms may render the equations stiff and thus severely restrict the time step (even with semi-Lagrangian advection approximations) one needs to combine the semi-Lagrangian formulation with semi-implicit time-stepping to obtain maximum benefit from the semi-Lagrangian approach. By combining a semi-Lagrangian treatment of advection and a semi-implicit treatment of gravity terms, it is possible to increase the time step substantially while maintaining numerical stability.

3.7 PHYSICAL PARAMETERISATION IN CLIMATE MODELS

Because of their large grid-box dimension, global climate GCMs do not explicitly represent small-scale process occurring within the atmosphere-surface-ocean continuum. In order to produce realistic simulations (Kalnay *et al.*, 1998), a climate model needs to have an accurate representation of the net effect of small-scale physical processes in the climate system. These processes proved to be important for model performance. Physical parameterisation is the representations of those processes in a model that are not explicitly governed by the dynamic atmospheric equations (Hewitson, 2001). The most important fields

of physical parameterisation include the radiation balance, clouds and precipitation processes (dynamic and convective), boundary layer processes, surface and sub-surface processes atmospheric chemistry and gravity wave drag.

As noted before, the primary factor that drives atmosphere circulation is the differential solar radiation between the poles and the equator and the subsequent radiation budget that needs to be in balance. The processes involved in the radiation budget are very complex and too time consuming to compute for numerical prediction purposes (Fu *et al.*, 1995). Hence simplified radiation schemes are used in atmospheric models (e.g., Katayama, 1974 see Haltiner and Williams, 1980). These simplifications and stochastic approximations of physical processes in the atmosphere are typical examples of physical parameterisation.

Cumulus convection plays a major role in the vertical transport of heat and moisture in the atmosphere. Cumulus parameterisation has been a topic of considerable interest since the first studies by Charney and Eliassen (1964) and Ooyama (1964) who focused on the growth of tropical cyclones. Following this development, many cumulus convection parameterisation schemes have been developed for atmospheric models. These vary from rather simplistic moist convective adjustment schemes (Kuo, 1974) to sophisticated approaches, which include more detailed cloud physics (Arakawa and Schubert, 1974; Anthes, 1977). While individual clouds might not be resolved in large-scale atmospheric models, a collection of these clouds may have an important impact on the large-scale heat and moisture budget of the atmosphere. Consequently, it is necessary to parameterise the effects of cumulus clouds as a function of the large-scale fields of temperature, moisture, and momentum (Albrecht, 1983).

Since cloud formation and rainfall are important for sustainable life on Earth, many parameterisation schemes representing cloud and precipitation processes have been developed over the last few decades to allow for more realistic simulations in global GCMs and NCMs. Cloud and rainfall parameterisation is linked to dynamic related atmospheric properties such as temperature, humidity and wind velocities at a specific time-step. Such parameterisation schemes, which are applied to “correct” the atmosphere at given time steps, are known as diagnostic schemes and are widely used in large-scale models (Slingo, 1987). Sophisticated prognostic schemes have also been developed to reflect microphysical processes in clouds and the interaction of cloud processes with the

surrounding atmosphere (Sundquist, 1978; Smith, 1990). Nevertheless, all these processes are still an oversimplification of real atmosphere-cloud processes.

2.8 MODEL SIMULATIONS ON LONGER TIME-SCALES

Weather refers to the day-to-day state of the atmosphere. It describes the formation and propagation of fronts and individual storms, daily precipitation, temperature, humidity, winds and Mean Sea Level Pressure (MSLP) patterns. While great progress has been made in the field of forecasts on longer time scales, the chaotic behaviour of the atmosphere hinders the predictability of day-to-day weather fluctuation beyond Lorenz's limit and there is no scientific basis for forecasting beyond this limit (AMS, 2001). Apart from the impact of chaos, accurate observations of the initial atmospheric state (initial conditions) are crucial for short-term weather forecasting.

In longer-term forecasts and simulations (seasonal and climate) initial conditions do have a detectable influence at the initial phase of the simulation, although they become less important as the simulation progresses in time. Here boundary forcing plays an important role in keeping the model simulation on track and prevents it from drifting. When boundary forcing such as fluxes from the upper ocean, ice sheets or land surface are coupled to the atmosphere and are allowed to evolve, longer time-scale model simulations may be achieved (Goddard *et al.*, 2001). Boundary forcing from changing Sea Surface Temperatures (SSTs) makes seasonal forecasting possible, while climate change scenarios may be produced when a model is forced with changing concentrations of greenhouse gases. It is obviously also important that energy is conserved in the formulation of the atmospheric equations of climate simulations.

CHPATER 4

CHARACTERISTICS OF THE PAST AND PRESENT CLIMATE OF ERITREA

4.1 INTRODUCTION

Historical data for large parts of Africa either does not exist or is not regarded as reliable. At present regional-scale observational records of temperature and rainfall are limited, and there is little prospect of reconstructing temperature and rainfall records from historical data alone unless more knowledge of paleoclimatology in Africa is gained. It is therefore sound to include proxy data from other sources, such as tree growth indices, ice-cores and sedimentary deposits along with historical data for paleoclimatic reconstruction over the past few centuries (Bradley, 1991). Despite the uncertainty in historical records, many researchers have searched for evidence of more extreme fluctuations in temperature over the past 500 years than observed since the industrial revolution that started in 1860 (Nicholson, 1979; MacCracken and Kutzbach, 1991).

Studies of past climates are useful in identifying mechanisms and processes that might have led to large changes in climate. These studies might also contribute to climate model verification and improvement (MacCracken and Kutzbach, 1991). However, such information is of little value in current social infrastructure and natural resource management activities.

A widely used and easily available observational dataset for more recent model comparison are the global reanalysis data set from the National Center for Environmental Prediction (NCEP) (Kalnay *et al.*, 1996) and European Centre for Medium-Range Weather Forecasts (ECMWF) (Gibson *et al.*, 1997). NCEP data is available for many variables since the mid-1970s, and it covers the African continent with a horizontal resolution of $2.5^{\circ} \times 2.5^{\circ}$. Some variables are also available on horizontal levels in the vertical. Although not particularly ideal for local or regional scale model verification (because of its coarse resolution), the NCEP reanalysis is most probably among the best data set presently available for this purpose.

In Eritrea there are a number of meteorological stations distributed all over the country. Observed data from most of these stations appear to be unreliable owing to a lack of continuity and standardization. Nonetheless, attempts are under way to incorporate some of the locally observed rainfall data to supplement NCEP reanalysis data in order to investigate past and present climate trends over Eritrea.

This chapter gives an introduction on how past climates evolved in the sub-Saharan Africa and Eritrea region. It also gives detail about the characteristics of the present Eritrea climate, and explores previous views on the driving mechanisms of atmospheric circulation and of persistent droughts that became more frequent over the past two decades.

4.2 OBSERVED CLIMATE PATTERNS

4.2.1 ATMOSPHERIC CIRCULATION

Describing characteristics of the present atmospheric general circulation provide an appropriate starting point for elaborating on the climate of Eritrea. Larger scale atmospheric circulation plays an important role in the occurrence of wet and dry spells in the region. Characteristics of global atmospheric circulation for January and July are well documented in the literature (Ahrens, 2000; Martyn, 1992; Nicholson and Flohn, 1980). Although it is beyond the scope of this chapter to provide detail of the global atmospheric circulation, it is worthwhile to firstly give an overview of the global circulation that affects Eritrea before addressing local climate properties, which extend from the climate of Eritrea to the climate in small-scale river basin catchments.

4.2.1.1 MEAN SEA LEVEL PRESSURE AND NEAR-SURFACE WIND PATTERNS

In reality there are a number of latitudinal synoptic-scale bands of alternating low and high-pressure systems that propagate in the atmosphere with their associated wind flow patterns. In the equatorial zone, a semi-stationary band of low-pressure systems occur on average. Due to solar heating and strong convection, a region of thunderstorms and frequent rain developed that is referred to as the Inter-Tropical

Convergence Zone (ITCZ). North and south of the ITCZ (at approximately 30° latitude), subtropical anticyclones occur which are associated with descending air masses that result in drier conditions. Further pole wards, mid-latitudes cyclones and high-pressure areas of the circumpolar regions are found.

Important for Eritrean climate are the Northern Hemisphere subtropical Bermuda-Azores anticyclone positioned over the eastern Atlantic Ocean (between 25°N and 35°N) and the Pacific anticyclone – both systems occur throughout the year. These two anticyclones developed in response to the convergence of air aloft near the upper-level jet stream that forms part of the well-known Hadley cell. Two wind patterns, namely prevailing westerlies to the north of these systems and easterly trade winds to the south are a result of the angular momentum balance of the planet's atmosphere. Easterly trade winds form a significant part of onshore mass flux over northeastern Africa. However, during May to September (spring season) the central Asian high-pressure cell decays to form a shallow Pakistani thermal low in association with the ITCZ. During winter (October to April), owing to the intense cooling of the Asian continent, a high-pressure cell develops over Asia to interact with the other Northern Hemisphere subtropical anticyclones. In the southern hemisphere, three clearly defined subtropical anticyclones appear over the three oceans that are separated by southern Africa, South America and Australia.

Synoptic-scale atmospheric circulation cells associated with subsidence and convection of air over specific regions have recently attracted a lot of interest, especially with respect to drought patterns (see section 4.4). In the tropics atmospheric circulation is governed to a great extent by Hadley cell circulation that is associated with convection over the ITCZ and subsidence over the subtropics. Subsidence in the subtropics is most pronounced over the oceans (Nicholson and Flohn, 1980). During the northward migration of the ITCZ in Boreal summer months (June-July-August (JJA)), convection accompanied by local forcing plays an important role in the weather of the Eritrea region. The northward migration of the ITCZ towards the Sahara is accompanied by the west African monsoon, which allows for air flow from the west over the northern African continent. Winds from the African monsoon often reach Eritrea from the west.

The central east African highland meandered across a north-south alignment (east of the Nile valley). Its northern boundary is located in Eritrea and its

southern boundary over central-east Africa. This highland, the Red Sea, the Gulf of Aden, the Gulf of Guinea and the high altitude Asian landmass all contribute noticeably to the weather of Eritrea by affecting the movement of air masses with dry or wet attributes depending on the origin of flow and route followed.

The near-surface wind and MSLP climate as illustrated in figure 4.1 (a), (b), (c) and (d) demonstrate the most important synoptic-scale atmospheric circulation features over Eritrea during the four Boreal seasons. The discussion, however, focuses on the JJA and December-January-February (DJF) seasons, owing to the similarity of these seasons to the remaining seasons (September-October-November (SON) and March-April-May (MAM)).

Boreal summer season (JJA)

The northward migration of the ITCZ marks the onset of the summer season in the Eritrea region, which happens in June. During the JJA season (Boreal summer season), counter-clockwise circulation around the Pakistani thermal low and clockwise rotation around the Bermuda high produce northerly winds that consists of cool and dry air. These winds propagate southwards from the Azores and Siberian highs before reaching the Eritrea region (figure 4.1(c)). The northerly winds confluence with West African monsoon flow from the southwest before flowing over Eritrea and the Red Sea region. The ITCZ forms where these two air masses “collide”. These wind patterns are referred to as *harmattan* over the Sahara and West Africa, and *Egyptian Current* in the northeast Africa section (Martyn, 1992).

The African monsoon flow originates from the Atlantic Ocean high-pressure system in the subtropics of the Southern Hemisphere. The flow propagates northwards across the equator where it turns eastwards as a result of the Coriolis force. When reaching the Gulf of Guinea, the flow therefore becomes westerly to southwesterly from where it advance across the Congo basin and Sahara towards northeast Africa. The unstable moist air in the African monsoon when reaching the African continent becomes drier as it flows over the African continent until it faced the dry and dust bearing of the Egyptian currents. The African monsoon persists during the May to September period (broader summer) with some minor changes in the MSLP fields and ITCZ location.

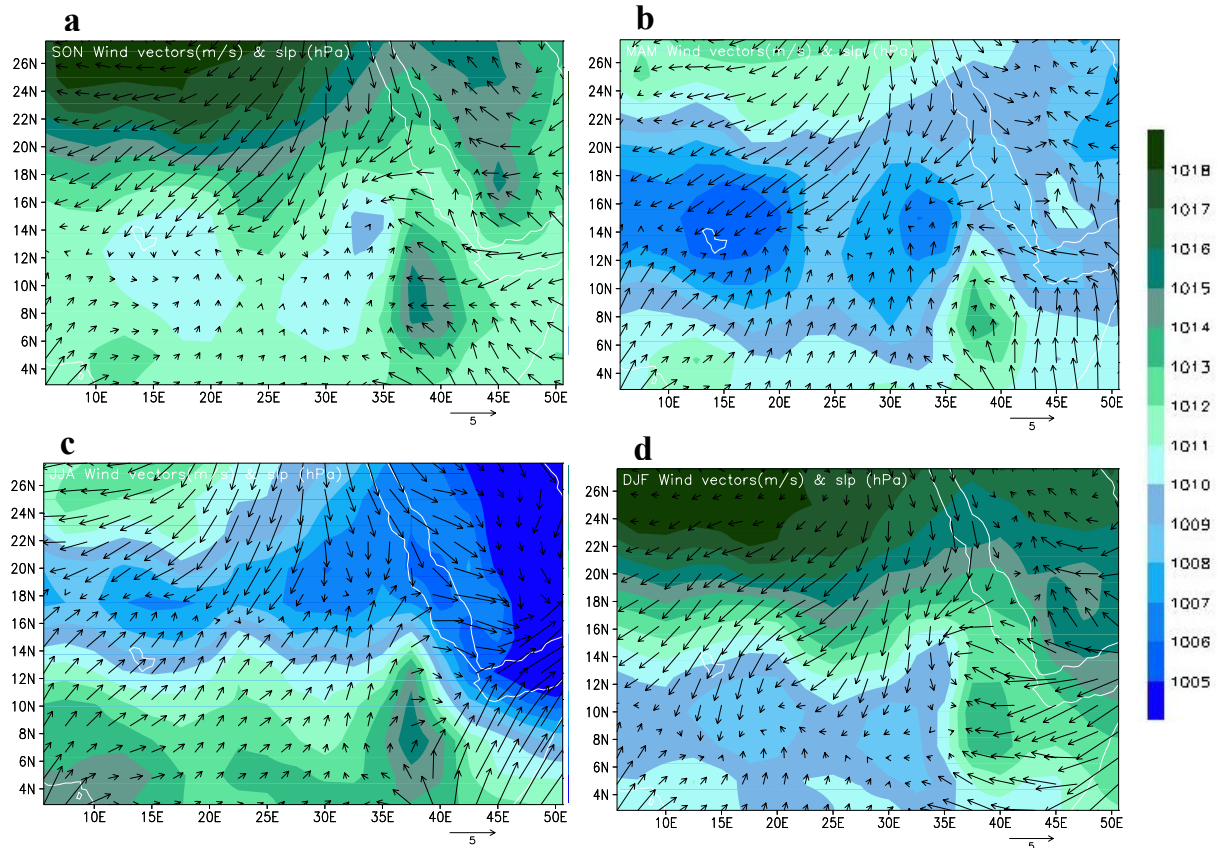


Figure 4.1: Observed seasonal Mean Sea Level Pressure (MSLP) in hPa and averaged near-surface winds ($\times 10 \text{ ms}^{-1}$) over the period (1948-2003) as obtained from NCEP reanalysis data. The maps represent the four Boreal seasons namely, (a) September to November (SON), (b) March to May (MAM), (c) June to August (JJA) and (d) December to February (DJF).

Boreal winter season (DJF)

During the Boreal winter season (DJF) the Asian continent cools down and the strong Siberian high-pressure system develops over central Asia. The clockwise rotation around this high result in intensified easterly trade winds towards Africa and a reverse in the Indian Monsoon flow. This allows for a strong easterly flow over the Red Sea and Eritrea (figure 4.1 (d)). The ITCZ migrates towards the south of the equator over east Africa, although it persists in the Northern Hemisphere over the west-African section.

Over the western parts of Eritrea, average winds flow parallel to the mountains of the central Highlands to move southwards to southwestwards. These winds contain little

moisture and allow for the prevalence of dry conditions over western Eritrea during DJF.

During the Boreal winter season circulation patterns are complex over the Red Sea region and the eastern escarpment of the Eritrea Highlands. Flow is predominantly from the east and southeast crossing the Red Sea before reaching Eritrea. Van Buskirk, *et al.* (1997) suggested the development of a cool humid inversion layer over the Red Sea ocean surface as a result of evaporation, with winds that is pushed to the west by synoptic gradients. These winds, under the influence of the central Highlands, “collide” with northerly flow from Egypt to form a small convergence zone. The former wind patterns are responsible for rainfall during the DJF season in the Red Sea and eastern escarpments of Eritrea, since moisture is imported from the Indian Ocean and Gulf of Eden.

4.2.1.2 MOISTURE ADVECTION AND RAINFALL PATTERNS

Tropical warm-season rainfall regimes are predominant on the African continent, although winter rains of extra-tropical origin prevail on its northern and southern extremes. Arid and semiarid zones, the Sahara and the Kalahari, mark the transition from tropical to extra-tropical influence. The primary control on rainfall in the tropical areas is the ITCZ, which advances northward to the Saharan margin in the Boreal summer and southward to the north of Kalahari in the Austral summer (Nicholson, 1986).

In Africa moisture flux becomes progressively less toward the north and south of the equator. It is evident that, even though the ITCZ's location is more northerly during the Boreal summer (JJA), the northward decrease of rainfall and moisture flux patterns seem to be not only controlled by the ITCZ, but also by the degree of convection, the availability of moisture and average synoptic forcing. Figure 4.2 (a), (b), (c) and (d) gives the daily precipitation, precipitable water, zonal and meridional moisture fluxes averaged over the season JJA and period 1948-2003. The climatology was calculated from the NCEP reanalysis data set. In general the moisture flux pattern are consistent with precipitation patterns (figure 4.2 (a), (b) and (c), (d)).

The west-Africa monsoon is responsible for substantial moisture flux from the Gulf of Guinea towards the ITCZ zone in Africa. Martyn (1992) linked these moisture

advection patterns to the general atmospheric circulation. The trade winds, blowing from the Atlantic high-pressure system in the Southern Hemisphere overwhelming consists of stable air. When crossing the equator while advecting northwards, the air becomes unstable due to the adherence of moisture. The resulting moisture transport is persisted until it meets the dry and dust bearing northeasterly and easterly Northern Hemisphere trade winds at ITCZ. The northward displacement of the ITCZ during JJA creates an opportunity for the African monsoon moisture to reach Eritrea, which also mark the beginning of the Boreal summer.

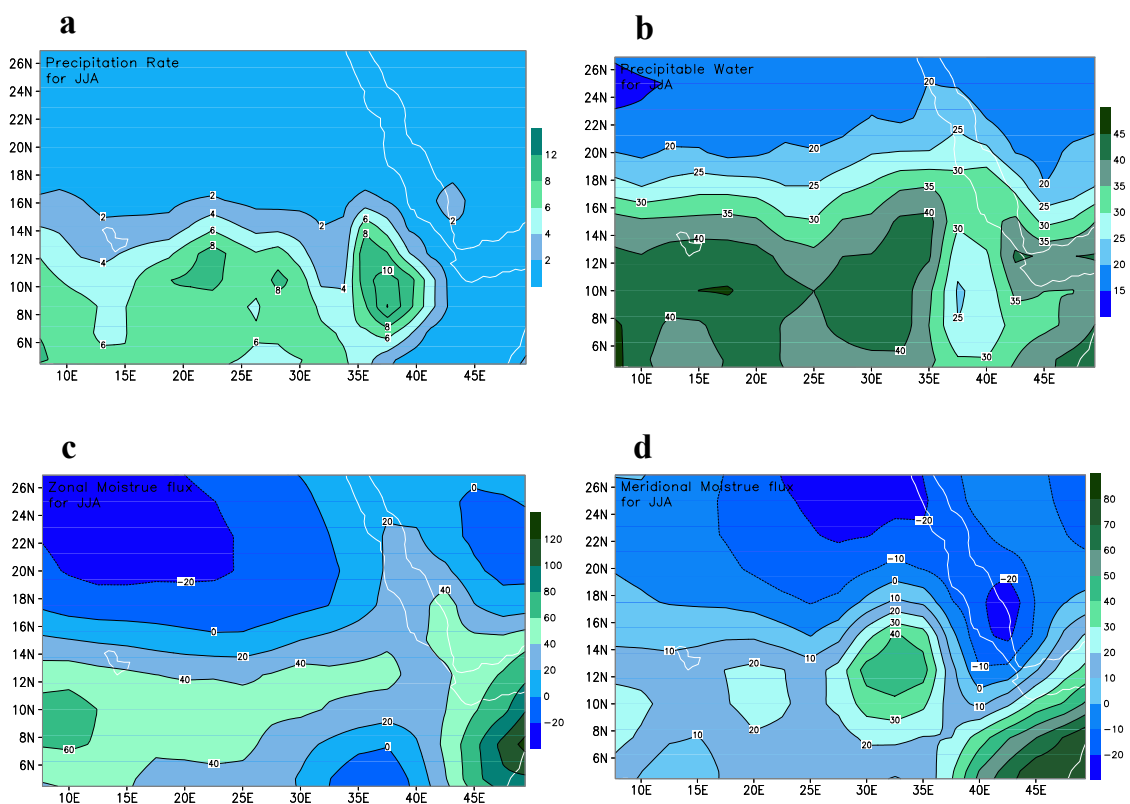


Figure 4.2: Observed (a) precipitation rate in mm per day, (b) precipitable water in kg m^{-2} , (c) zonal moisture flux and (d) meridional moisture flux in $\text{kg m}^{-1}\text{s}^{-1}$ averaged over the months June to August (JJA) and period 1948-2003. The climatology was calculated from the NCEP reanalysis data set.

Boreal summer season (JJA)

The driving mechanisms of Boreal summer rainfall over Eritrea are consistent with those that drive the Sahelian climate. It is mainly associated with tropical

circulation and constrained, to a large extent, by convective activities in the ITCZ. Over Eritrea rainfall extends from May to September, while reaching a peak during July and August. During this season the eastern Lowlands experience dry conditions. Martyn (1992) suggested this to be associated with the so-called foehn effect that appears on the lee side of mountains when air descends from a higher altitude. However, this is not affecting the eastern escarpments of Eritrea the eastern facing highlands are characterized by a bimodal (during JJA and DJF seasons) rainfall pattern as shown in figure 4.3. The higher rainfall along the eastern escarpment may be attributable to local influences such as evapotranspiration from a densely covered forest surface.

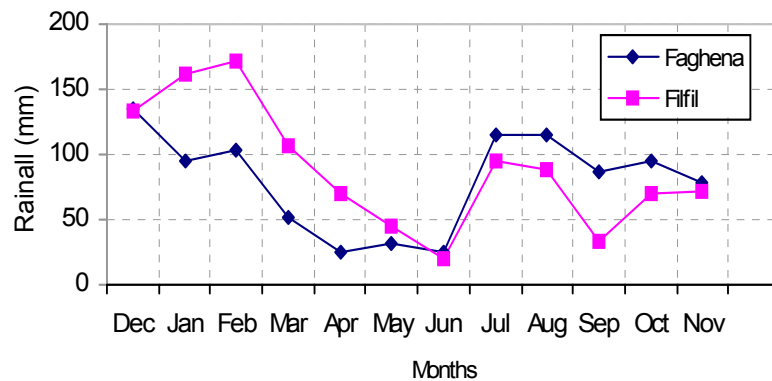


Figure 4.3: Observed mean monthly rainfall in mm for Filfil (1928-63) and Faghena (1947 to 1962) as obtained from the Department of Water Resources (DWR) of Eritrea. These two stations are found along the eastern escarpment of the Eritrea Highlands that is covered with remnants of the tropical rain forest and referred to as Green Belt.

Boreal winter season (DJF)

During DJF circulation and moisture advection patterns over Eritrea is not affected by tropical atmospheric systems since the ITCZ moves towards southern Africa in the eastern section of Africa. During the Boreal winter season winds bring moisture from northwestern Indian Ocean and Gulf of Eden. The moisture transport is responsible for rainfall in the Red Sea and along the eastern escarpment of the central Highland of Eritrea. On the Highland plateau and the western part of Eritrea, dry conditions prevail owing to the foehn effect.

4.3 OBSERVED CLIMATE TRENDS AND VARIABILITY

It has been well understood that climate variability, whether associated with internal or external climate system forcing, appears to modify the normal prevailed climate state of the atmosphere which in turn reinforce conditions that might lead to droughts or floods in different locations of the globe.

The Southern Oscillation (SO) is the best-defined and understood mode of international climate variability. Extreme phases of the SO are characterized by global-scale shifts in atmospheric circulation cells (normally Walker cells) and with a marked, high amplitude modulation of equatorial Pacific Ocean sea surface temperature anomalies (Ropelewski & Halpert, 1991) that include the formation of El Niño events. Currently, some percentage of interannual variability on the globe appears to be related to changes in tropical oceans temperatures associated with El Niño events. It is expected that greenhouse warming might equalize temperatures in the eastern and western Pacific Ocean by warming the cooler eastern Pacific Ocean. The heat of the warmer western Pacific is largely absorbed by increased evaporation. Such an expected decrease in El Niño events might obviously also reduce interannual variability on other parts of the globe (Rind, 1991).

The response of the climate over the northern east Africa region (Eritrea, Ethiopia, Somalia and Djibouti) to the SO and El Niño events is not well documented. Most studies focused on the western Sahle or central eastern Africa domain (Kenya, Tanzania, Uganda, Burundi and Rwanda). The climate behavior of the former region, especially over Eritrea and Ethiopia, shares some degree of similarity to that of the central eastern Africa region during periods when tropical circulation dominates. It was found that El Niño events are normally associated with positive rainfall anomalies over the entire eastern Africa region – with the exception of Sudan (Schreck and Fredrick, 2003).

In recent years observed increased temperatures that might be attributed to global warming might have already disturbed climate patterns over eastern Africa. With this in mind, Schreck and Fredrick (2003) studied climate variability over eastern Africa where they compared the recent climate to a longer-term climate. They concluded that the recent climate was associated with a rapidly intensifying global warming signal. They suggested that if the observed global warming trend

continues to intensify in coming decades, the climate and ENSO responses may be altered significantly over eastern Africa. The possible response of the future climate of this region under conditions of enhanced greenhouse gases concentrations will be discussed in more detail in chapters 5 and 6 of this document. This section will focus on observed trends and variability over the domain illustrated in figure 4.4, with specific emphasis on the Eritrea sub-domain (gray area).

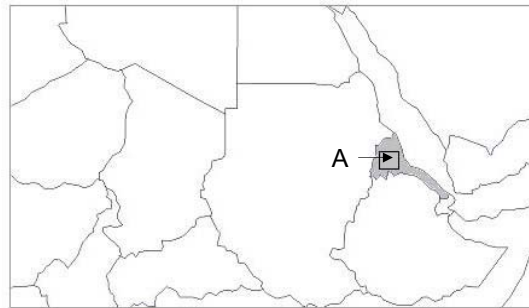


Figure 4.4: The domain that will be considered in PRECIS nested climate model (NCM) simulations. Eritrea is indicated in gray. In the following sections NCEP reanalysis data are spatially averaged over the box A.

4.3.1 RAINFALL

Trends and variability in rainfall is a matter of great importance, and a reliable long record of rainfall at different locations over the area of interest is essential when determining trends and investigating variance. Owing to many difficulties associated with rainfall measurement over Eritrea the use of station data alone is not recommended. For a country like Eritrea it is important to compare other moisture-related variables, such as stream flow and soil moisture with precipitation to generate a broader picture of long-term rainfall trends. Such analyses, however, are not addressed in this study.

As indicated in figure 4.5, the annual rainfall as recorded at Asmara (located on the central Highlands) shows a negative trend of approximately $0.87 \text{ mm}\cdot\text{year}^{-1}$. During 1955-1960 and around 1980 anomalously high rainfall episodes were recorded in comparison to other decades. Prior to 1955 rainfall fluctuated around

the mean with a smaller variability. The dry episode during the last five years in the figure 4.5 was more severe than ever recorded since 1900.

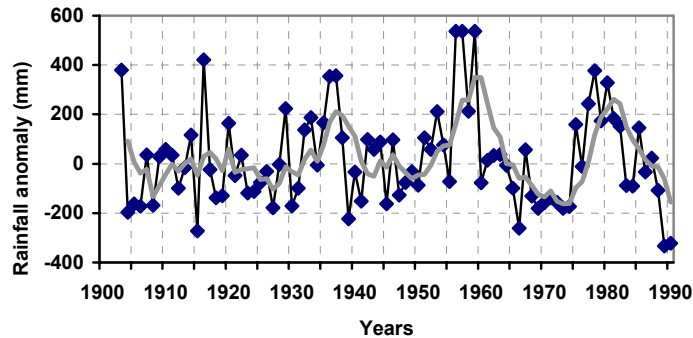


Figure 4.5: Annual rainfall anomalies (black line) and 5-years moving averages (gray line) over the period 1900-1990 for Asmara that is located on the central Highlands of Eritrea as obtained from the Department of Water Resources (DWR).

4.3.2 NEAR-SURFACE AIR TEMPERATURE

Variability of near-surface air temperatures calculated from NCEP reanalysis data over the period 1950 to 2000 for the four seasons DJF, MAM, JJA and SON were spatially averaged over both the entire domain of figure 4.4 and the box-area **A** in figure 4.4. Figures 4.6 (a), (b), (c) and (d) illustrate the weighted average time series of observed near-surface temperature anomalies ($^{\circ}\text{C}$) for the four seasons as calculated over the entire domain of figure 4.4. The gray lines represent five-year moving averages. Similarly, figures 4.7 (a), (b), (c) and (d) give the weighted average anomalies as calculated over the box-area **A**. According to these figures there are no obvious differences in air temperature variability over the two selected domains.

Figure 4.7 (a) shows a significant increasing trend in near-surface temperatures for the JJA season over the period 1948 to 1965. In contrast to an increase trend, it is interesting to note that temperature variability decreased over the same period. The general trends of near-surface temperatures during the SON and MAM seasons are similar to that of JJA, although higher variability appears in the SON and MAM time series. The trend of near-surface temperatures during DJF is not significant, but a warming episode appeared over the last decade.

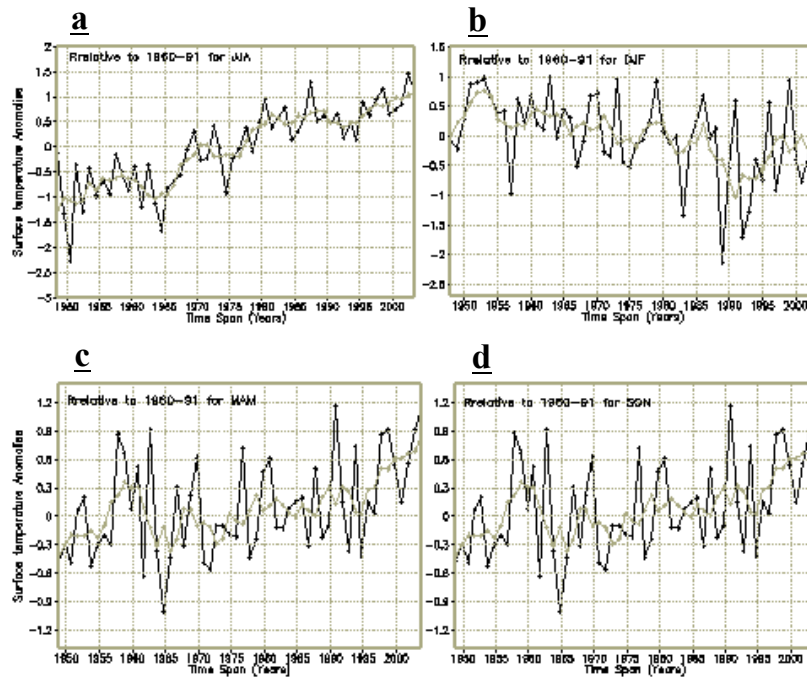


Figure 4.6: Weighted average time series (1950 to 2000) of near-surface temperature anomalies ($^{\circ}\text{C}$) as calculated from NCEP reanalysis data for the seasons (a) JJA, (b) DJF, (c) MAM and (d) SON and the entire domain of figure 4.4. Gray lines denote five-year moving averages.

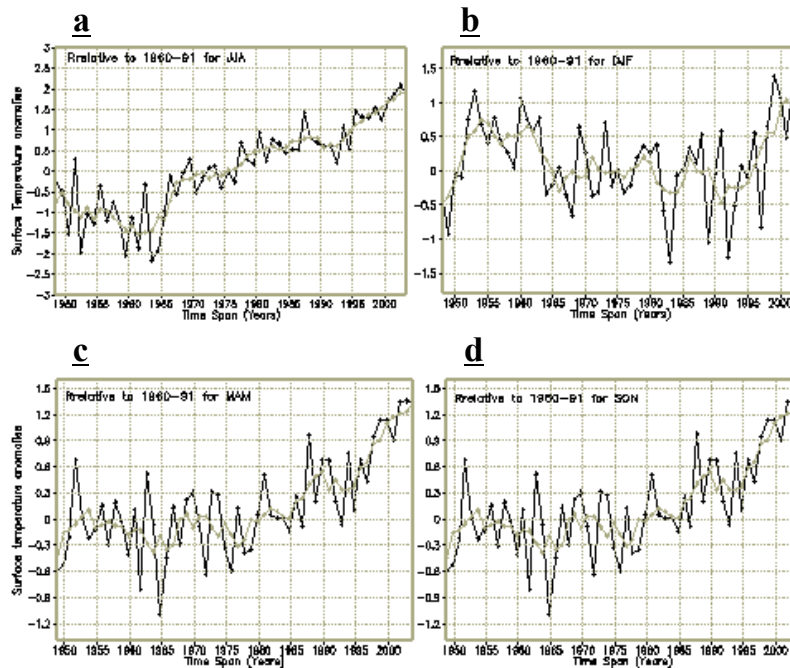


Figure 4.7: As figure 4.6 but averaged over box-area A.

4.3.3 MEAN SEA LEVEL PRESSURE

Variability of MSLP calculated from NCEP reanalysis data over the period 1950 to 2000 for the four seasons DJF, MAM, JJA and SON were spatially averaged over both the entire domain of figure 4.4 and the box-area **A** in figure 4.4. Figures 4.8 (a), (b), (c) and (d) illustrate the weighted average time series of observed MSLP anomalies (hPa) for the four seasons as calculated over the entire domain of figure 4.4. The gray lines represent five-year moving averages. Similarly, figures 4.9 (a), (b), (c) and (d) give the weighted average anomalies as calculated over the box-area **A**.

The MSLP during JJA (figure 4.9(a)) as well as in many of the other figures in 4.8 and 4.9 experienced a profound sink for the subsequent 10 years following 1954. It is interesting to compare this episode with rainfall in figure 4.5. During the same period Eritrea experienced persistent wet conditions. Higher rainfall is normally associated with a drop in MSLP since lower pressures is an indication of instability in the atmosphere. The MSLP anomalies do not show any significant trend, although it appears that MSLPs increased since the 1970s, but stabilized to a great extent thereafter.

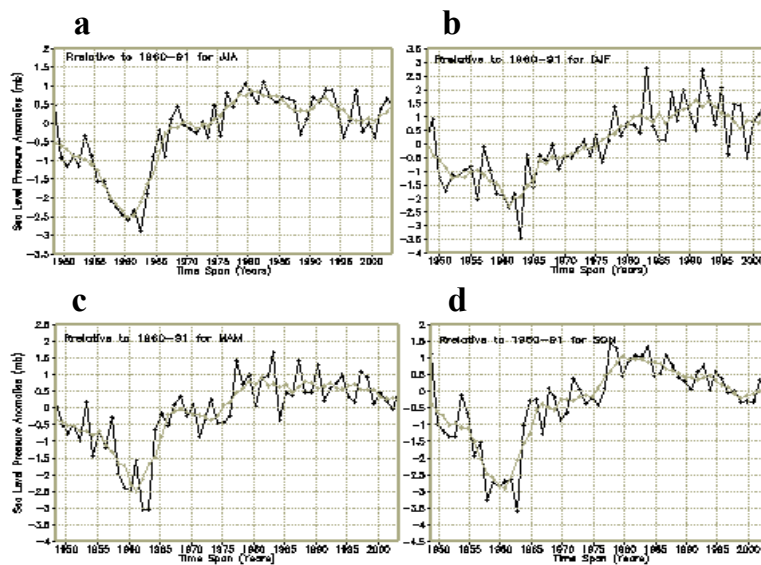


Figure 4.8: Weighted average time series (1950 to 2000) of Mean Sea Level Pressure (MSLP) anomalies (hPa) as calculated from NCEP reanalysis data for the seasons (a) JJA, (b) DJF, (c) MAM and (d) SON and the entire domain of figure 4.4. Gray lines denote five-year moving averages.

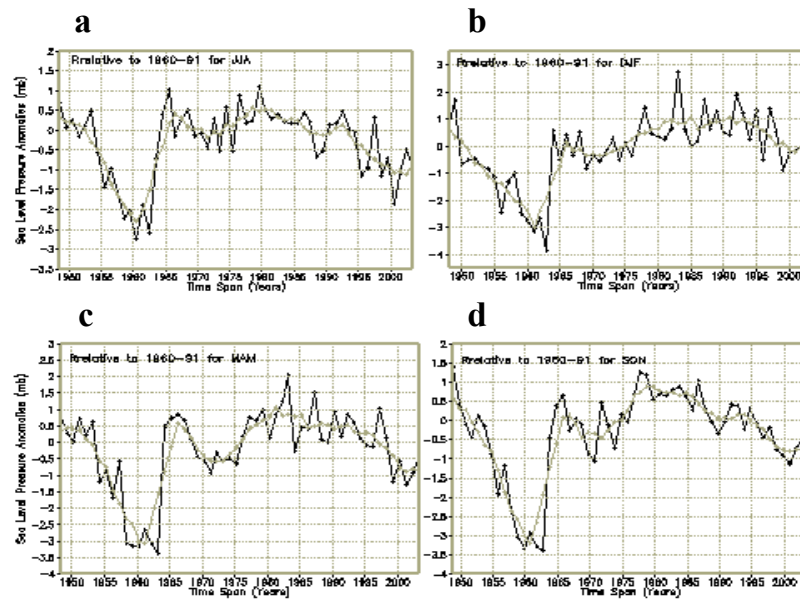


Figure 4.9: As figure 4.8 but averaged over box-area A.

4.4 DROUGHT EVENTS

Recent and present climate records of sub-Saharan Africa, and more particularly Eritrea, show frequent drought events that might be associated with the ENSO phenomenon. This section explores possible atmospheric mechanisms that might have led to these dry episodes.

4.4.1 BACKGROUND

There is strong evidence that the 16th and 18th centuries were generally wetter in the Soudano-Sahelian region than more recent decades, although drought episodes occurred in the 1680s and in the early to mid 18th century from 1738 to 1756 (Nicholson, 1981). Since then droughts became more frequent and more severe, particularly in the early 19th century (1800s to 1830s) and throughout the 20th century. In more recent decades trends pointed towards increasing arid conditions over large parts of Africa, which suggest that temperatures may have increased (Bradley, 1991).

The present climate of Sub-Saharan Africa is dominated by frequent drought events, which appear on the inter-annual and perhaps inter-decadal time scale. Drought is regarded a natural disaster that inflicts severe damage to ecosystems

and society in Africa. Despite many efforts to determine the driving mechanisms that cause droughts, scientists are still not sure whether more recent drought episodes evolve from natural forcing, such as ENSO, or from greenhouse warming.

4.4.2 PROPOSED DROUGHT MECHANISMS

Many researchers showed interest in the mechanisms that drove the persistent drought episodes that occurred in the Sahel-Sahara region over the last two decades. A general feeling is that these drought episodes might follow from a combined forcing from both natural and anthropogenic influences.

Charney (1975) attempted to relate the droughts in the Sahel region to biogeophysical feedback mechanism. According to his hypothesis the clearance of vegetation cover due to human activities, such as overgrazing, lead to an enhanced albedo. A higher albedo leads to a smaller fraction of radiation that is absorbed by the surface of the Earth, which in turn reduces heat and instability of the near-surface atmosphere. These conditions will result in higher pressures, increased subsidence and even dryer conditions. Walker and Rowntree (1977) emphasized the importance of soil moisture to the climate system and hypothesized that once the soil of a region gets wet, it produces a feedback to the atmosphere and biosphere for several weeks in advance. Nevertheless, initial sustained aridity and ground dryness alone could cause a desert to persist. As an extension of the research by Charney (1975), Cunnington and Rowntree (1986) indicated that any decrease in adiabatic heating, weather due to a reduced albedo or increased moisture availability, should lead to less instability and obviously less buoyancy. Rainfall will only appear if the lower atmosphere has enough energy to push the air upwards across the condensation level and higher. Reduced surface temperatures and adiabatic cooling might therefore lead to less rainfall.

Changes in synoptic and smaller scale atmospheric circulation patterns are also playing an important role in sustaining or suppressing conditions for persistent droughts. For example, the southward migration of the subsidence band of the Hadley cells in the subtropics promotes dry condition (Nicholson, 1886; 1991; Nicholson and Flohn, (1980). Nicholson (1983) suggested that the relative position of the ITCZ might modulate rainfall fluctuations (especially droughts). Similarly, Lamb (1978) and Foland *et al.* (1986) suggested that the gradual

infringement of the Saharan desert, which might be caused by regional or synoptic forcing, appears to be substantially influenced a southerly shift of the ITCZ. Owen and Folland (1988) indicated that global SST fluctuations were instrumental for initiating the humid 1950s and dry 1984s of the Sahel. Druyan and Hastenrath (1990) proposed that southward expansion of the mid-tropospheric jet might be the symptom of summer drought in the region.

CHAPTER 5

FUTURE CLIMATE PROJECTIONS FOR ERITREA FROM GCM SIMULATIONS

5.1 INTRODUCTION

A variety of paleoclimate, present and future simulations performed by GCMs intended to address the likelihood positive or negative trends in temperature and precipitation variability. At present there exists a general global inter-model consistency of possible changes as a result of greenhouse warming. Despite of an increase in global temperatures, diurnal temperature variability might likely decrease owing to a reduction in the latitudinal temperature gradient. Precipitation might increase owing to more evaporation (Mitchell, 1991; Rind, 1991). In some areas of the world the moisture content of the atmosphere might also increase without any noticeable changes in rainfall totals (Rind, 1991). The response of the general circulation of the atmosphere will obviously determine which areas might become drier and which areas might expect higher rainfall.

The objective of this chapter is to explore temperature and rainfall responses for the months January and July to model simulated climate change projections over the domain defined in figure 4.4, but with specific emphasis on the Eritrea sub-domain. Firstly results from greenhouse simulations from six GCMs used in the Inter-governmental Panel on Climate Change (IPCC) initiative will be analyzed in order to search for inter-model consistency signals in temperature and rainfall simulations. The A2 and B2 scenarios from the Special Report on Emission Scenarios (SRES) will be considered.

5.2 GLOBAL FUTURE CLIMATE CHANGE SIMULATIONS

The logic behind constructing future climate change simulations has been explained in depth in Chapter 9 of the report of the IPCC Working Group 1

(Cubasch, *et al.*, 2001). It is worthwhile to briefly review the basics adopted in this report merely on the basis of contextual relevance and importance.

Studies on projections of possible future climate change use a hierarchy of coupled ocean/atmosphere/sea-ice/land surface models to provide indicators of global response as well as possible regional patterns of climate change. These types of more comprehensive fully coupled global climate models configuration was introduced in the late 1980s and are generally referred to as Atmosphere-Ocean Global Climate Models or Atmosphere-Ocean General Circulation Models (AOGCMs).

These highly sophisticated fully coupled GCMs evolved in such a way that models of the main components (atmosphere, land, ocean and sea ice) were mostly developed separately before they were gradually coupled. Most recently, sulphur cycle components have been incorporated to represent the emissions of sulphur and how they are oxidized to form aerosol particles. Currently in progress is the coupling of the land carbon cycle and ocean carbon cycle. The atmospheric chemistry component currently is modeled outside the climate model. The general trend in the evolution of GCMs development goes with notion of modeling of the Earth's climate system realistically so that all the components can interact and, thus, the predictions of climate change will continuously take into account the effect of feedbacks among components.

Despite these rapid developments in GCMs, it is yet hardly possible to produce accurate future climate change projections as a result of uncertainty. Reliable projections of future climate change as a result of increased greenhouse gas emissions could contribute significantly to early precaution actions, which might facilitate adaptation. Nevertheless, they are the only scientific resources currently available to produce some degree of guidance what might be expected in future climates.

Recently, the IPCC Working Group 1 released its third assessment report, and as part of this initiative prepared future climate change projections for Earth by introducing SRES greenhouse and aerosol forcing to AOGCMS. These SRES scenarios have been constructed to explore the future climate response to estimated greenhouse gas and aerosol precursor emissions. This response was simulated by using the only tool available for this purpose, namely GCMs.

The six GCMs used in the IPCC report are:

1. Canadian Centre for Climate modelling and analysis (CCCma)
2. UK Hadley Centre for climate prediction and Research (HadCM3)
3. Japanese Centre for climate system Research (NIES99)
4. Australian Commonwealth Scientific and Industrial Research Organization (CSIRO)
5. USA Geophysical Fluid Dynamics Laboratory (GFDL99)
6. German Climate Research Centre (ECHAM4)

5.3 GREENHOUSE GASSES AND AEROSOLS EMISSION SCENARIOS

GCMs are used to generate future climate change projections from prescribed atmospheric concentrations of greenhouse gasses and aerosols based upon specific emission scenarios. These forcing agents are the sole inputs to make a suite of projected future climate changes that illustrate the possibilities that might lie ahead.

In 1996, the IPCC began the development of a new set of emissions scenarios, effectively to update and replace the well known IS92 scenarios (figure 5.1). Four different narrative storylines, which are illustrated below, were developed to describe the relationship between emission driving forces and their evolution and to add context for the scenario quantification as obtained from IPCC, WG1 (2001). The SRES scenarios do not include additional climate initiatives, which means that no scenarios are included that explicitly assuming implementation of the emissions targets of the Kyoto Protocol. However, greenhouse emissions are directly affected by non-climate change policies designed for a wide range of other purposes. Further more, government policies can, to varying degrees, influence the greenhouse gas emission drivers and this influence is broadly reflected in the storylines and resulting scenarios. In this chapter, as noted earlier, the six GCM projections that emanate from the A2 and B2 SRES scenarios are explored. The SRES scenarios are illustrated in figure 5.1.

The A1 SRES scenario describes a future world of very rapid economic growth, global population that peaks in mid-century and declines thereafter, and the rapid introduction of new and more efficient technologies. Major underlying the themes

are convergence among regions, capacity building and increased cultural and social interactions, with a substantial reduction in regional differences in per capita income. The A1 SRES scenario family develops into three groups that describe alternative directions of technological change in the energy system. The three A1 groups are distinguished by their technological emphasis: fossil intensive (A1F1), non-fossil energy sources (A1T), or a balance across all sources (A1B) (where balanced is defined as not relying too heavily on one particular energy source, on the assumption that similar improvements rates apply to all energy supply and end use technologies).

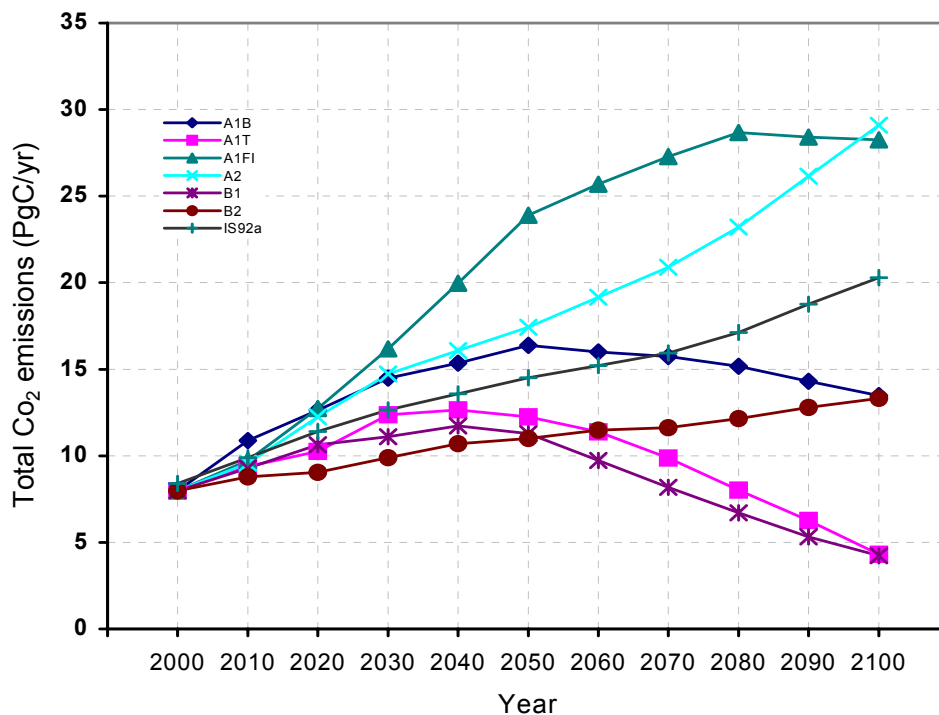


Figure 5.1: Anthropogenic emission projections of CO₂ for the six SRES scenarios, A1B, A2, B1 and B2, A1F1 and A1T plus the updated and replaced well known the IS92a scenario as obtained from the IPCC Special Report on Emissions Scenarios (SRES) dataset (appendix II).

The A2 SRES scenario describes a very heterogeneous world. The Underlying them is self-reliance and preservation of local identities. Fertility patterns over regions converge very slowly, which results in continuously increasing population. Economic development is primarily regionally oriented and per capita economic

growth and technological change are more fragmented and slower than in other storylines.

The B1 SRES scenario describe a convergent world with the same global population, that peaks in mid-century and declines thereafter, as in the A2 storyline, but with rapid change in economic structures toward services and information economy, with reductions in material intensity and the introduction of clean and resource-efficient technologies. The emphasis is on global solutions to economic, social and environmental sustainability, including improved equity, but without additional climate initiatives.

The B2 SRES scenario describes a world in which the emphasis is on local solutions to economic, social and environmental sustainability. It is a world with continuously increasing global population, at a rate lower than A2, intermediate levels of economic development, and less rapid and more diverse technological change than in the B1 and A1 storylines. While the scenario is also oriented towards environmental protection and social equity, it focuses on local and regional levels.

5.4 IPCC GCM CLIMATE PROJECTIONS FOR ERITREA

IPCC GCM future climate projections of air temperature and precipitation rate (daily rainfall) relative to the base-line climatology (1961-1990) for January and July are investigated. The investigation explores projected changes for the 2080s with the A2 and B2 SRES scenarios. The domain under investigation is indicated in figure 4.4 with emphasis on the Eritrea sub-domain (shaded region in figure 4.4). The objective is to measure the aerial extent of the projected change and to explore if there exists inter-model consistency among the GCMs. High level of inter-model agreement gives an indication of the higher probability of the event to occur ahead and narrowing the range of uncertainty posed by both the natural randomness of the climate system and model physics (architecture) where the former uncertainty can only be quantified here.

The methodology followed to extract the statistical summaries of the projected climate changes from the Eritrea sub-region (denoted with letter “A” in the subsequent GCM maps) was done in two-steps. Firstly the coarse GCM boxes were replicated or regirded to finer grid boxes to suit the extraction along the

borders. Secondly the statistical summary was extracted from region “A” by masking out the remaining data. The scheme generates grid boxes based upon the original coarse grid box and broadcasts its value to the offsprings. In other words, the algorithm duplicates the coarse grid box into finer grid boxes with out sharing information from the adjacent grid boxes. For more information consult the “EXPAND” module in IDRISI software. The idea was to avoid additional uncertainty associated with interpolation. The GCM maps presented in the subsequent sections are, however, in their original resolution.

5.4.1 IPCC SIMULATED CLIMATE CHANGE SCENARIOS FOR JULY

5.4.1.1 AVERAGE NEAR-SURFACE TEMPERATURE PROJECTIONS

A2 and B2 SRES scenarios GCM projections of near-surface temperature for the 2080s as simulated by the six IPCC GCMs over the domain in figure 4.4 for July are illustrated in figures 5.2 and 5.3, respectively. Owing to the coarse resolution of the GCMs, no detail is available for Eritrea. However, averages of grid boxes that cover Eritrea were considered in the analysis that follows.

All the GCM projections showed above baseline near-surface temperature projections for 2080s for the whole domain with slight differences in the spatial distribution in both SRES scenarios. Accordingly, the HadCM3, CCCma, CSIRO, ECHAM4, GFDL99 and NIES99 GCMs project signals of near-surface temperature enhancement for the A2 and B2 SRES scenarios (figures 5.2 and 5.3). As shown in figure 5.4, there exists strong inter model consistency for near-surface temperatures among the GCMs. The NIES99 GCM simulated the smallest signal of A2 (+1.59 °C) and B2 (+0.92 °C).

The spatially averaged GCM near-surface temperature departures for Eritrea are in the order of +3.39 °C and +2.24 °C for the A2 and B2 SRES scenarios, respectively (figure 5.4(a)). The spatially averaged minimum (figure 5.4(b)) and maximum (figure 5.4(c)) values for Eritrea are in the range of +2.68°C and +4.3°C for the A2 SRES scenario, and +1.77°C and +2.99°C for the B2 SRES scenario. These two figures indicate the range of change fields in the considered sub-domain, i.e., figure 5.4(b) captures a grid box with the minimum value while figure 5.4(c) a grid box with the maximum value.

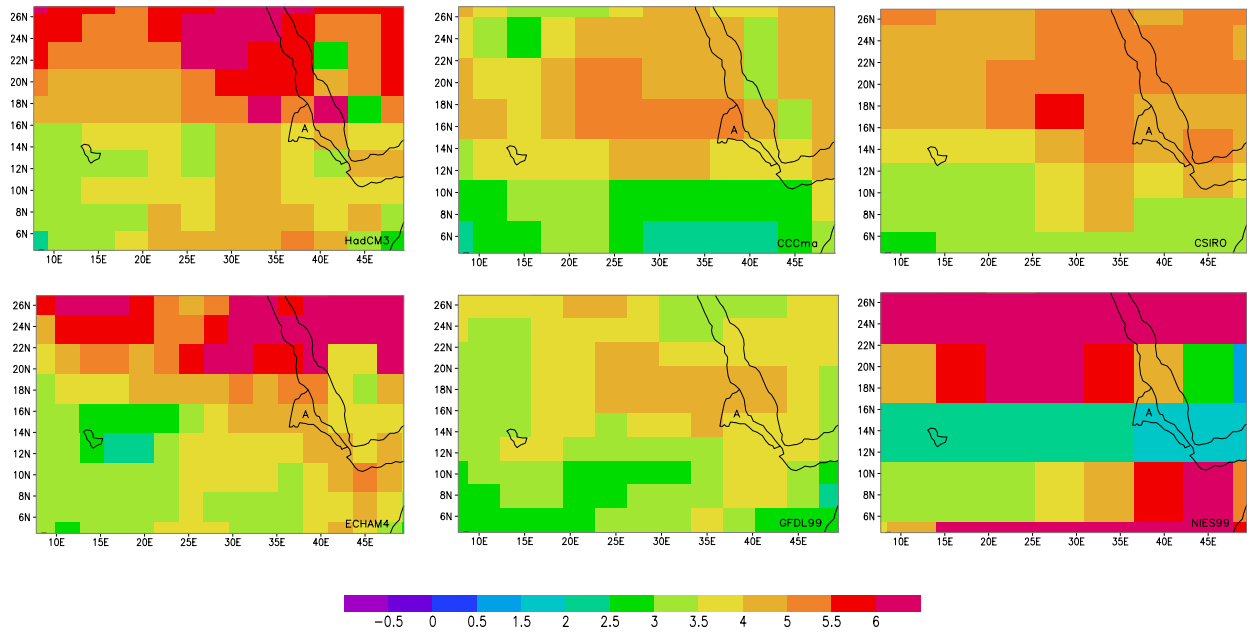


Figure 5.2: July near-surface temperature ($^{\circ}\text{C}$) projections for the 2080s relative to 1961-90 for the six IPCC GCMs (indicated in the right bottom of each plot) for the A2 SRES scenario. Eritrea is indicated in letter "A".

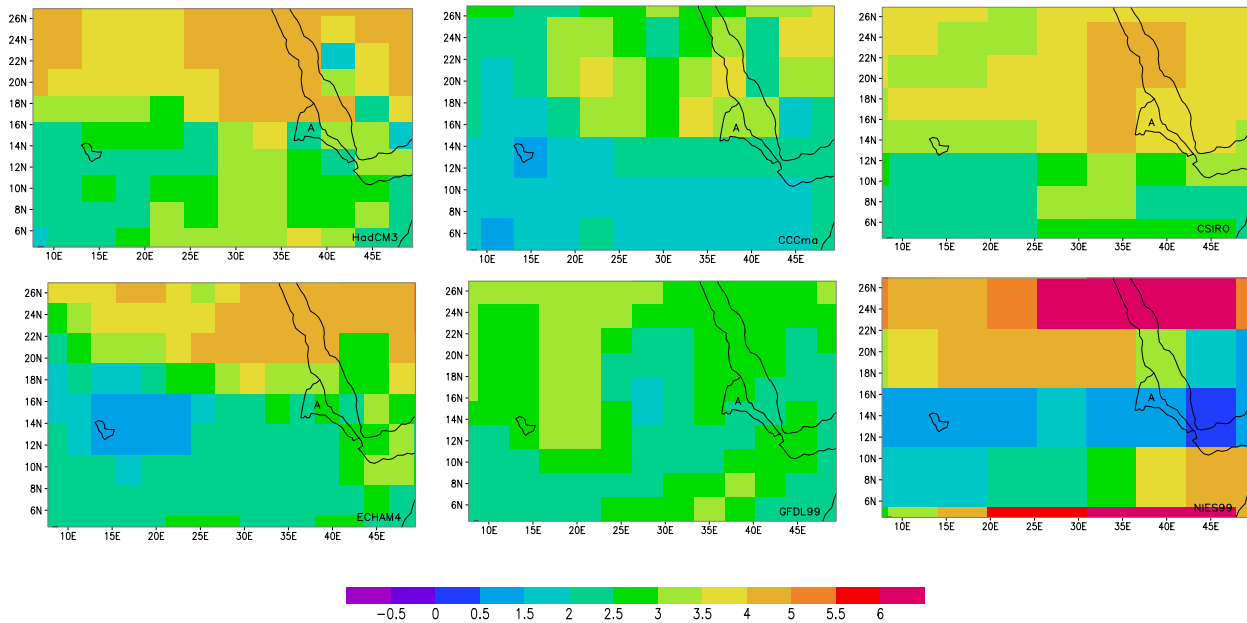


Figure 5.3: As figure 5.2 but for the B2 SRES scenario

This section indicates, according to the GCMs, that there exists a good possibility for warmer near-surface conditions during July in 2080s for Eritrea, with a 100% spatial coverage of positive anomalies (figure 5.4(d)).

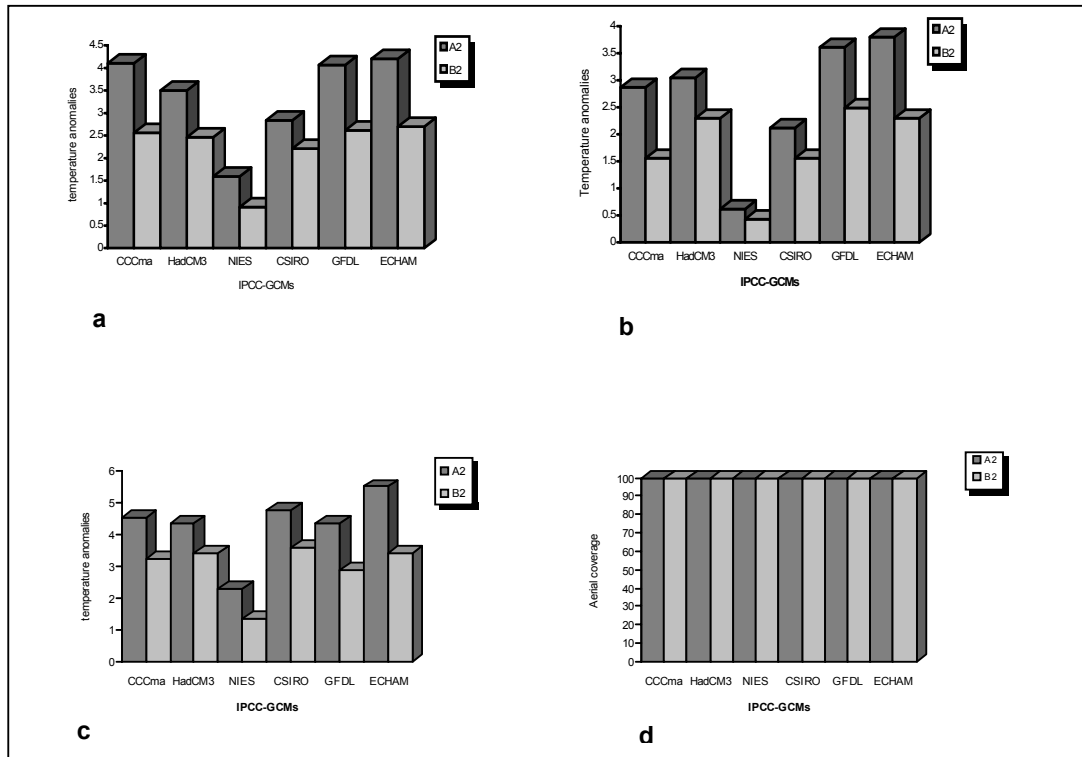


Figure 5.4: Spatially averaged near-surface temperature ($^{\circ}\text{C}$) projections for July 2080s for the A2 and B2 SRES scenarios over the Eritrea domain. The graphs denote spatial (a) averages, (b) minimum, (c) maximum and (d) aerial coverage (%) of positive anomalies of near-surface temperatures.

5.4.1.2 AVERAGE RAINFALL PROJECTIONS

Precipitation rate projections in $\text{mm}\cdot\text{day}^{-1}$ for the 2080s as simulated by the six IPCC GCMs with the A2 and B2 SRES scenarios for July are illustrated in figures 5.5 and 5.6, respectively. Again, due to the coarse grid resolution no detail is available for Eritrea.

Unlike the consistent above-baseline near-surface temperature projections, mixed signals of above and below baseline rainfall appear in the GCM projections. Note

that according to most IPCC GCMs large parts may expect drier condition comparing to present climate. The CSIRO and CCCma GCMs, in particular, simulated a rainfall decrease over most of the region under both SRES scenarios. According to grid boxes that cover Eritrea the majority of IPCC GCMs indicate a general increase of rainfall over Eritrea. That is in contrast to the bias towards drier conditions over the complete domain. In this regard, the HadCM3, ECHAM4, GFDL99 and NIES99 simulated wetter condition for Eritrea, while the remaining two GCMs (CCCma and CSIRO) simulated relatively drier conditions in comparison to the present climate. Despite of the wetter conditions projected by the majority of IPCC GCMs, mixed signal occur that imply a lack of inter model consistency amongst the IPCC GCMs as illustrated in figure 5.7. This poses uncertainty on what to expect in rainfall totals over the coming decades.

The spatial averaged GCM rainfall departures for Eritrea are in the order of $+0.4 \text{ mm. day}^{-1}$ and $+0.5 \text{ mm.day}^{-1}$ for the A2 and B2 SRES scenarios, respectively (figure 5.7(a)). The spatially averaged, minimum (figure 5.7(b)) and maximum (figure 5.7(c)) values for Eritrea are in the range of -0.6 mm.day^{-1} and $+1.6 \text{ mm.day}^{-1}$ for the A2, and -0.5 mm day^{-1} and $+1.8 \text{ mm day}^{-1}$ for the B2 SRES scenarios.

Generally, the analysis shows that one might expect an increase in rainfall for July in the 2080s for the Eritrea, with mixed signals where the CSIRO GCM simulated the smallest percentage of wetter grid boxes (17.6%) while the HadCM3 and NIES99 with 100% wetter grid boxes (figure 5.7(d)).

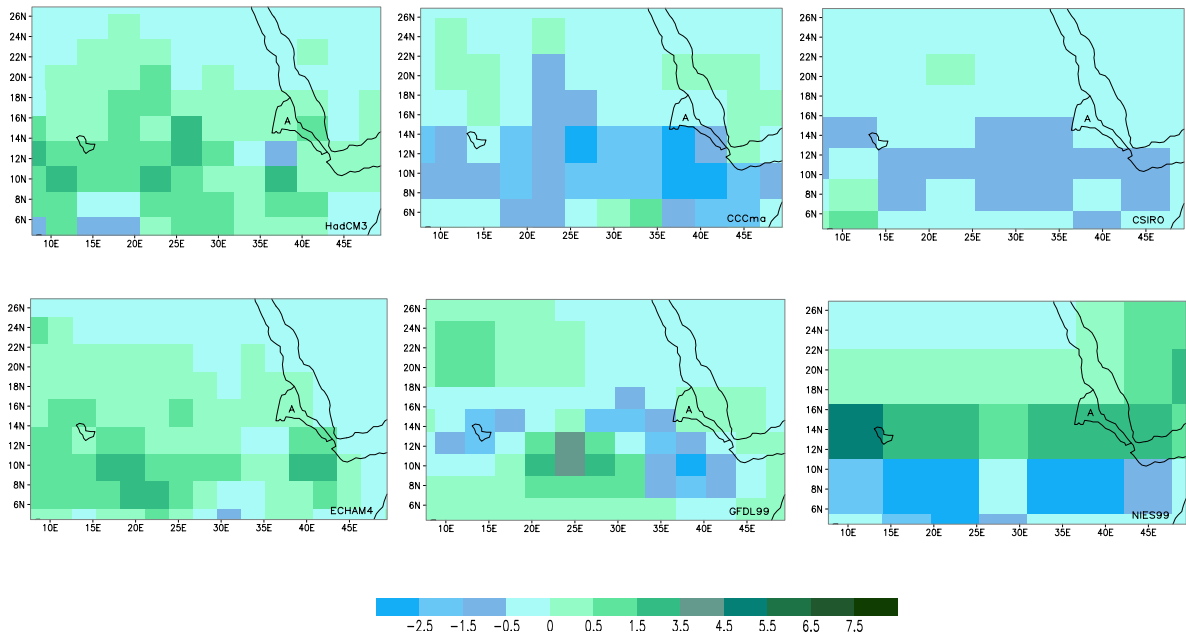


Figure 5.5: July rainfall ($\text{mm}\cdot\text{day}^{-1}$) projections for the 2080s relative to 1961-91 for the six IPCC GCMs (indicated in the right bottom of each plot) for A2 SRES scenario. Eritrea is indicated in letter "A".

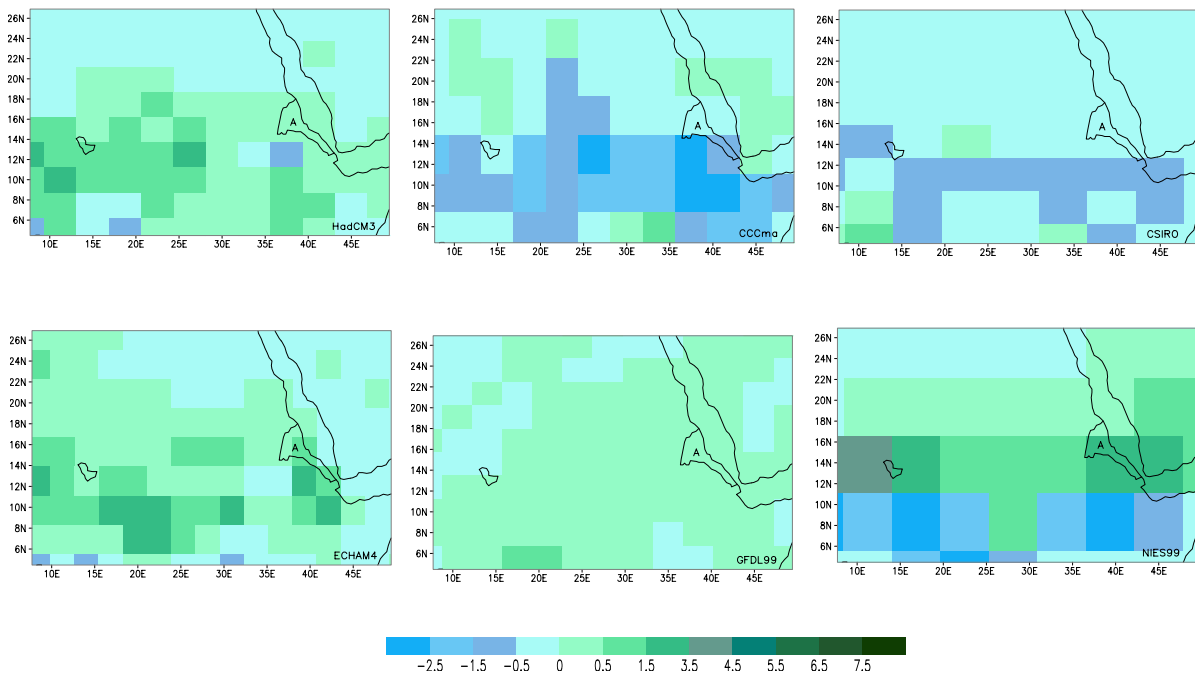


Figure 5.6: As figure 5.5 but for the B2 SRES scenario

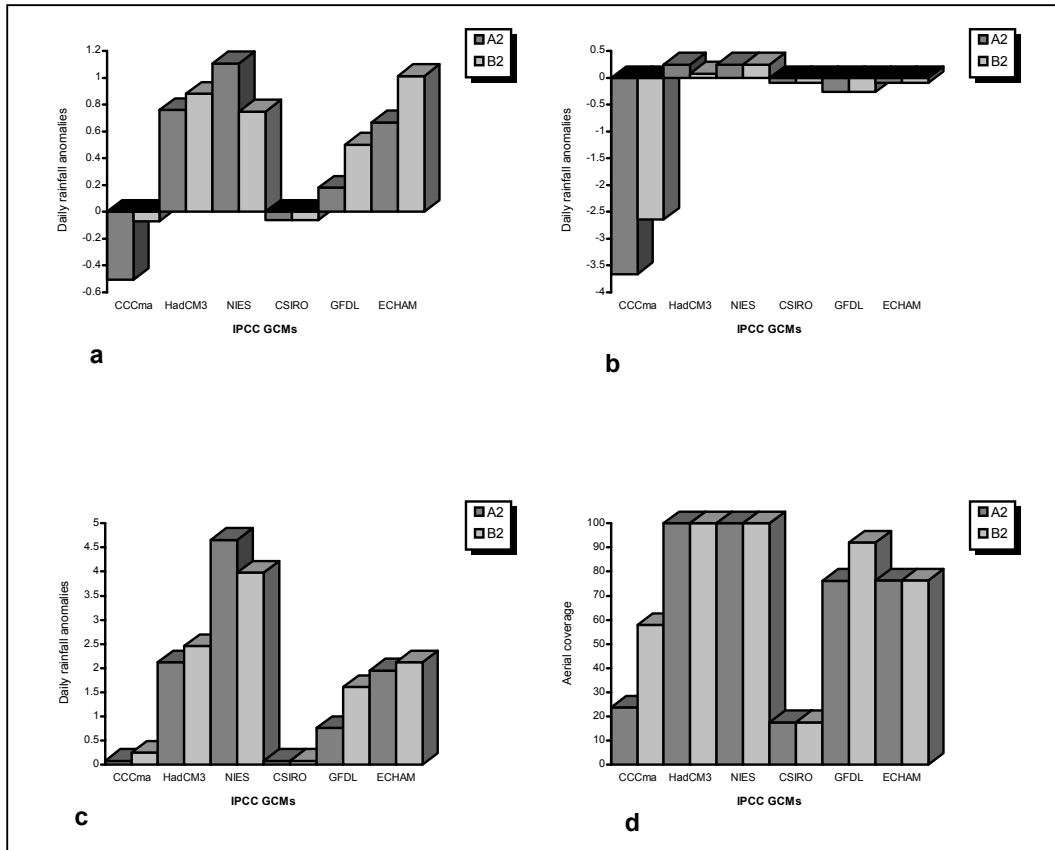


Figure 5.7: Spatially averaged rainfall (mm day⁻¹) projections for July 2080s for the A2 and B2 SRES scenarios over the Eritrean domain. The graphs denote spatial (a) averages, (b) minimum, (c) maximum and (d) aerial coverage (%) of positive anomalies of rainfall.

5.4.2 IPCC SIMULATED CLIMATE CHANGE SCENARIOS FOR JANUARY

5.4.2.1 AVERAGE NEAR-SURFACE TEMPERATURE PROJECTIONS

A2 and B2 SRES scenarios GCM projections of near-surface temperature for the 2080s as simulated by the six IPCC GCMs over the domain in figure 4.4 for January are illustrated in figures 5.8 and 5.9, respectively.

In agreement with the July simulations, above baseline near-surface temperature departures are generated for the 2080s. The spatial distribution of the projections, however, is less uniform than for July. When the whole domain is considered, the

GCMs captured locations of maximum near-surface temperature enhancement differently. The CCCma, for instance, simulated maximum near-surface temperature values over the western section, the ECHAM4 and GFDL99 over the southern section, while the CSIRO produce maximum values over the northern section of the domain. Nevertheless, apart from differences in magnitude, there is a plausible spatial agreement between all GCM simulations forced by the two SRES scenarios (A2 and B2).

The possibility that one might expect warmer January near-surface temperatures over Eritrea in the 2080s are simulated for both the A2 and B2 SRES scenarios (figure 5.10). Interesting to note is that there appear to be a stronger inter model consistency in average near-surface temperature projections compared to the July simulations (figure 5.4(a)) because of the comparable signal captured by NIES99 i.e., 4.42°C (A2 SRES scenario) and 3.38°C (B2 SRES scenario).

The spatial averaged GCM near-surface temperature departures for Eritrea are in the order of +3.9°C and +3.1°C for the A2 and B2 SRES scenarios, respectively (figure 5.10(a)). The spatially averaged minimum (figure 5.10(b)) and maximum (figure 5.10(c)) values for Eritrea are in the range of +3.4°C and +4.7°C for the A2, and +2.6°C and +3.8°C for the B2 SRES scenarios.

In general, the analysis concludes that one might expect an increase in the trend of January near-surface temperatures towards the 2080s over the Eritrea sub domain with a 100% spatial coverage of positive anomalies (figure 5.10(d)).

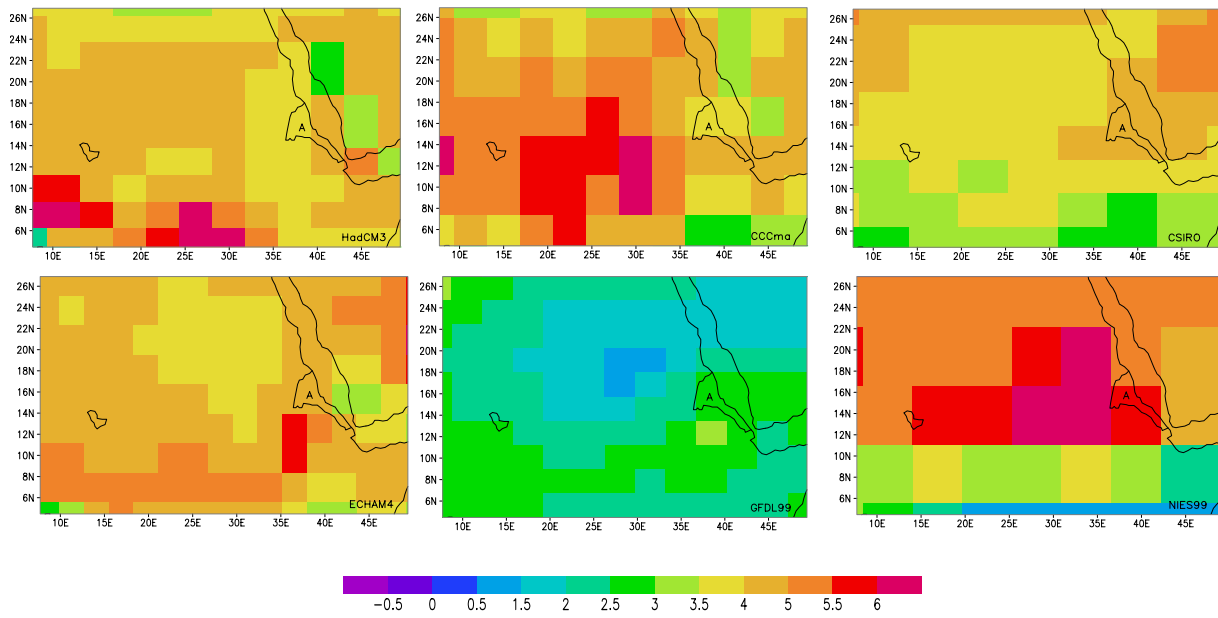


Figure 5.8: January near-surface temperature ($^{\circ}\text{C}$) projections for the 2080s relative to 1961-90 for the six IPCC GCMs (indicated in the right bottom of each plot) for the A2 SRES scenario. Eritrea is indicated in letter "A".

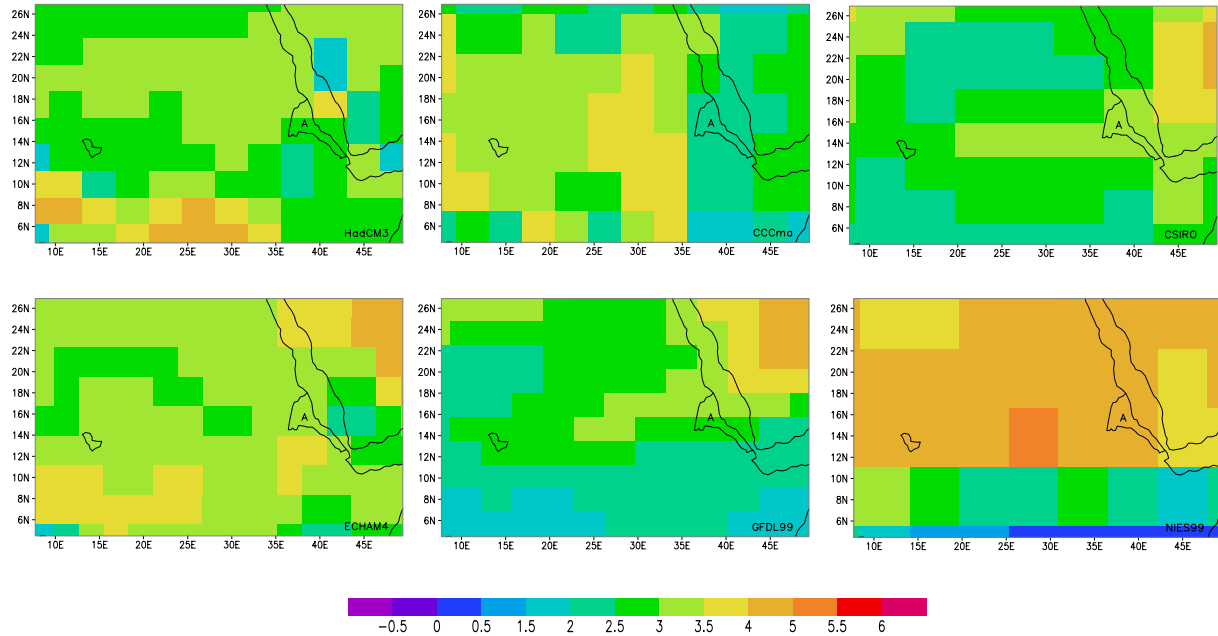


Figure 5.9: As figure 5.8 but for the B2 SRES scenario

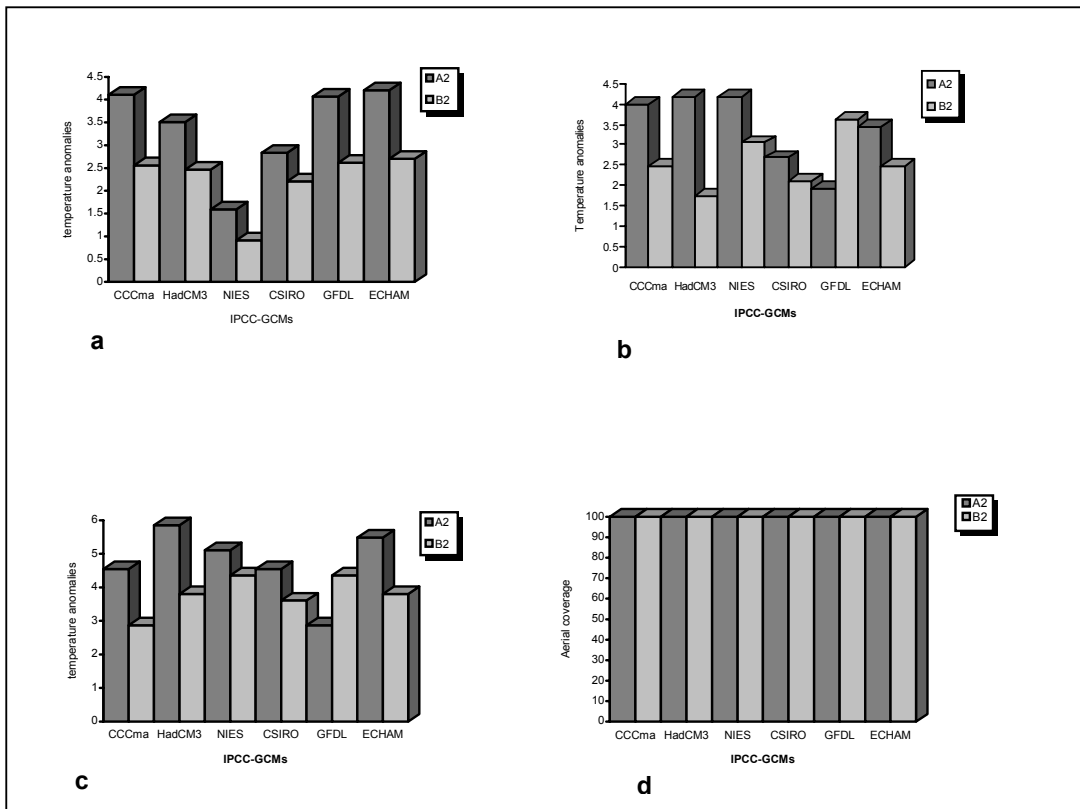


Figure 5.10: Spatially averaged near-surface temperature ($^{\circ}\text{C}$) projections for January 2080s for the A2 and B2 SRES scenarios over the Eritrea domain. The graphs denote spatial (a) averages, (b) minimum, (c) maximum and (d) aerial coverage (%) of positive anomalies of near-surface temperatures.

5.4.2.2 AVERAGE RAINFALL PROJECTIONS

Precipitation rate projections in $\text{mm}\cdot\text{day}^{-1}$ for the 2080s as simulated by of the six IPCC GCMs with the A2 and B2 SRES scenarios for January are illustrated in figures 5.11 and 5.12, respectively.

The projected January rainfall departures should be viewed from the perspective of observed regional rainfall behavior. During January, most of the region experiences dry condition (Boreal winter) and thus any projected changes by the IPCC GCMs on non-rainfall parts can only be a fluke. Some parts of the domain, however, receives rainfall associated with tropical circulation (the southern

extreme) or with regional disturbances (Ethiopia and eastern section of Eritrea) and thus, the analysis only focus on these regions.

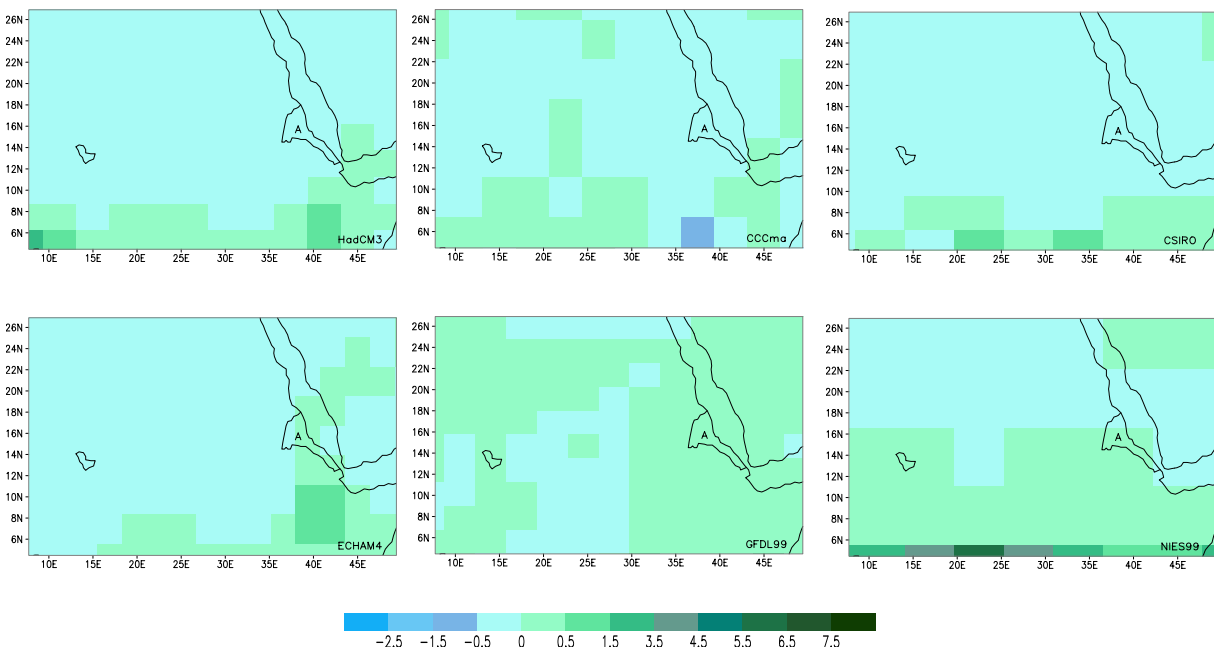


Figure 5.11: January rainfall (mm.day⁻¹) projections for the 2080s relative to 1961-91 for the six IPCC GCMs (indicated in the right bottom of each plot) for A2 SRES scenario. Eritrea is indicated in letter "A".

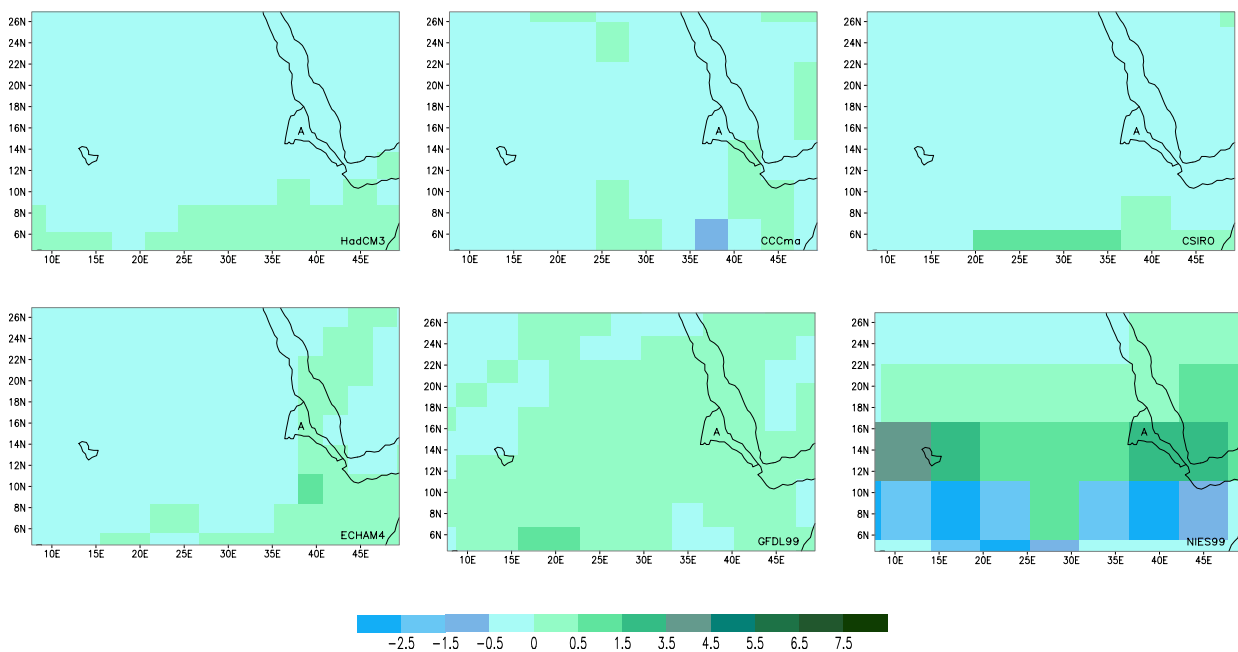


Figure 5.12: As figure 5.11 but for the B2 SRES scenario

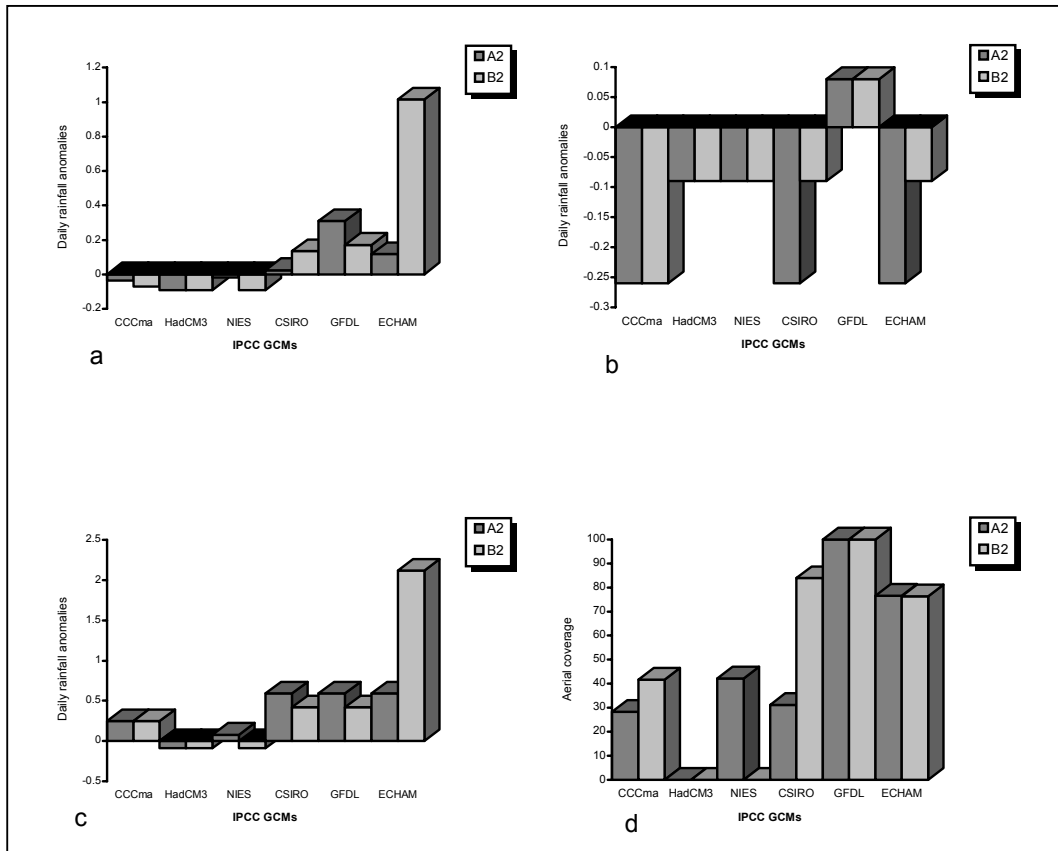


Figure 5.13: Spatially averaged rainfall (mm day⁻¹) projections for January 2080s for the A2 and B2 SRES scenarios over the Eritrean domain. The graphs denote spatial (a) averages, (b) minimum, (c) maximum and (d) aerial coverage (%) of positive anomalies of rainfall.

Similar to the July climate projections, the January rainfall projections are also associated with a great extent of uncertainty. This is again attributed to mixed signals of projected rainfall distribution amongst IPCC GCM simulations. The majority of GCMs (ECHAM4, NIES99, CSIRO and CCCma) show an increase in rainfall for both SRES scenarios. The GFDL99 simulated wetter conditions for the B2 SRES scenario, although a decrease in rainfall appear over the southwestern section of the domain for the A2 SRESS scenario. The HadCM3 simulated drier conditions over most of the domain for both the A2 and B2 SRES scenarios.

January precipitation projections for the 2080s for the considered scenarios over the Eritrea sub domain is regarded as uncertain since most of area under investigation is located in the summer rainfall region. For this reason, the January (presently dry winter) grid box values should be scrutinized with caution when constructing the histograms in figure 5.13.

CHAPTER 6

CLIMATE CHANGE SIMULATIONS USING THE PRECIS REGIONAL CLIMATE MODEL SYSTEM

6.1 INTRODUCTION

Assessing the impact of climate change on the biosphere, and in particular on society, is important for developing mitigation or adaptation strategies. The response of climate to greenhouse warming is based upon estimated scenarios that are generated by GCMs. Unfortunately GCM results are the only projected climate change information available, and impact assessment exercises often use results as basis for conclusions. Apart from the great extent of uncertainty in GCM simulations of certain variables, it also provides information on fairly coarse resolution. Grid point values, for example, are expressed as the spatial average over areas that cover hundreds of kilometers. Present IPCC GCM climate change projections are therefore lacking local detail that is important for impact studies on national and regional levels. An appropriate option would be to make use of the averaged results from GCMs to drive finer resolution models, such as RCMs, that is nested within the GCM to obtain more spatial detail in climate change projections.

This chapter discusses the current regional-scale climate over the eastern section of the Sahel and its probable future evolution by placing major emphasis on the Eritrean sub-region. The PRECIS RCM system developed by the Hadley Center in the UK was used for this purpose.

6.2 MODEL DESCRIPTION

The PRECIS RCM system is a fine resolution atmospheric and land surface model that may be nested over a limited area in a GCM. Dynamical flow, clouds and precipitation formation, radiation processes, land surface and deep soil characteristics are all included in the model. The PRECIS RCM system incorporates the current version of the HadRM3H RCM, which has similar dynamics and physics

employed by the HadCM3 GCM. Both the RCM and GCM employ identical representations of both the grid scale dynamics and the sub-grid physics. In this way the RCM produces high-resolution simulations for a defined region, which are consistent with the large-scale simulation of the GCM.

The atmospheric component of the PRECIS RCM system is a hydrostatic version of the full primitive equations, i.e. vertical acceleration in the atmosphere is assumed to be small of hydrostatic equilibrium and hence vertical motions are diagnosed separately from the equations of state. It has a complete representation of the Coriolis force and employs a regular latitude-longitude grid in the horizontal and a hybrid vertical coordinate. A terrain following σ -coordinate (σ =pressure/surface pressure) is considered at the lower four levels with purely pressure coordinates at the top three levels. A hybrid of these two coordinates is used between these upper and lower levels. The model has 19 vertical levels in the atmosphere (from the surface to 30 km in the stratosphere = 0.5 hPa) and four levels in the soil. The model equations are solved in a spherical polar coordinates and the latitude-longitude grid is rotated so that the equator lies inside the region of interest in order to obtain quasi-uniform grid box area throughout the region.

The PRECES RCM system can run at two different horizontal resolutions, namely a $0.44^\circ \times 0.44^\circ$ and a $0.22^\circ \times 0.22^\circ$ resolution (giving grid boxes of approximately 50km x 50km and 25km x 25km, respectively). Whilst a more realistic land-sea mask and fine scale detail is expected at 25km resolution, the time to complete such a simulation will take approximately six times longer than the time to complete a 50km resolution run over the same area. Two thirds of the increase in simulation time is attributed to a fourfold increase in the number of grid points, and the rest from taking a smaller time step. The time step associated with the physical parameterization in the model remains the same (five minutes) for both resolutions to maintain numerical stability.

The HadRM3H (PRECIS) RCM requires prescribed surface and lateral boundary conditions. For present-day simulations surface boundary conditions are only required over water, where the model needs time series of SSTs and sea-ice. Observed SST and sea-ice (on a $1^\circ \times 1^\circ$ grid) data are used with an atmosphere-only present-day GCM simulation that generates output that serves as lateral boundary conditions for the RCM present-day simulation. For future climate change simulations

SSTs and sea-ice obtained from a coupled GCM simulation are used to provide the lower boundary forcing for the atmospheric GCM and RCM simulations. There is no prescribed constraint at the upper boundary of the RCM. The lateral boundary conditions comprise the standard atmospheric variables of MSLP, horizontal wind components, temperature and humidity. Since certain configurations of the HadRM3H RCM contain a full representation of the sulphur cycle, boundary conditions for sulphur dioxide, sulphate aerosols and associated chemical species are also required. The lateral boundary conditions are updated every 6 hours, while surface boundary conditions are updated once a day. The model uses a relaxation method (Davies and Turner, 1977) that is implemented across a four-point buffer zone at each level in the vertical. Values in the HadRM3H RCM are relaxed towards the values interpolated in time from data saved every 6 hours from the GCM integration (Jones *et al.*, 2001; Wilson *et al.*, 2003).

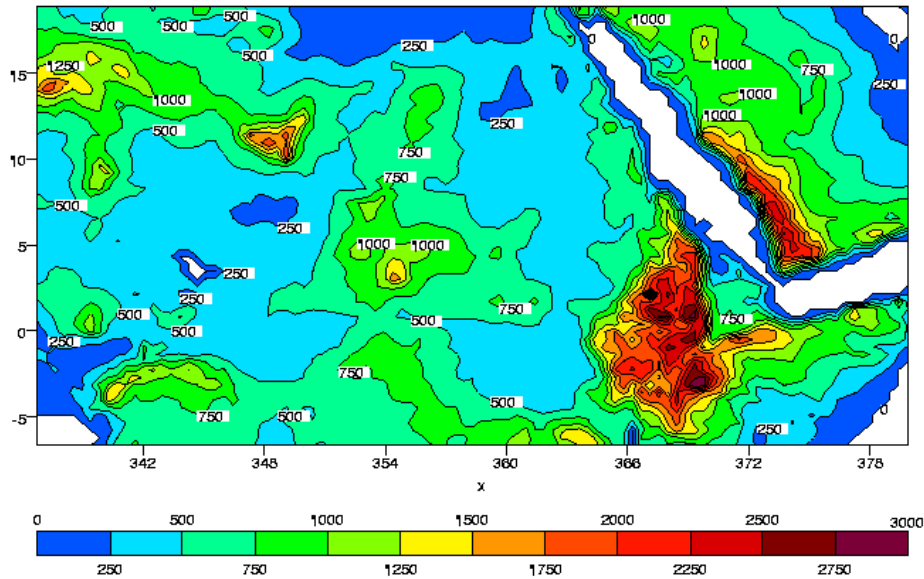
6.3 EXPERIMENTAL DESIGN

6.3.1 MODEL DOMAIN AND CONFIGURATION

The PRECIS RCM system is employed to generate regional-scale simulations over the model domain spanning from about 5°N to 51°N and 2.5°E to 28°E (figure 6.1(a)). This domain includes the Sahara desert, sub-Saharan Africa, the Red Sea region, the Gulf of Aden and a part of the Middle East.

The model domain was optimally expanded for reasons of model stability by considering the inherent dynamics of the region as detailed in chapter 4, i.e., in order to allow for the full development of internal mesoscale circulation patterns and to capture relevant regional forcing. To address this issue, three one month runs were performed with different model domain size as explained in Jones *et al.* (2001). The output maps are, however, not presented here for reasons of redundancy concerns. An attempt was also made to place the boundaries away from complex topography (figure 6.1(a)), particularly over the southern region where the Eastern Africa steep mountains occur. This was done to avoid noise due to the mismatch between the coarse resolution driving data and the high-resolution model topography. Despite the large domain, the study will focus on sub-Saharan Africa with emphasis on the Eritrea sub-domain.

(a)



(b)

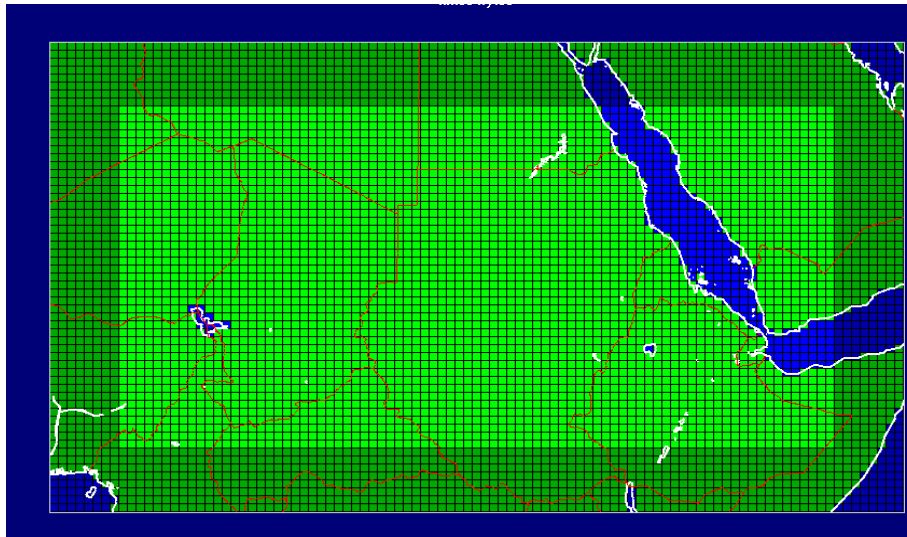


Figure 6.1: The figures illustrate the PRECIS RSM system model topography (a) in meters and model domain (b) with the grid resolution of $0.44^\circ \times 0.44^\circ$.

In this experiment, the model was configured to operate at a spatial resolution of $0.44^\circ \times 0.44^\circ$ and 13 horizontal levels in the vertical. Output was collected at the 1000, 900, 850, 800, 700, 600, 500, 400, 300, 250, 200, 100 and 50 hPa pressure levels. Only selected diagnostics are, however, available on these levels. The

remaining diagnostics are available at different levels related to the hybrid coordinate levels described in the previous Section.

The HadRM3H RCM requires at least one year for a spin-up period to bring the moisture and temperature fields in the deep soil in equilibrium with the atmospheric forcing. Data from the spin-up period is excluded from the analysis in this chapter.

6.3.2 PRESENT CLIMATE SIMULATION

A 31-year simulation (1960-1990) was completed with the PRECIS RCM system as baseline or control simulation. The one year (1960) simulation was considered a spin-up period. Results from a global simulation generated by the HadAM3H (atmosphere only) GCM were prescribed as boundary input to the PRECIS RCM system. In the HadAM3H GCM simulations observed SSTs and sea-ice input of the HadISST data series (1960-1990) were prescribed as lower boundary forcing.

The observed evolution of greenhouse gases over this period of 31-years was used to provide relevant information on atmospheric composition. In addition the observed evolution of anthropogenic emissions of sulphur dioxide were prescribed and its evolution and impact on atmospheric composition was simulated within the sulphur cycle component of the HadAM3H GCM, and eventually, the PRECIS RCM system.

6.3.3 Future Climate Simulations

Similar to the baseline simulation the PRECIS RCM was forced by HadAM3H GCM derived boundary conditions. In these simulations the A2 and B2 emission scenarios from the Special Report on Emission Scenarios (SRES), also known as the A2 and B2 SRES scenarios, were considered. The sea surface boundary conditions, however, were derived from changes in SSTs and sea-ice simulated by matching integrations of the coupled ocean-atmosphere HadCM3 GCM. (i.e., using the same emissions scenarios and providing initial conditions to the HadAM3H GCM).

To be more specific, the boundary conditions for the PRECIS RCM system, as detailed by Arnell *et al.* (2003), were derived through a two-stage process from

the HadCM3 GCM which is a coarse resolution ocean-atmosphere general circulation model (AOGCM) and the HadAM3H GCM, a higher resolution Atmospheric General Circulation Model (AGCM). The HadCM3 GCM has a spatial resolution of $3.7^{\circ} \times 2.5^{\circ}$ with 19 atmospheric levels in the vertical. This model was applied to generate a transient climate change simulation (a simulation with gradually increasing observed and projected emission scenarios) over the period 1850 to 2100. The HadAM3H GCM is an improved version of the atmospheric component of the HadCM3 GCM from resolution perspective. It has a spatial resolution of $1.88^{\circ} \times 1.24^{\circ}$ and has the same number of vertical levels with the HadCM3 GCM.

Climate change projections of the 2070s and 2080s (2070-2090) were considered in simulations performed by the PRECIS RCM system over the domain under investigation (figure 6.1).

6.4 VERIFICATION METHODS

In an effort to validate the performance of the PRECIS RCM system over the Eritrea region in terms of simulating the standard meteorological variables, i.e., rainfall, temperature, wind patterns and pressure fields, the months of July and January were considered. The baseline climate simulation of 30 years (1961-1990) was compared with observational data obtained from the National Center for Environmental Prediction (NCEP) reanalysis dataset 1948 to 2003 (Kalnay *et al.*, 1996). It is worthwhile to note, however, that variation in grid projection and resolution between observed and simulated data pose difficulties for quantitative analysis. The NCEP reanalysis data is available on a $2.5^{\circ} \times 2.5^{\circ}$ horizontal resolution, while the PRECIS RCM system generates output on a $0.44^{\circ} \times 0.44^{\circ}$ grid resolution. The PRECIS RCM system output diagnostics, as noted earlier, are in the rotated grid projection where the equator is shifted to within the model domain, while NCEP data are in a latitude-longitude format.

The PRECIS RCM system output diagnostics were first transformed to a standard grid projection, which provides approximate horizontal resolution of $0.45^{\circ} \times 0.43^{\circ}$ over the Eritrean region. The NCEP fields were interpolated to the RCM grid dimensions by using a bilinear interpolation scheme. Although the NCEP field was considerably smoothed, two similar grids enabled direct comparison for verification purposes. The reverse case was also considered where the PRECIS

RCM fields were regridded into the NCEP grid resolution. Root Mean Square (RMS) differences (errors) and Pattern or Anomaly Correlation (ACs) were calculated and model performance were expressed in a similar way as demonstrated in Taylor (2000) - see Appendix A.

The RMS difference is a common accuracy measure for model-simulated fields. RMS differences may be calculated by averaging the individual squared differences of RCM and observed (or the driving GCM) fields at each grid point, followed by square root computation to measure the degree of spatial discrepancy. RMS difference may also be calculated for a single grid point over a given period of time to measure the temporal discrepancy.

AC is commonly employed and is calculated in a similar way as the RMS difference, but measures the degree of association between the RCM and observed (or the driving GCM) fields.

6.5 RESULTS AND DISCUSSIONS

The HadAM3H GCM fields would have been supplementary to the results of the baseline fields of the PRECIS RCM system to address the consistency issue. The GCM output dataset is, however, not supplied along with the PRECIS software. For this reason, the inclusion of the driving GCM maps and the associated discussions are deemed impossible to reflect in this work.

6.5.1 MEAN SEA LEVEL PRESSURE

The observed MSLP climatology (1961-1990) for July over the model domain (figure 6.1 (b)) is presented in figure 6.2(a).

During July (Boreal summer), a low-pressure zone is observed over northeastern section of the model domain, which is most probably part or an extension of the trough that developed over the Indo-Asia region centered in Pakistan. This low-pressure region normally strengthens during July with meridional elongation across the Sahel-Sahra in Africa to induce regional pressure gradients and flow patterns associated with tropical atmospheric circulation during the Boreal summer. A low-pressure gradient (trough) is observed over Eritrea and Ethiopia, which presumably is attributed to the East African steep topography forcing. On

the eastern side of this depression, a shallow ridge developed in response of the East African rift valley (figure 6.2(a)).

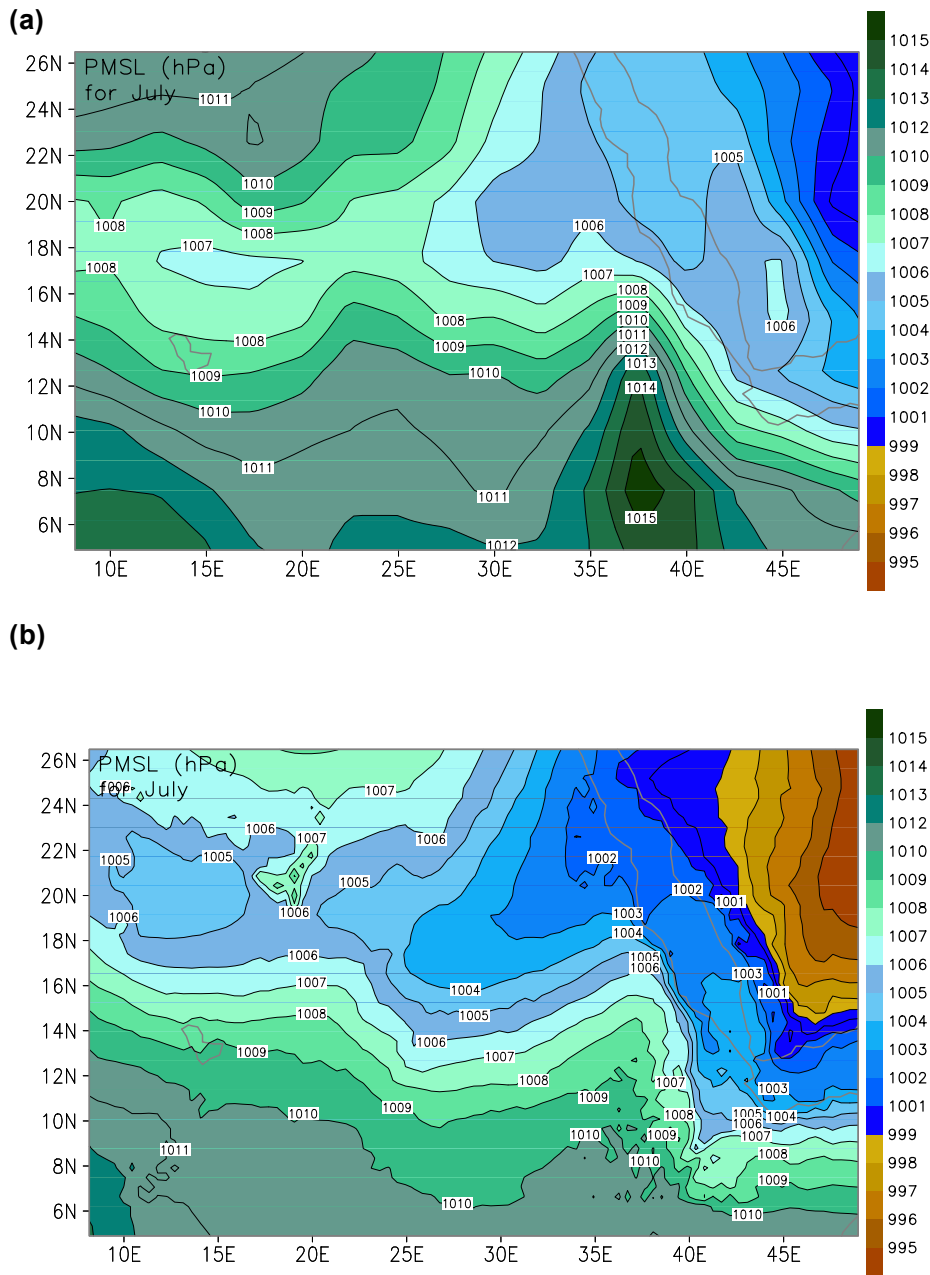
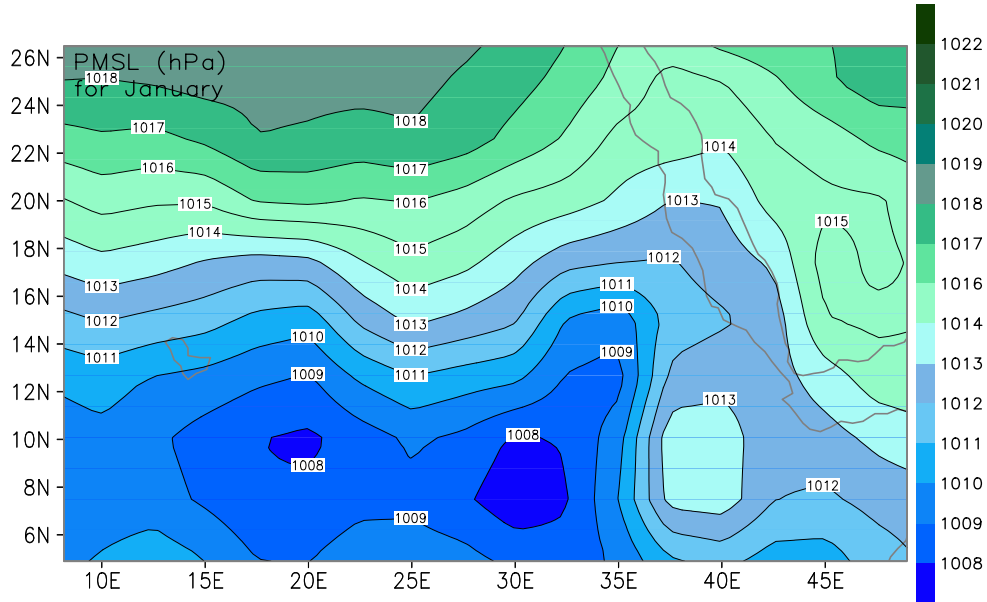


Figure 6.2: Average of Mean Sea Level Pressure (MSLP) for July (1961-1990) as obtained from (a) the NCEP reanalysis data and (b) the baseline integration of the PRECIS RCM system. The contour interval is 1 hPa.

(a)



(b)

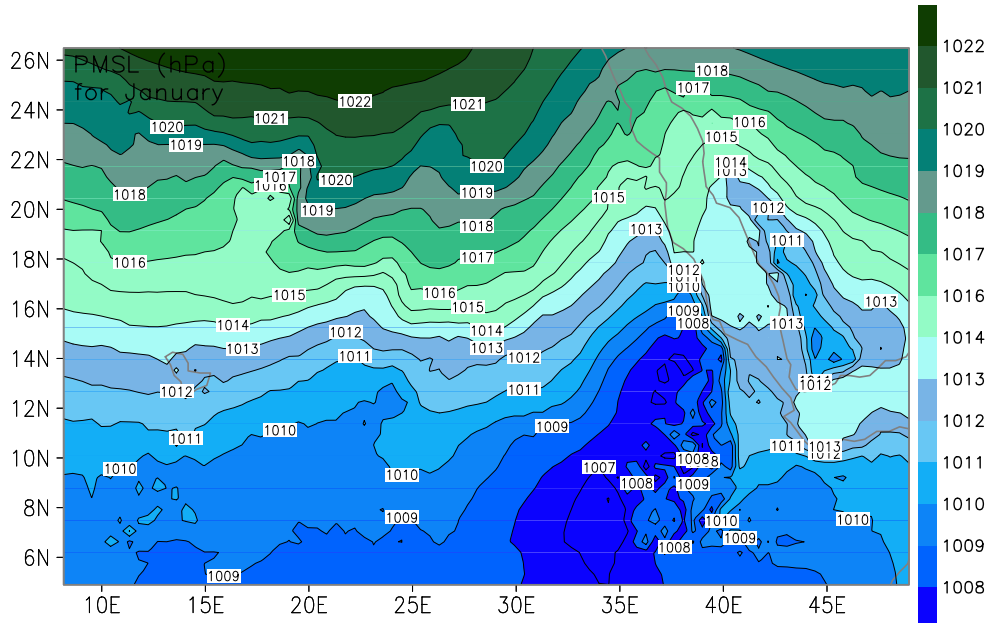


Figure 6.3: Average of Mean Sea Level Pressure (MSLP) for January (1961-1990) as obtained from (a) the NCEP reanalysis data and (b) the baseline integration of the PRECIS RCM system. The contour interval is 1 hPa.

As illustrated in figure 6.2(b), the PRECIS RCM system captured the observed MSLP patterns (figure 6.2(a)) associated with tropical atmospheric circulation and the influence of the local topography during July. The influence of the East African rift valley is clearly resolved in the PRECIS RCM system despite not available in the NCEP reanalysis fields (if local knowledge is to be integrated), most probably owing to the relative coarse resolution of the NCEP reanalysis fields. West of the trough a shallow ridge is captured along the lower areas to the west of the mountains (figure 6.1).

The observed MSLP pattern during January over the PRECIS RCM system domain (figure 6.3(a)) is characterized by a southward shift of the low and high-pressure systems in comparison to the July climatology (figure 6.2(a)). The PRECIS RCM system managed to capture the most important pressure systems (figure 6.3(b)), though with much more detail as a result of the finer resolution.

6.5.2 NEAR-SURFACE WIND PATTERNS

The observed near-surface wind streamline climatology (1961-1990) for July over the PRECIS RCM system domain is presented in figure 6.4(a).

The ITCZ is the line where trade or monsoon winds from the Southern Hemisphere meet trade or monsoon winds from the Northern Hemisphere. During July the ITCZ shifts north of the equator both in the western and eastern section of the Sahelian region (see Chapter 4 for details). Two wind components, namely a southwesterly and a northeasterly component, dominate in the Eritrean region nearly throughout the year. The ITCZ is located where these winds meet. The PRECIS model simulated the patterns of these winds realistically (figure 6.4(b)) as compared to the NCEP reanalysis climatology.

There are, however, some differences between the wind patterns simulated by the PRECIS RCM system and NCEP wind (figure 6.4(a) and (b)). Firstly, the model clearly captures the wind disturbances that are caused by the East African topography which can be justified by the absence of this feature in the upper air circulation system of the model climate. It is, however, impossible to show this altered features are the true winds of the real world since there is lack of observed data of comparable resolution as explained in section 6.6. A second difference between the model simulated and observed fields are the northward

displacement of the mean (1961-1990) position of the ITCZ relative to the NCEP climatology. The displacement is presumably caused by the amplified pressure gradient evident in the model climate (figure 6.2(b))

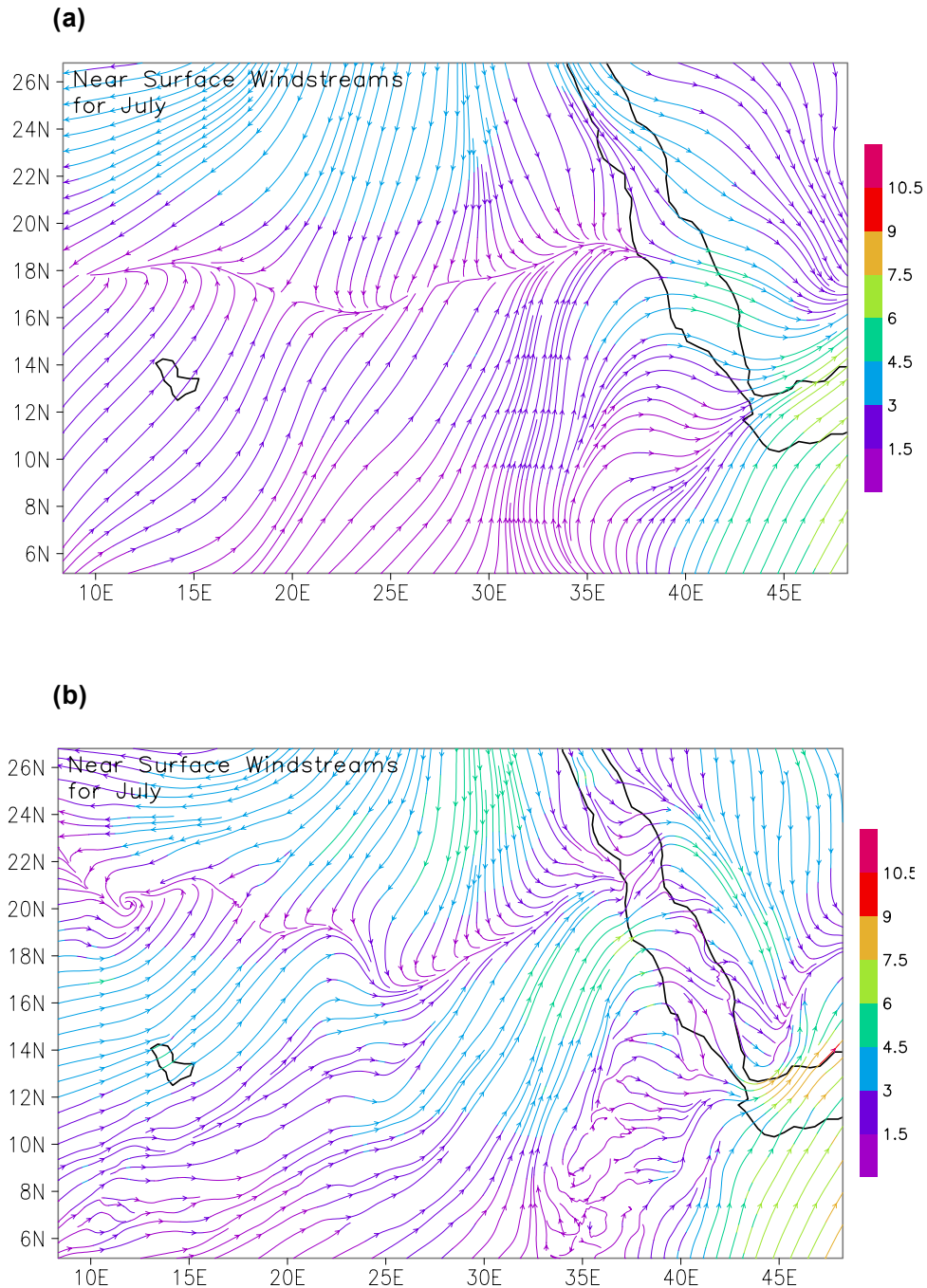


Figure 6.4: Near-surface wind streamlines for July (1961-1990) as obtained from (a) the NCEP reanalysis data and (b) the baseline integration of the PRECIS RCM system.

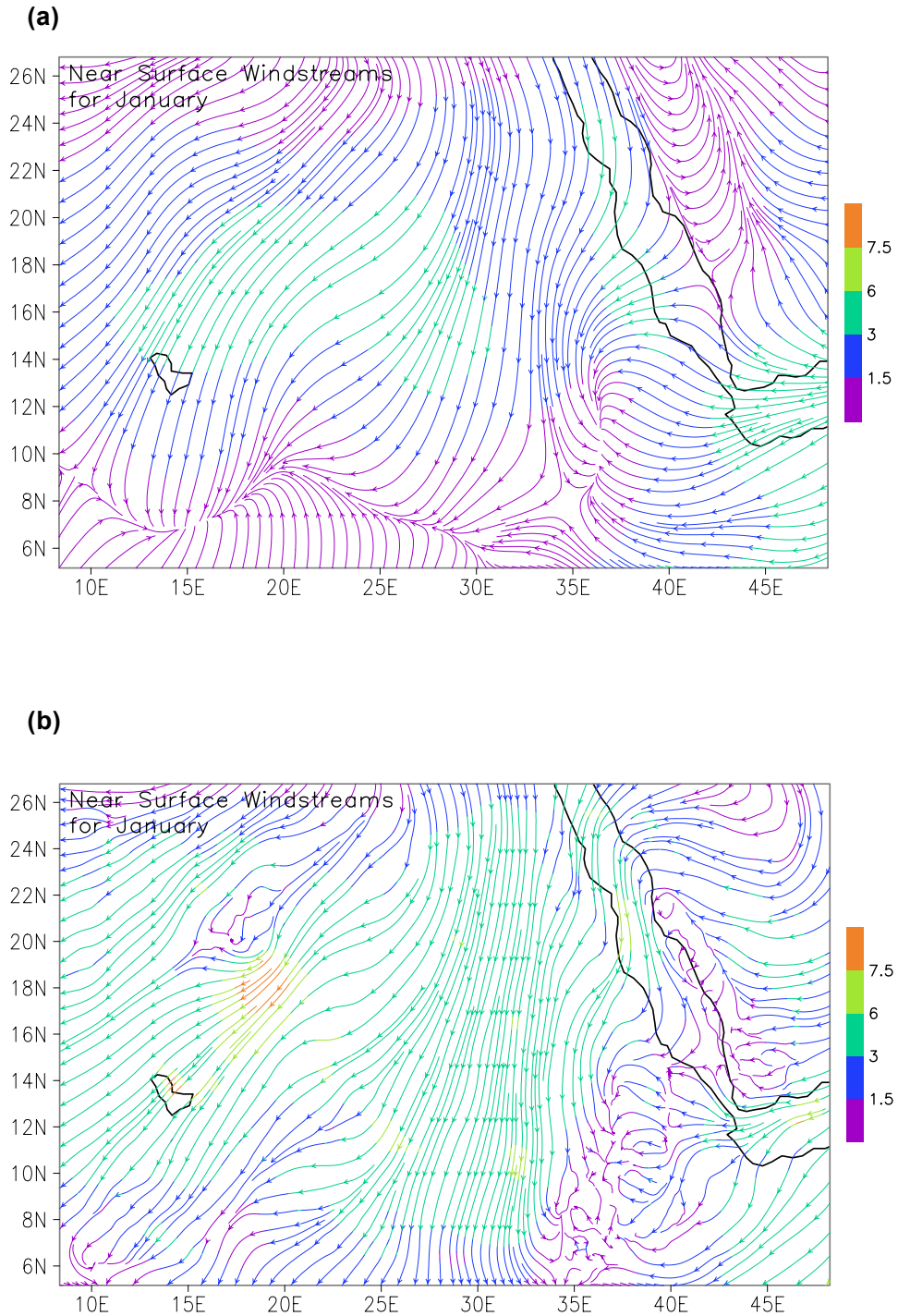


Figure 6.5: Near-surface wind streamlines for January (1961-1990) as obtained from (a) the NCEP reanalysis data and (b) the baseline integration of the PRECIS RCM system.

The observed near-surface wind streamline climatology (1961-1990) for January over the PRECIS RCM system domain is presented in figure 6.5(a). The PRECIS RCM system well simulated the observed wind patterns (figure 6.4(b)), especially the dominance of the northerly winds and its flow along the Red Sea channel. The model, however, severely exaggerated the northeasterly winds. This intensification of winds causes a southward displacement of the ITCZ, which is quite unrealistic. This might be the reason for the model's inability to capture the observed January precipitation rate over the southern part of the model domain (see section 6.5.3).

6.5.3 PRECIPITATION RATE

The NCEP climatology (1961-1990) of daily precipitation distribution for July over the PRECIS RCM system domain is demonstrated in figure 6.6(a).

Precipitation during the Boreal summer reaches its peak in July. Precipitation totals are the highest over the southern section of the model domain. The observed meridional decrease in rainfall towards the north (figure 6.6(a)) is, to a large extent, caused by more active convective activity associated with the ITCZ in the south. The convection is driven by the convergence of the West African monsoon and the northeasterlies. During July a trough develops over the region as a result of summer heat. The influence of the east African steep topography causes a northward shift in rainfall over southern Eritrea, Central and southwestern Ethiopia. This is in comparison of rainfall over the central section of the Sahel latitude (eastern Sudan; refer to chapter 4 for comprehensive coverage of seasonal climatology).

The model successfully captured the meridional gradient of precipitation rate south of the ITCZ (figure 6.5(b)) as well as the gradient toward the Sahara desert. When qualitatively visualized, rainfall patterns compare well with the NCEP reanalysis climatology. The NCEP precipitation maximum in central Ethiopia is, however, not captured in the model climate. The PRECIS RCM system simulated scattered patches of maxima over the mountainous landscape of Eritrea, which could be attributed to local forcing that is captured in the finer resolution of the model.

The NCEP climatology (1961-1990) of daily precipitation distribution for January over the PRECIS RCM system domain is illustrated in figure 6.7(a), while model results for the same month are given in figure 6.7(b).

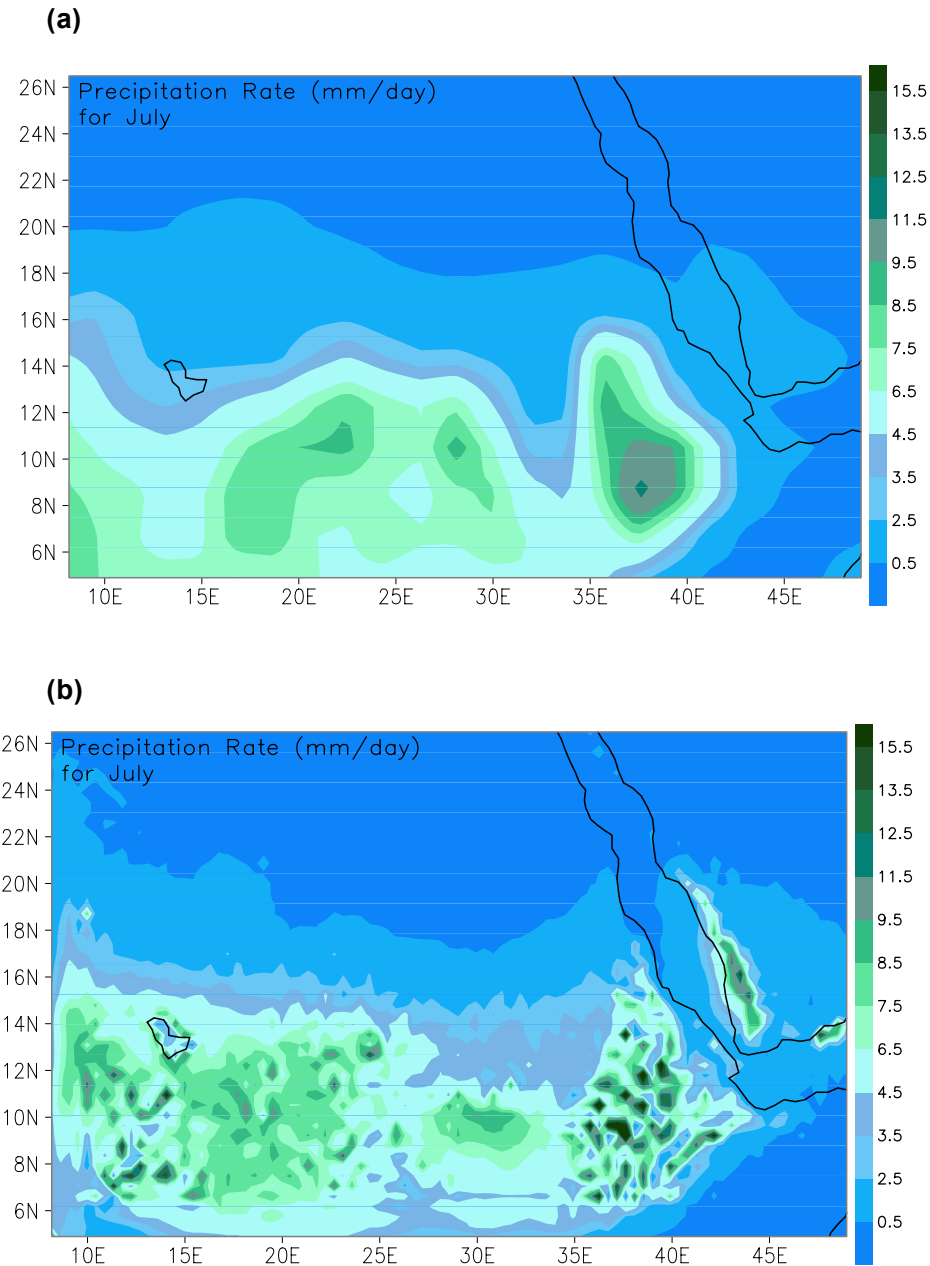


Figure 6.6: Precipitation rate (mm/day) for July (1961-1990) as obtained from (a) the NCEP reanalysis data and (b) the baseline integration of the PRECIS RCM system.

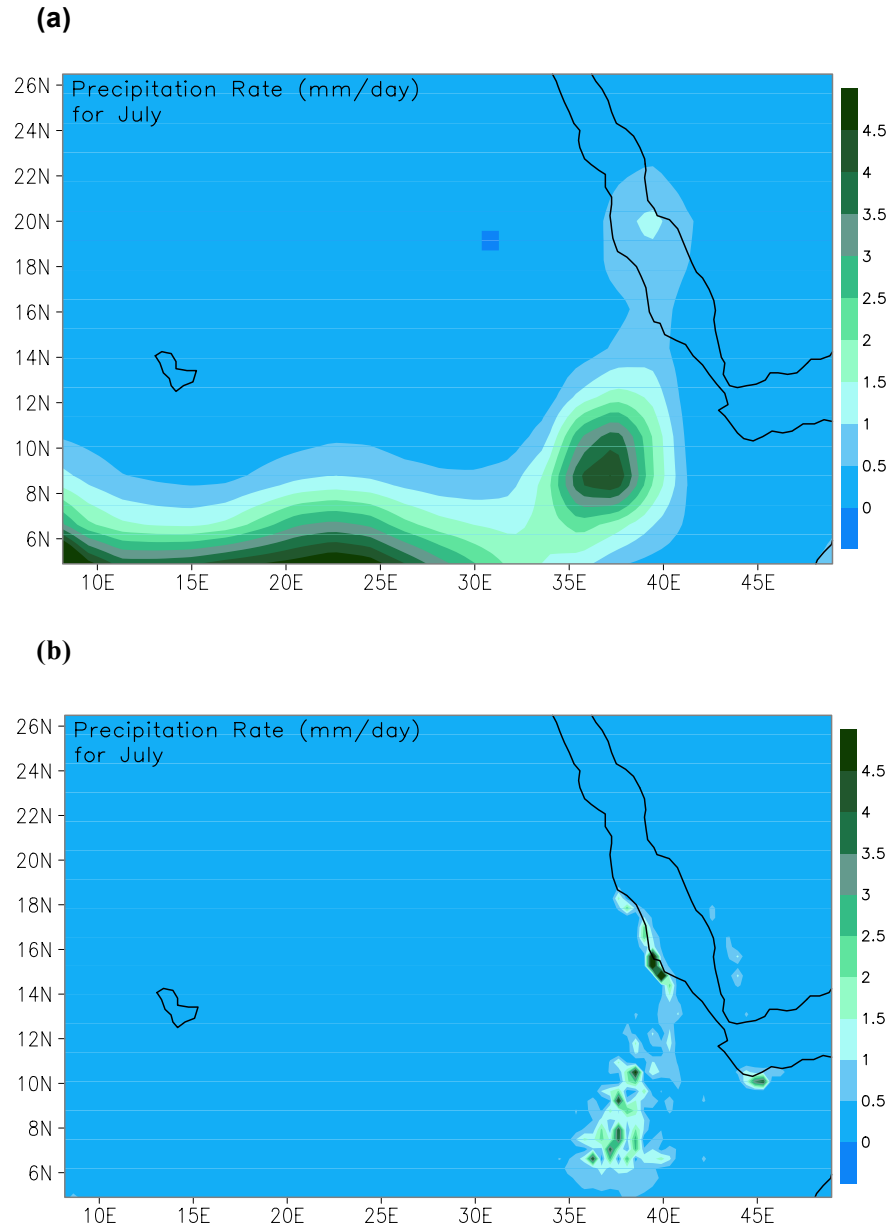


Figure 6.7: Precipitation rate (mm/day) for January (1961-1990) as obtained from (a) the NCEP reanalysis data and (b) the baseline integration of the PRECIS RCM system.

During January, the rainfall distribution associated with tropical circulation is captured in the southern section of the domain (figure 6.7(a)). The zonal elongation of rainfall with its maxima centered at 37°E and 8°N is also present in the NCEP data. The scanty rainfall over the Red Sea coastal area may be attributed by regional disturbances (not part of the ITCZ). During January, the

circulation patterns and the associated moisture advection systems are mainly associated with the trough developed in response of the Egyptian currents and its affiliated portion plowing through the Gulf of Aden and the Red Sea channel driven by regional/ synoptic pressure gradients (figures 6.4(a)) and 6.5(a)). The ITCZ shifts south of the Equator during January in the south eastern section of the domain, and the region, generally, experiences dry condition (boreal winter).

When the PRECIS RCM system climate is viewed in the light of the ascribed regional behavior, it severely misses the NCEP rainfall band over the ITCZ. This is because of the exaggerated intensification of the surface pressure and northeasterly winds in the model climate. The model, however, simulated the regional cyclonic induced rainfall along the east African steep topography and the Red Sea coastal area, especially over the eastern escapement of Eritrea (green belt).

6.5.4 SURFACE TEMPERATURE

The NCEP climatology (1961-1990) of surface temperatures for July and January over the PRECIS RCM system domain is illustrated in figures 6.8(a) and 6.9(a), while model results for the same months are given in figures 6.8(b) and 6.9(b).

Although a clearly defined latitudinal temperature gradient occur in both the July and January climatologies, it is characterized by spatially reversed surface temperature maxima and minima prevalence and their associated gradient in the south-north orientation despite the lower temperatures dominance in the region during January, i.e., the higher temperature zone is in the northern section of the domain during July while it is found in the southern section during January. The variation is mainly driven by the meridional shift of solar insolation. During the boreal summer the apparent position of the Sun shifts towards the Northern Hemisphere whilst during the boreal winter it migrates towards the Southern Hemisphere.

The influence of synoptic or regional scale forcing that constrains cold air mass movement (*harmattan* over the Sahara and West Africa, and *Egyptian Current* in the north-east Africa section; Martyn, 1992; figure 6.5(a)) is significant during January or the Boreal winter. The cold air advection that largely originates from the cold Asian continent has a marked effect on cold air temperatures in January over the PRECIS RCM domain. This is particularly evident in the central Sahara Desert (western

Sudan and Chad) where a southward penetration of the cold air is observed as lower temperatures. This intrusion is, however, hampered by the warm tropical climate with its maximum in southern Sudan and Central Africa (figure 6.9(a)). The warmer climate is mainly associated with the position of the ITCZ (figure 6.5(a) in the Northern Hemisphere over central and western Africa during the Boreal winter.

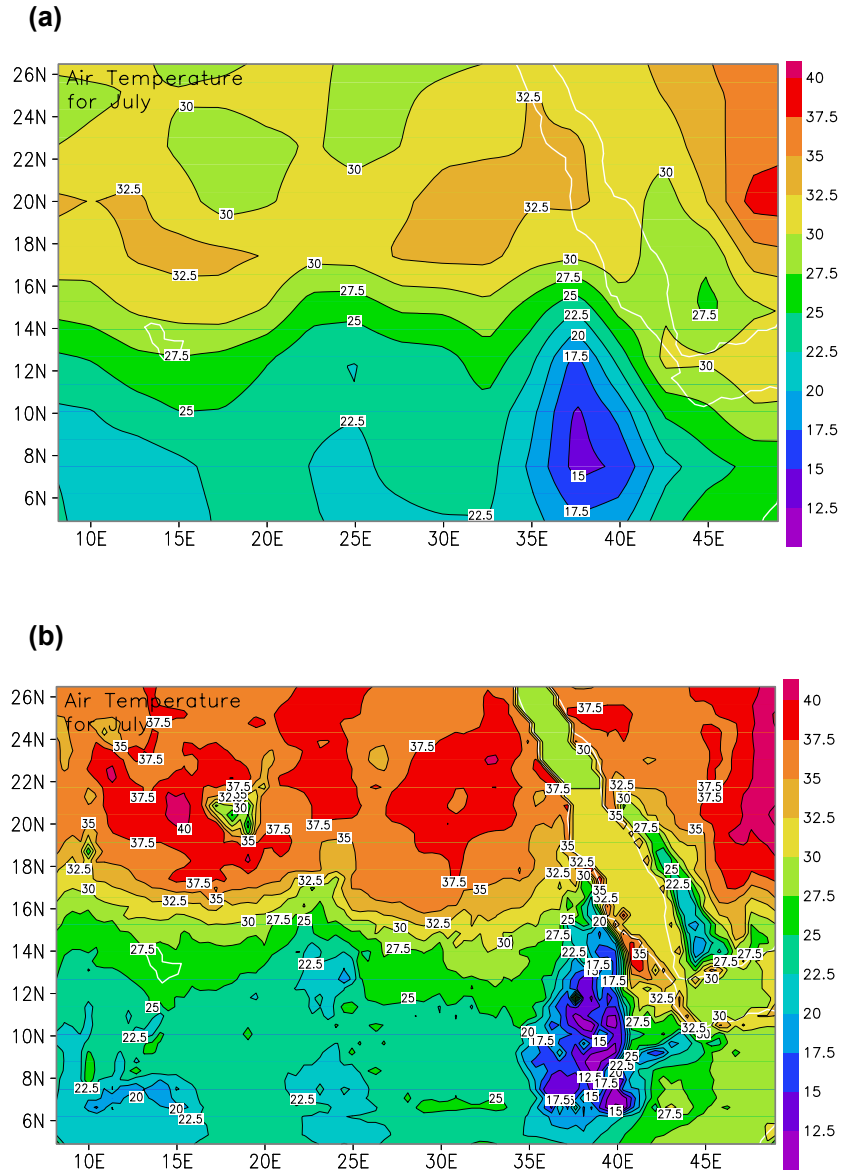


Figure 6.8: Surface temperature ($^{\circ}\text{C}$) for July (1961-1990) as obtained from (a) the NCEP reanalysis data and (b) the baseline integration of the PRECIS RCM system.

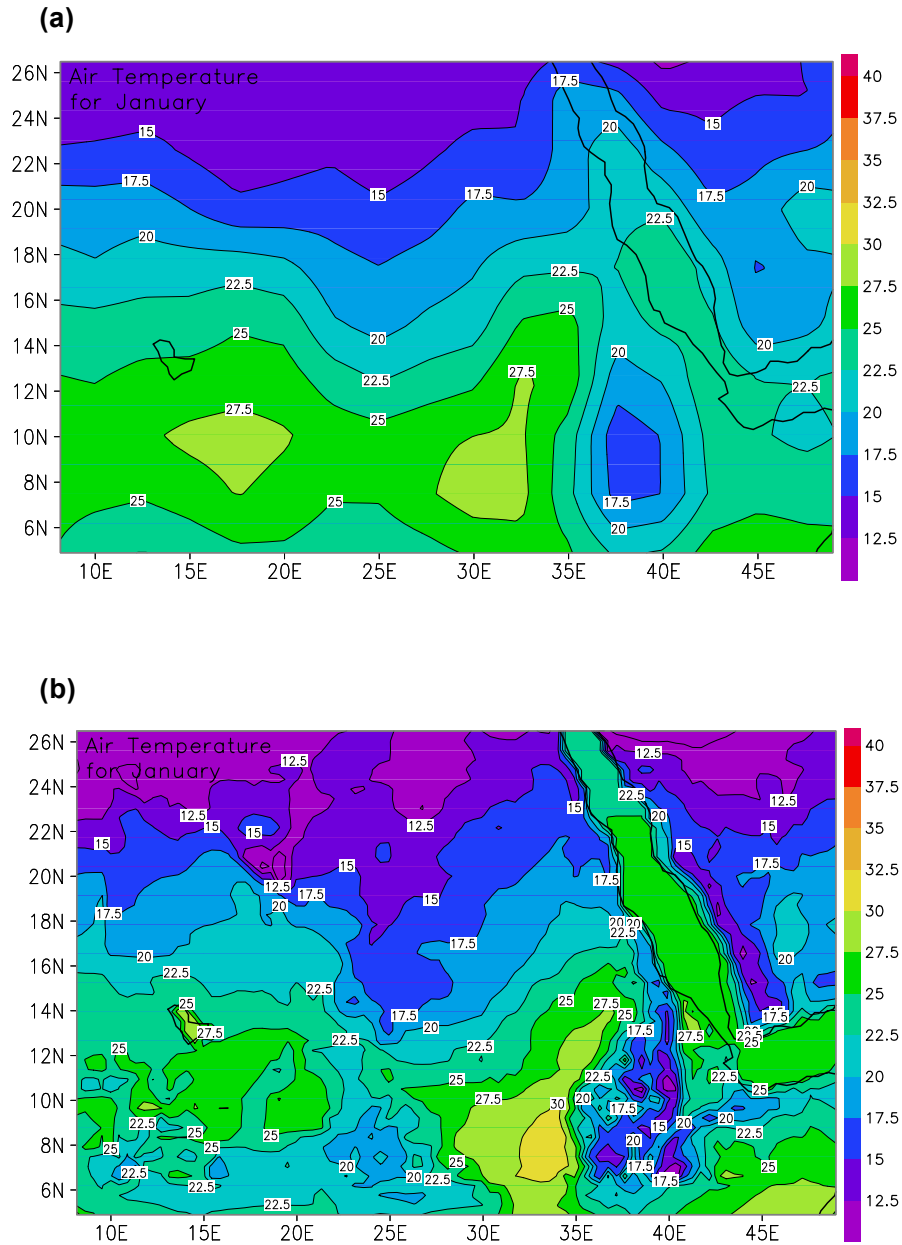


Figure 6.9: Surface temperature ($^{\circ}\text{C}$) for January (1961-1990) as obtained from (a) the NCEP reanalysis data and (b) the baseline integration of the PRECIS RCM system.

The influence of low-level topography and mountain shields along the western Ethiopia border and Eritrea are significant and responsible for a northerly meandering of higher temperatures during January (figure 6.9(a)). Another interesting phenomenon, which might also play a role, is the local convergence zone between

the Egyptian Current and the warm air advection from the Gulf of Aden (figure 6.5(a)). In general, the relative importance of central east Africa topography forcing in modifying winter air temperature propagation is, however, largely suppressed because of cold air from central Asia, in comparison to the July climate (figure 6.8(a)). During July, higher temperatures appear over the northern section of the PRECIS RCM domain. The Central east African mountain range affects the climate of July in such a way that a steep surface temperature gradient with its minimum (less than 15°C) occurs over the plateaus located in central and southern Ethiopia.

When the PRECIS RCM system and NCEP surface temperatures over the study domain are compared, it is clear that there are fairly high spatial similarities in both the July and January fields. In this regard the model successfully simulates the meridional surface temperature gradient for July (figure 6.8(b)) and January (figure 6.9(b)).

However, there are some differences between the NCEP and PRECIS RCM system climates. These variations are not necessarily model errors. They might to a great extent reflect the model's ability to resolve sub grid scale processes owing to its finer resolution in comparison to the NCEP climate. In this regard, the model captures more diverse surface temperature over the domain, particularly over the central east Africa complex landscape. The model also managed to simulate surface temperature patterns in the eastern African rift valley as well as the Danakil depression which is more than 100m deep below sea level (the hottest spot on the globe where the information can be found from known web search engines). These temperatures are not well captured in the NCEP data.

6.6 MODEL EVALUATION

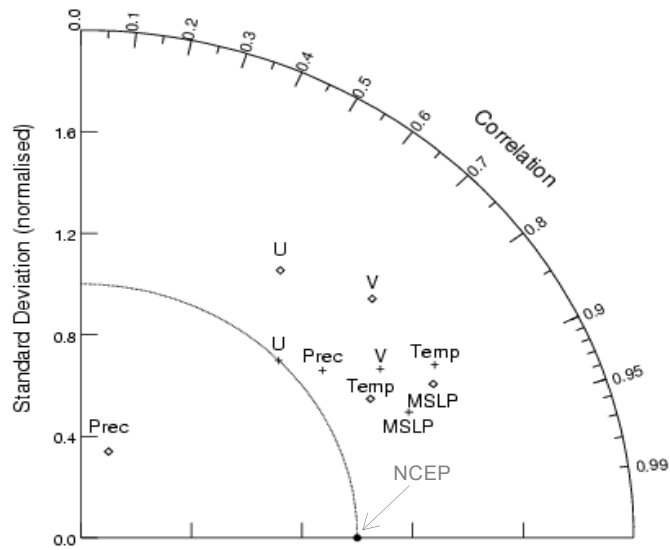
The lack of reliable observations over the PRECIS RCM system domain made the model verification effort difficult. As a result the model was verified against the coarser resolution NCEP reanalysis fields (Kalnay *et al.*, 1996). A standard skill of measures (table 6.1) and Taylor (2000) scheme (figure 6.10) were applied to investigate model performance.

The performance of the PRECIS RCM system was based upon the climatology of the months July and January. Verification focused on variables discussed in the preceding sections. The model provided relatively realistic portrayal of the surface

temperature, MSLP, circulation and precipitation rate for July. Similarly, the January fields of surface temperature and MSLP were plausible. Nevertheless, it manifested relatively weak skill in simulating the observed circulation features (near surface wind components) during January. The model also severely underestimated the rainfall of January. The poor skill might be attributed to the simulation of higher pressure fields and the consequential strengthening of the northerly winds which led to a southward displacement of the ITCZ from its mean state position in the central and western section of the model domain. The model performance on daily precipitation for January, therefore, remains a source of uncertainty (figure 6.10). Results are also listed in Table 6.1. for the case where the NCEP reanalysis dataset was interpolated into the PRECIS RCM grid resolution.

The model generally revealed a tendency to over estimate the annual variability on most of the considered variables relative to the NCEP reanalysis climatology, with the exception of daily precipitation in January which is severely underestimated. One must, however, keep in mind that NCEP fields are smoothed considerably and might therefore not be a perfect reflection of climate variability over a fine resolution spatial scale figure (6.10(a)). To address this snag, however, the effect of resolution was also considered (figure 6(b)) where the PRECIS model outputs were regirded into the NCEP resolution in order to suppress the effect of sub-grid details captured in the PRECIS climate. Accordingly, the model variables are relatively clustered around the one value standard deviation (threshold value that defines the nature of variability) and slightly displaced toward the reference (figure 6.10(b)). This implies there is an improvement in the model's skill comparatively.

(a)



(b)

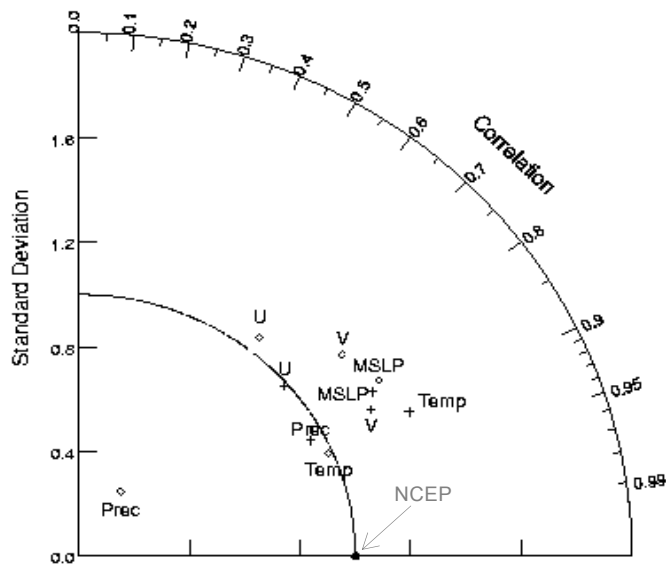


Figure 6.10: Model evaluation diagram for all considered variables for July (+) and January (\diamond). The top panel (a) shows when the NCEP fields are interpolated to the PRECIS resolution while (b) shows the reverse. The Root Mean Square (RMS) difference values and standard deviations were normalized with observation to suite the analysis. The RMS difference is the proportional distance between NCEP (reference) and PRECIS RCM fields. The radial distance is the standard deviation and the angular coordinate is the pattern correlation. See figure A.1 for the geometric relationship among these three measures of standard skill) (after Taylor, 2000)

Table 6.1: Model performance over all grid points (91x51) covering the PRECIS RCM system domain as compared to the corresponding NCEP reanalysis fields for January and July. Variables are surface temperature (°C), MSLP (hPa), precipitation rate (mm.day⁻¹) and the horizontal wind components (m.s⁻¹) on different temporal scales.

VARIABLES	Time Span	Standard Deviation				RMS difference		Pattern Correlation (AC)	
		Observed		Model		Jan	Jul	Jan	Jul
		Jan	Jul	Jan	Jul				
Surface Temperature	1960s	4.28	4.51	5.01	6.76	2.68	4.44	0.87	0.90
	1970s	4.32	4.63	5.30	6.64	2.66	3.90	0.88	0.90
	1980s	4.60	4.80	5.24	6.66	2.63	4.22	0.87	0.90
	30 yrs	4.38	4.61	5.18	6.68	2.61	4.14	0.89	0.88
MSLP	1960s	2.99	3.12	4.07	4.24	2.34	1.37	0.85	0.85
	1970s	3.06	3.14	4.40	4.06	2.26	1.31	0.89	0.88
	1980s	3.25	3.32	4.58	3.96	2.06	1.47	0.88	0.86
	30 yrs	3.08	3.18	4.35	4.08	2.18	1.33	0.90	0.85
Daily precipitation	1960s	1.20	3.41	0.30	3.29	1.31	2.17	0.30	0.82
	1970s	0.95	3.07	0.32	3.25	1.0	2.43	0.25	0.80
	1980s	0.65	2.75	0.36	3.15	0.68	2.39	0.25	0.81
	30 yrs	0.92	2.93	0.33	3.21	0.98	2.00	0.28	0.80
U-Winds	1960s	1.32	1.76	1.52	1.99	1.51	1.50	0.56	0.73
	1970s	1.21	1.70	1.54	1.76	1.56	1.54	0.52	0.76
	1980s	1.18	1.80	1.65	1.70	1.58	1.50	0.48	0.73
	30 yrs	1.22	1.91	1.56	1.80	1.53	1.48	0.56	0.72
V-winds	1960s	1.29	1.91	1.74	2.56	1.63	1.37	0.74	0.85
	1970s	1.24	1.94	1.77	2.49	1.72	1.317	0.74	0.88
	1980s	1.23	2.15	1.78	2.50	1.64	1.47	0.73	0.86
	30 yrs	1.24	1.97	1.76	2.51	1.65	1.33	0.75	0.85

6.7 CLIMATE CHANGE SCENARIO PROJECTIONS WITH THE PRECIS RCM SYSTEM

Climate change projections generated by the PRECIS RCM system for the A2 and B2 SRES scenarios are presented (see section 6.6.3). For the sake of avoiding redundancy, however, the 2070s (2071 to 2080) pattern maps are not included. Only results from the 2080s (2081 to 2090) simulations are discussed. Nonetheless, the analysis confirmed that there are similar projected trends in surface temperature and daily rainfall projections between the years discussed and the 1970s.

6.7.1 SURFACE TEMPERATURE

6.7.1.1 JULY PROJECTIONS

Future scenarios for the 2080s of surface temperatures as simulated by the PRECIS RCM system for the A2 and B2 SRES scenarios and for July are illustrated in figures 6.11(a) and 6.11(b), respectively. Owing to the fine resolution of the PRECIS RCM system, as opposed to the IPCC GCM projections (chapter 5), detailed regional manifestations of surface temperatures are captured.

PRECIS RCM system projections showed above baseline surface temperature anomalies for July in the 2080s over the entire PRECIS RCM system domain for both SRES scenarios, which are consistent with IPCC GCM results, in general, and the HadCM3, in particular. According to the PRECIS RCM system simulation, one might expect a profound surface temperature increase over the Sahara desert ($> 4.5^{\circ}\text{C}$ for the A2 SRES scenario and $> 2.5^{\circ}\text{C}$ for the B2 SRES scenario) with a decreasing gradient towards the south.

The likelihood of increasing surface temperatures under conditions of the A2 and B2 SRES scenarios for July in the 2080s over the entire Eritrea sub-domain is also a possibility. According to the PRECIS RCM system one might expect a warming signal in the range of $+3.5^{\circ}\text{C}$ to $+5.5^{\circ}\text{C}$, and $+1.5^{\circ}\text{C}$ to 3.0°C for the A2 and B2 SRES scenarios, respectively.

6.7.1.2 January projections

Future scenarios for the 2080s of surface temperatures as simulated by the PRECIS RCM system for the A2 and B2 SRES scenarios and for January are illustrated in figures 6.12(a) and 6.12(b), respectively.

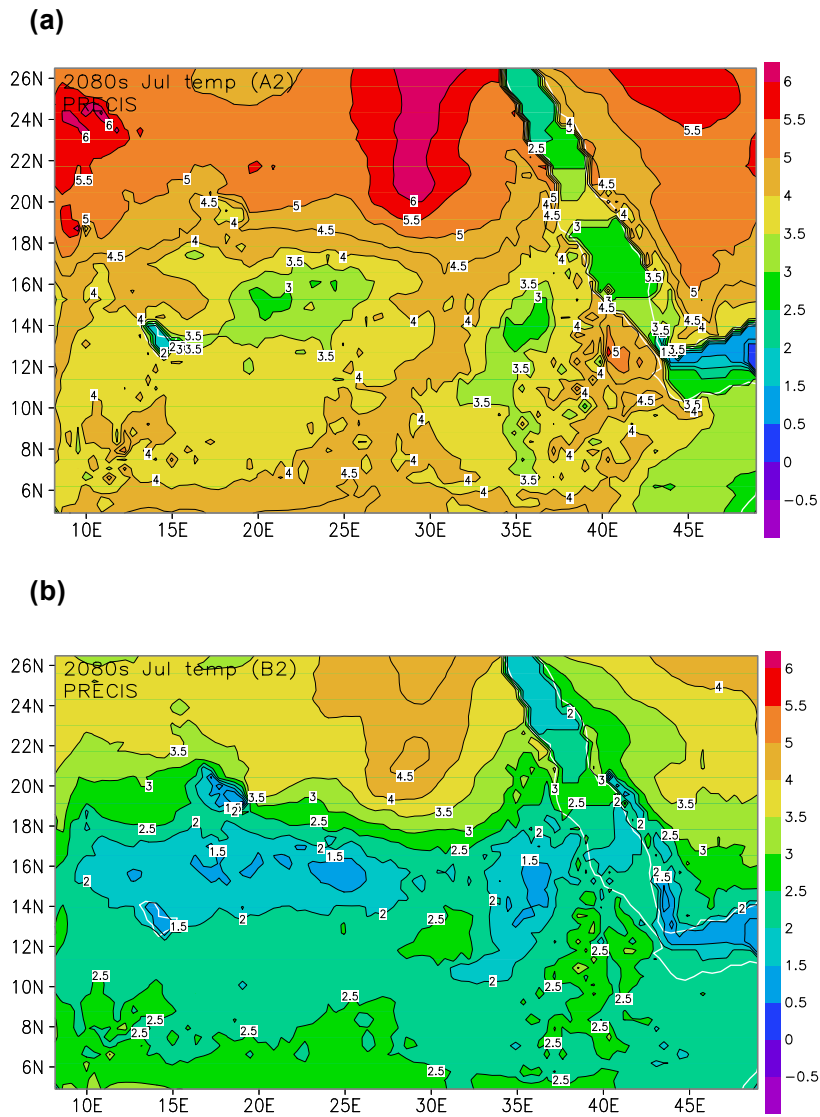


Figure 6.11: Surface temperature ($^{\circ}\text{C}$) climate change anomalies as generated by the PRECIS RCM system for July in the 2080s relative to the baseline climate of 1961 to 1990. Simulations are for the (a) A2 and (b) B2 SRES scenarios and the isotherm interval is 0.5°C .

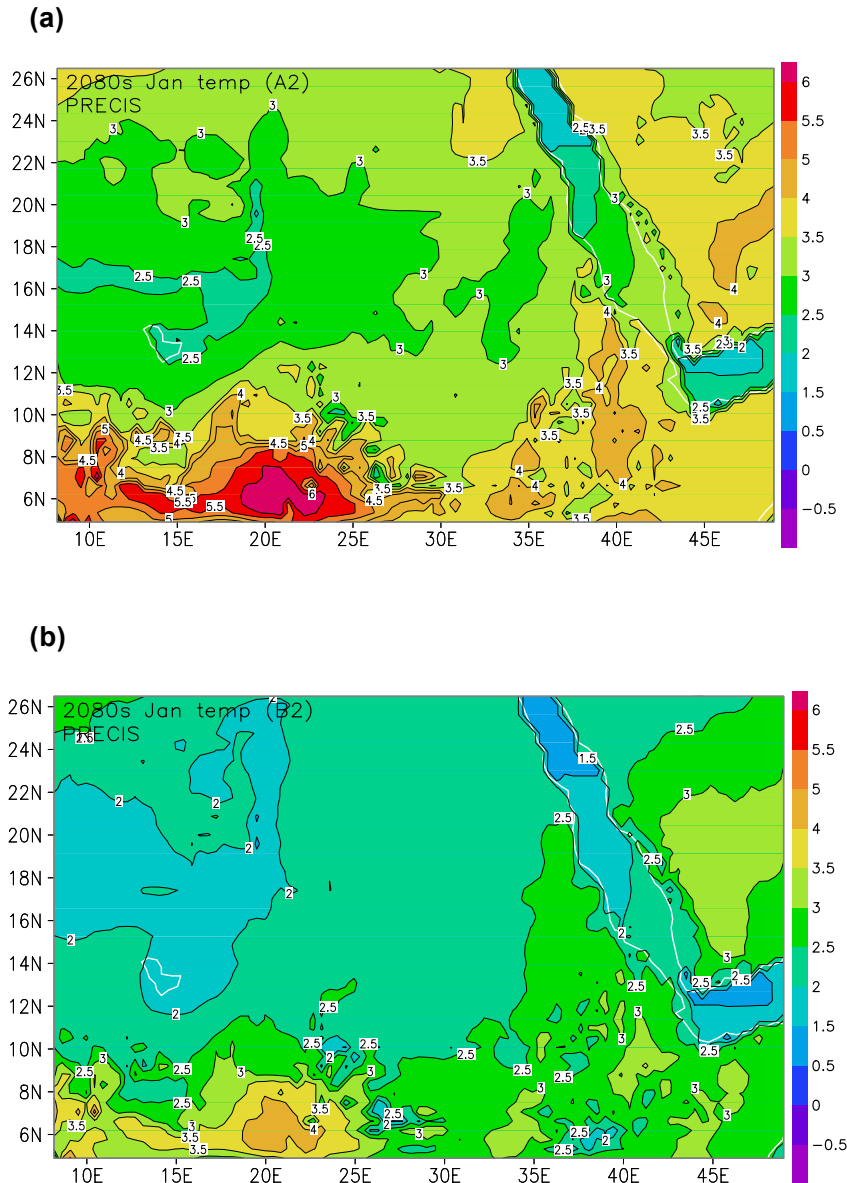


Figure 6.12: Surface temperature ($^{\circ}\text{C}$) climate change anomalies as generated by the PRECIS RCM system for January in the 2080s relative to the baseline climate of 1961 to 1990. Simulations are for the (a) A2 and (b) B2 SRES scenarios and the isotherm interval is 0.5°C .

The January 2080s projections are indicative of above baseline surface temperature conditions for both the A2 and B2 SRES scenarios. The model simulated maximum surface temperature deviations ($> 6^{\circ}\text{C}$ for the A2 SRES scenario and $> 4.5^{\circ}\text{C}$ for the B2 SRES scenario) over the southwestern part of the PRECIS RCM domain.

The PRECIS RCM system generated projected surface temperatures in the range of +3.0°C to +4.5°C and +2.5°C to 3.5°C for the A2 and B2 SRES scenarios, respectively. There is some degree of spatial consistency between PRECIS RCM system results and the HadCM3 GCM (figures 5.8 and 5.9 in the preceding chapter) simulated fields for both SRES storylines

6.7.2 PRECIPITATION RATE

6.7.2.1 JULY PROJECTIONS

Future scenarios for the 2080s of the precipitation rate as simulated by the PRECIS RCM system for the A2 and B2 SRES scenarios and for July are illustrated in figures 6.13(a) and 6.13(b), respectively.

The PRECIS RCM system generated mixed spatial signals of rainfall anomalies over the study domain. The model indicates that one might expect an increase in rainfall over most of the Sahel region under the conditions of both the A2 and B2 SRES scenarios. Some parts, however, might experience relatively drier condition than the baseline climate.

Although there is a spatial consistency between the PRECIS RCM system and its driving GCM (HadCM3), the lack of inter-model consistency amongst the IPCC-GCMs adds to a significant degree of uncertainty on what to expect with respect to future rainfall. This uncertainty makes it difficult to determine the impact of climate change and to define vulnerabilities.

Projections of precipitation rate for the 2080s over the Eritrea sub-domain under conditions of both the A2 and B2 SRES scenarios are similar to projections for the Sahel region. Rainfall seems to increase over most of Eritrea relative to the baseline climate. An average increase of +1.5 mm.day⁻¹ in daily rainfall during summer (July) is simulated with a maximum increase projected for the southwestern part of the PRECIS RCM system domain (+3.0 mm day⁻¹).

6.7.2.2 JANUARY PROJECTIONS

Future scenarios for the 2080s of the precipitation rate as simulated by the PRECIS RCM system for the A2 and B2 SRES scenarios and for January are illustrated in figures 6.14(a) and 6.14(b), respectively.

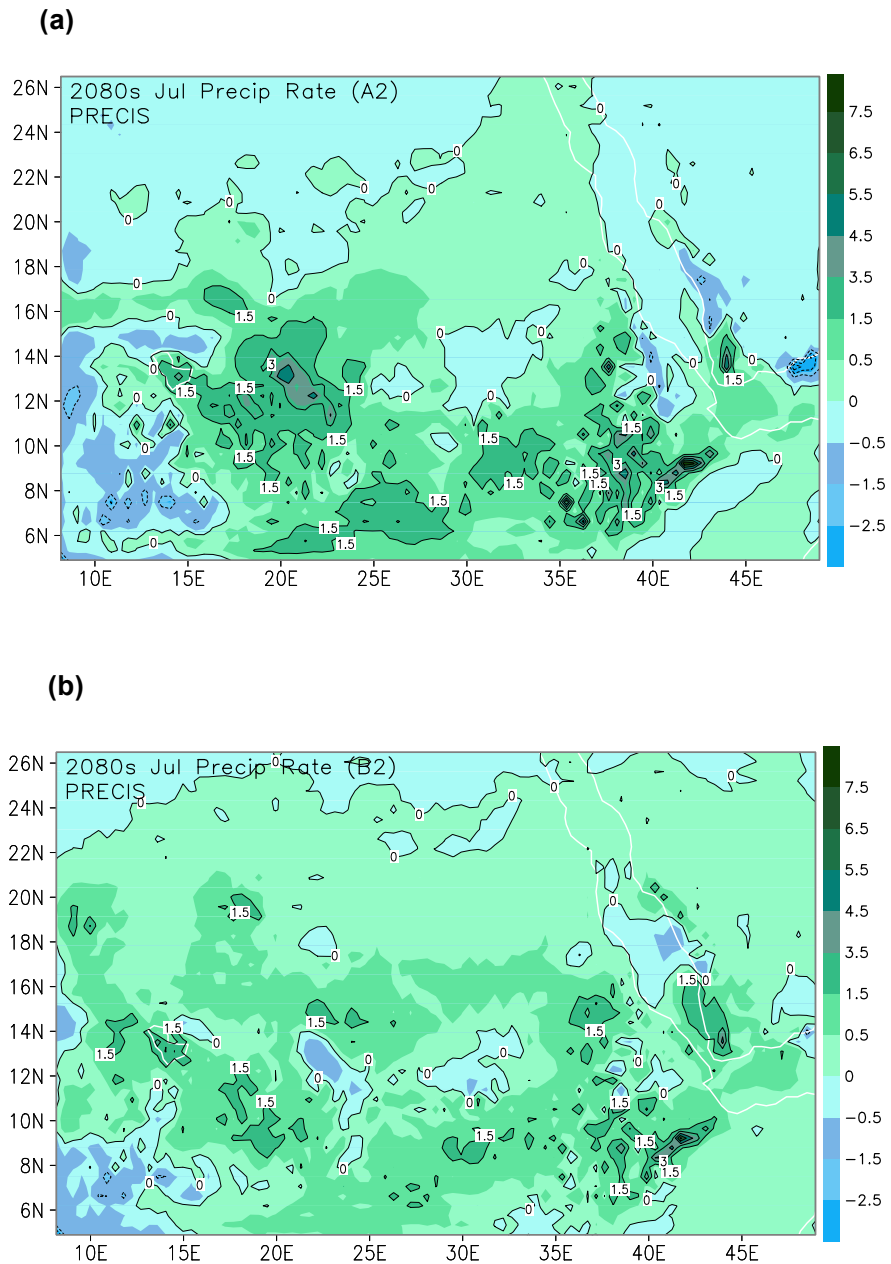


Figure 6.13: Precipitation rate ($\text{mm}\cdot\text{day}^{-1}$) climate change anomalies as generated by the PRECIS RCM system for July in the 2080s relative to the baseline climate of 1961 to 1990. Simulations are for the (a) A2 and (b) B2 SRES scenarios and contour intervals are 1.5mm.

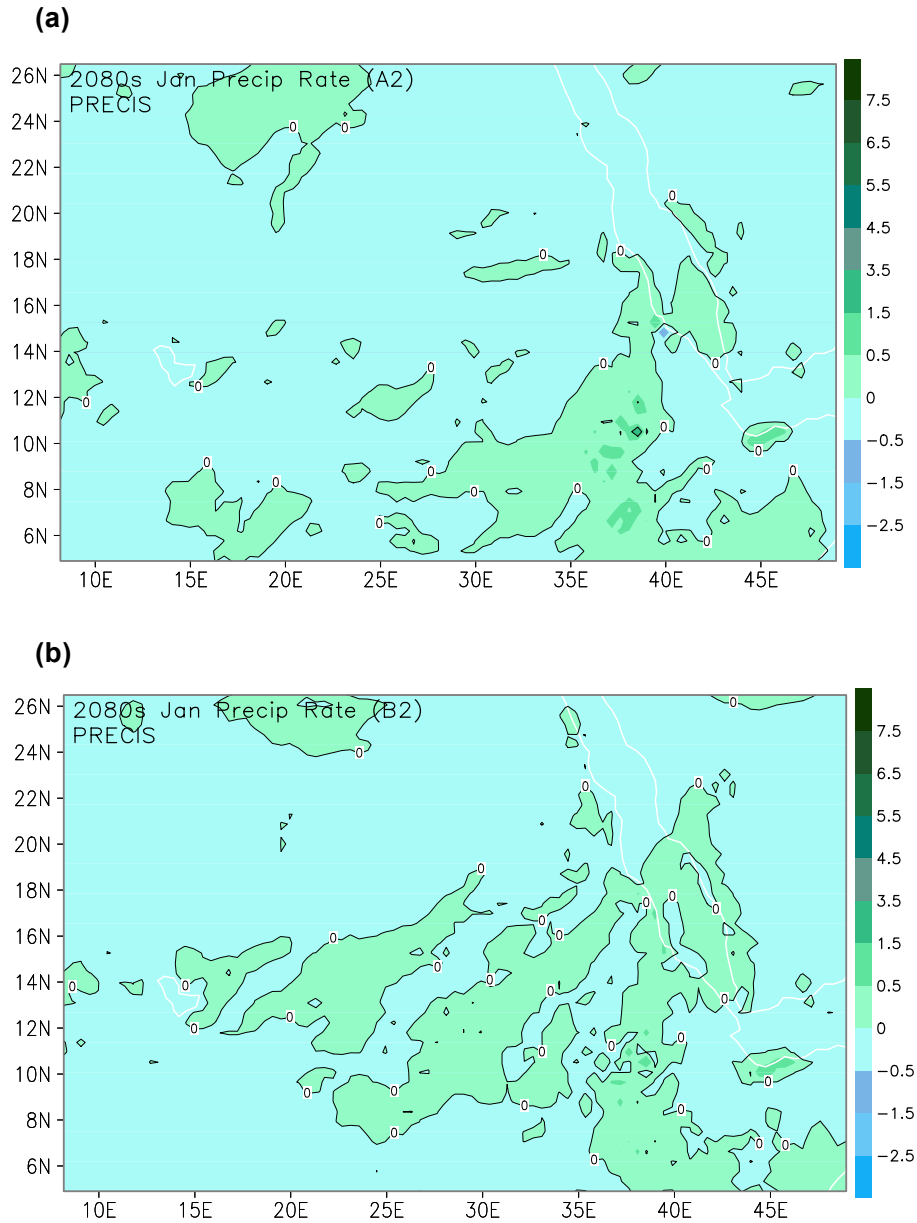


Figure 6.14: Precipitation rate ($\text{mm}\cdot\text{day}^{-1}$) climate change anomalies as generated by the PRECIS RCM system for January in the 2080s relative to the baseline climate of 1961 to 1990. Simulations are for the (a) A2 and (b) B2 SRES scenarios and contour intervals are 1.5mm.

According to PRECIS RCM system simulations, daily rainfall might increase in some parts of the winter rainfall region in the 2080s. The January rainfall projection has a greater degree of uncertainty than the July projection, not only because of a lack of consistency amongst the IPCC-GCMs, but also because of the weaker skill of the PRECIS RCM system (table 6.1) in representing the

present climate of the region (figure 6.7(b)). The lack of consistency between the RCM and HadCM3 projections (figures 5.10 and 5.11 in the preceding chapter), consequently, renders the reliability of the PRECIS RCM system fields and projections for January unsuitable for use in impact and vulnerability studies.

On the basis of PRECIS RCM system simulations, one might expect an increase in the daily rainfall of January during the 2080s under conditions of both the A2 and B2 SRES scenarios in the Eritrea sub-domain.

CHAPTER 7

CONCLUSIONS

The present climate of Sub-Saharan Africa has been dominated by persistent drought events, especially over the last two decades, which perhaps are accentuated by interannual and interdecadal climate variability. The origin of these drought events is still vague, since it is not yet clear whether it evolved from natural forcing, such as ENSO or from anthropogenic induced climate change. This study, however, suggests that there is a stronger likelihood the droughts are a result of natural variability, based upon the region's increasing rainfall respond to enhanced greenhouse concentrations. The study also indicates that the rainfall of the region is sensitive to atmospheric circulation features, such as the relative position of the ITCZ (Lamb, 1978; Foland *et al.*, 1986). Whether the influence of the southward migration of the subsidence band of the Hadley cells (Nicholson, 1886; 1991; Nicholson and Flohn, 1980) or the African Easterly Jet (AEJ: Druyan and Hastenrath, 1991) on the sensitivity of the time evolution of daily rainfall extends to the region needs further investigation. The response of climate variables in the region to anthropogenic greenhouse gas and aerosol emission induced climate change is therefore still a study field that needs attention.

The study reveals that the performance of the PRECIS RCM system in simulating most of the considered atmospheric variables shows plausible harmony with observed spatial patterns. The model was relatively skillful in simulating surface temperature, MSLP, near surface wind components and precipitation rate for July. Similarly, the January fields of surface temperature and MSLP are also relatively plausible. This prescribed skill should be attributed to the full representation of the climate system (land surface, sea, atmosphere and sulphur cycle and other chemical species) in the model. There are, however, some differences between the PRECIS RCM system results and NCEP observations, apparently caused by the effect of regional details and sub grid-scale processes in the model climate in account of its finer resolution of $0.44^{\circ} \times 0.44^{\circ}$, in comparison to the NCEP's resolution of $2.5^{\circ} \times 2.5^{\circ}$.

Nevertheless, the PRECIS RCM system manifests a very weak skill in simulating the observed circulation features such as near surface wind components during January. The model also severely underestimates the rainfall climate of January and its variability. The logic behind the model's weak skill in simulating the said variables might be attributed to the amplified simulation of pressure fields in the model climate and the consequential strengthening of the northerly winds which bring about a more southward displacement of the ITCZ from its mean position in the central and western sections of the model domain. The model performance on daily precipitation for January, therefore, remains a great source of uncertainty. The study therefore suggests that the model might also have biased over the study region and that there is a need for recalibration or improvement.

The climate change projections for the A2 and B2 SRES scenarios by the PRECIS RCM system show significant surface temperature enhancement for both the months of July and January relatively to the base-line climate (1961-1990) for the 2070s and 2080s. According to the climate change simulations, one might expect a profound surface temperature increases during July over the Sahara desert. The January projections also indicate above baseline temperatures. The study found similar trends over the Eritrea subdomain, and confirms that the PRECIS RCM system projections for the 2080s are consistent with the driving HadCM3 and other IPCC GCMs.

Mixed spatial climate change signal were identified for daily precipitation. Accordingly, PRECIS RCM system simulations indicated that rainfall might increase in most of the Sahel and the winter rainfall regions under conditions of the A2 and B2 SRES scenarios during July and January, respectively. Some regions, however, might expect drier condition relative to the base line climate. Similarly, rainfall trends projections for the Eritrea sub-domain are in agreement with those of the Sahel and the winter rainfall regions. Whilst, the PRECIS RCM system and HadCM3 July climate change projections are found to be consistent, there is a lack of inter-model agreement among the IPCC GCMs in simulating rainfall deviations. The study concludes that the January rainfall projections remain a source of uncertainty, not only because of lack of consistency among the IPCC-GCMs, but also because of the weaker skill of the PRECIS RCM system in representing the present climate.

Finally, the study concludes that the climate projections generated by the PRCES RCM system during the tropical circulation system dominance (June-July-August) are plausible and might be potentially utilized for further studies in climate change impact assessment in order to develop mitigations and adaptation strategies. The study also recommends that a future increase in temperature and rainfall might have an influence on all climate sensitive activities, and should therefore be viewed from different dimensions in a holistic manner.

APPENDIX A

MODEL VERIFICATION TECHNIQUES

A.1 INTRODUCTION

Forecast Verification is the process of determining the quality of forecasts. A wide variety of forecast verification procedures exist, but all involve measures of the relationship or set of forecast, and the corresponding observation(s). Any forecast verification method thus necessarily involves comparisons between matched pairs of forecasts and the observations to which they pertain (Wilks, 1995).

The methods employed in the model evaluation section of chapter 6 will be illustrated briefly here. Accordingly, the objective measures of skill or accuracy and their relationship that constitutes the basics of Taylor (2000) scheme are briefly highlighted.

A.2 TAYLOR DIAGRAM

A.2.1 THEORETICAL BASIS

The statistic most often used to quantify pattern similarity is the correlation coefficient. The term "pattern" is used here in its generic sense, not restricted to spatial dimensions. Consider two variables, f_n and r_n , which are defined at N discrete points (in time and/or space). The correlation coefficient (R) between f and r is calculated with the following formula:

$$R = \frac{\frac{1}{N} \sum_{n=1}^N (f_n - \bar{f})(r_n - \bar{r})}{\sigma_f \sigma_r},$$

where \bar{f} and \bar{r} are the mean values, and σ_f and σ_r are the standard deviations of f and r , respectively. For grid cells of unequal area, the above formula would normally be modified in order to weight the summed elements by grid cell area (and the same weighting factors would be used in calculating σ_f and σ_r). Similarly, weighting factors for pressure thickness and time interval can be applied when appropriate.

The correlation coefficient reaches a maximum value of one when for all n , $(f_n - \bar{f}) = \alpha(r_n - \bar{r})$, where α is a positive constant. In this case the two fields have the same centered *pattern* of variation, but are not *identical* unless $\alpha = 1$. Thus, from the correlation coefficient alone it is not possible to determine whether two patterns have the same *amplitude* of variation (as determined, for example, by their variances).

The statistic most often used to quantify differences in two fields is the root-mean-square (RMS) difference, E , which for fields f and r is defined by the following formula:

$$E = \left[\frac{1}{N} \sum_{n=1}^N (f_n - r_n)^2 \right]^{1/2}.$$

Again, the formula can be generalized for cases when grid cells should be weighted unequally.

In order to isolate the differences in the patterns from differences in the means of the two fields, E can be resolved into two components. The overall "bias" is defined as

$$\bar{E} = \bar{f} - \bar{r}$$

and the centered *pattern* RMS difference by

$$E' = \left\{ \frac{1}{N} \sum_{n=1}^N [(f_n - \bar{f}) - (r_n - \bar{r})]^2 \right\}^{1/2}.$$

The two components add quadratically to yield the full mean-square difference:

$$E^2 = \bar{E}^2 + E'^2.$$

The pattern RMS difference approaches zero as two patterns become more alike, but for a given value of E' , it is impossible to determine how much of the error is due to a difference in structure and phase and how much is simply due to a difference in the amplitude of the variations.

The correlation coefficient and the RMS difference provide complementary statistical information quantifying the correspondence between two patterns, but for a more complete characterization of the fields, the variances (or standard deviations) of the fields must also be given. All four of the above statistics (R , E' , σ_f and σ_r) are useful in comparisons of patterns, and it is possible to display all

of them on a single, easily interpreted diagram. The key to constructing such a diagram is to recognize the relationship between the four statistical quantities of interest here,

$$E'^2 = \sigma_f^2 + \sigma_r^2 - 2\sigma_f\sigma_r R,$$

and the Law of Cosines,

$$c^2 = a^2 + b^2 - 2ab \cos \phi,$$

where a , b , and c are the lengths of the sides of a triangle, and ϕ is the angle opposite side c . The geometric relationship between R , E' , σ_f and σ_r is shown figure A.1.

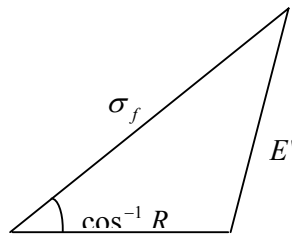


Figure A.1: Geometric relationship between the correlation coefficient, R , the pattern RMS difference, E' and the standard deviations, σ_f and σ_r , of the test and reference fields, respectively.

With the above definitions and relationships it is now possible to construct a diagram that statistically quantifies the degree of similarity between two fields. One field will be called the "reference" field, usually representing some observed state. The other field will be referred to as a "test" field (typically a model-simulated field).

APPENDIX B**PYTHON CODE FOR MODEL
OUTPUT MANIPULATION**

```

"""
*****
This python script transforms the PRECIS model output to the
correct regional axis and regrids NCEP to PRECIS model
resolution
*****
"""
# the following is only needed to confirm the path where the
target #files are found.
import os, sys
here = os.getcwd()
there = os.path.dirname(sys.argv[0])
if there == '': there = os.path.expanduser('~') + '/' + \
'path/'
if here != there:
    if os.path.isdir(there):
        os.chdir(there)
    else:
        print 'File not found!'
        sys.exit()
path = '../final_folder/'
*****
from genutil import statistics
from regrid import Regridder
import cdms, MV, MA, cftime, time, cdutil

*****
f1 = path + 'precis file'
precis = cdms.open(f1)
f2 = path + 'ncep file'
ncep = cdms.open(f2)
*****
s = precis('variable name')
r = ncep('variable name')
# retrieving the information
ax0=s.getAxis(0)      # time bounds
ax1=s.getAxis(1)      # lat bounds
ax2=s.getAxis(2)      # lon bounds

*****
# transforming the sigma levels to pressure
ax1.id='pressure'
ax1.units='hPa'
ax1.Length=vertical leves
ax1.First=L1

```

```

ax1.Last=Ln
ax1.axis='Z'
ax1[:]=[L1. , L2 , ..... ,Ln]
#*****
# Horizontal grid transformation
# Lat
lats=MV.arange(59,typecode=MV.Float)*R+Y0 #where R:
#Estimated resolution and Y0 intial Y value.
lat=cdms.createAxis(lats)
ax1=s.setAxis(1,lat)
lat.id='latitude'
lat.units='degree_north'
lat.designateLatitude()
#Lon
lons=MV.arange(99,typecode=MV.Float)*R+X0
lon=cdms.createAxis(lons)
ax2=s.setAxis(2,lon)
lon.id='longitude'
lon.units='degree_east'
lon.designateLongitude()
"""
*****
  Regarding of the NCEP Reanalysis data to the transformed
  PRECIS output grid
*****
"""
inprecis = s.getGrid() # Get the target grid
outncep = s.getGrid()
regncep = r.regrid(outncep)
"""
*****
* (Statistical analysis)
*****
"""
# Representation of time-span
# for precis
precistime1 = cdttime.comptime(year 1)
precistime2 = cdttime.comptime(year 2)
# for ncep
nceptime1 = cdttime.comptime(year 1)
nceptime2 = cdttime.comptime(year 2)
# query the spatial and temporal domains that should be
#included in the analysis
precis1 = precis('precis variable', time = (precistime1,\
precistime2), longitude = (x1,x2,'oo'),\
latitude = (y1,y2,'oo'))
ncep1 = ncep('ncep variable', time = (nceptime1, nceptime2),\
longitude = (x1,x2,'oo'),\
latitude = (y1,y2,'oo'))
#*****
# calculating averages of the two fields
avg_precis = cdutil.averager( precis1, axis='(time)',\
weights=['equal'])
avg_ncep = cdutil.averager( ncep1, axis='(time)',\
weights=['equal'])

```



```
# calculating the RMS between the two fields
rmse = statistics.rms( avg_precis,avg_ncep, axis='xy',\
weights=['equal','equal'])
# calculating the standard deviation
sd_precis = statistics.std( avg_precis, axis='xy',\
weights=['equal','equal'])
sd_ncep = statistics.std( avg_ncep, axis='xy',\
weights=['equal','equal'])
# calculating the pattern correlation
ac_60s=statistics.correlation(avg_precis ,avg_ncep,\
axis='xy', weights=['equal','equal'] )
```

REFERENCES

- Ahrens, C.D., 2000: *Meteorology today: An introduction to weather, climate, and the environment*, 6th ed., Brooks/Cole, Pacific Grove.
- Albrecht, B.A., 1983: *A cumulus parameterization for climate studies of the tropical atmosphere, Part I: model formulation and sensitivity test*, J. Atmos. Sci. 40: 2166-2181.
- America on line service, 2002: *Lonely planet World Guide Destination Eritrea*
<http://www.lonelyplanet.com/destinations/africa/eritrea/>
- AMS Statement, 2001: *Seasonal to interannual climate prediction (adopted by AMS Council 14 January 2001)*. Bulletin of the American Meteor. Soc., 82: 701-703, 710.
- Anthes, R.A., 1977: *A cumulus parameterization scheme utilizing a one-dimensional cloud model*, Mon. weather Rev., 105: 270-286.
- Arakawa A. & W.H. Schubert, 1974; *Interaction of a Cumulus Cloud Ensemble with the Large Scale Environment*, Part I, J. Atmos. Sci. 31: 674-701.
- Arnell, N.W., D.A. Hudson & R.G. Jones, 2003: *Climate scenarios from a regional climate model: Estimating change in runoff in southern Africa*, J. Geophys. Res., 108(D16), 4519, doi:10.1029/2002JD002782.
- Awosika, L.F., E.S. Diop, T.F. Downing, M. El-Raey, D. Le. Sueur, C.H.D. Magadza, S. Touré & C. Vogel, 2001: *The Regional Impacts of Climate Change*, IPCC Special Report on Climate Change
<http://www.grida.no/climate/ipcc/>.
- Bach, W., 1988: *Modelling the climatic response to greenhouse gases*, in Gregory, S. (ed), *Recent climatic change: A regional Approach*, Belhaven Press, London, pp. 8-19.
- Bjerknes, V., 1904: *Das problem von der wettervorhersage*, betrachtet vom standpunkt der mechanik und der physik. Meteor. A., 21 1-7.
- Bradley, R.S., 1991: *Pre-instrumental climate: How has climate varied during the past 500 years*, in Schlesinger, M.E. (ed), *Greenhouse-Gas-Induced climate change: A critical appraisal of simulations and observations*, Elsevier Scie., Amsterdam, pp. 391-409.
- Central Intelligence Agency (CIA), 2002: *World fact book of 2002*.
<http://www.cia.gov/cia/publications/factbook/goes/er.html>

- Charney, J.G, 1975: *Dynamics of deserts and drought in the Sahel*, Quart. J. Roy. Meteor. Soc. Vol.101, No. 428:193-202.
- Charney, J.G. & A. Eliassen, 1964: *On the growth of the hurricane depression*, J. Atmos. Sci.21: 68-75.
- Charney, J.G, R. Fjørtoft & J.von. Neumann, 1950: *Numerical integration of the barotropic vorticity equation*, Tellus, 2, 237-254.
- Cubasch, U. & R.D. Cess, 1990: *Processes and modeling. Climate Change: The IPCC Scientific Assessment*, Cambridge University Press, Cambridge.
- Cubasch, U., G.Meehl, G.J. Boer, G.J. Stouffer, M. Dix, A. Noda, C.A. Senior, S. Raper & K.S. Yap, 2001: *Projections of Future Climate Change*, in Houghton, J.G., Y. Ding, D.J. Griggs, D.J. Griggs, M. Noguer, P.J. van der Linden, X. Dai, K. Maskell & C.A. Johnson (eds), *Climate Change 2001: The scientific Basis*, contribution of working group I to the Third Assessment Report of the Intergovernmental Panel on Climate Change. Cambridge University Press, Cambridge, pp. 525-582
- Cunnington, W.M. & P.R. Rowntree, 1986: *Simulations of the Saharan atmosphere dependence on moisture and albedo*, Quart. J. Roy. Meteor. Soc. 112: 971-999.
- Davies, H.C., 1976: *A lateral boundary formulation for multi-level prediction models*, Quart. J. Roy. Meteor. Soc. 102: 405-418.
- Davies, H.C. & R.E. Turner, 1977: *Updating prediction models by dynamical relaxation: an examination of the technique*, Quart. J. Roy. Meteor. Soc. 103: 225-245.
- Drury, S.A., S.P. Kelley & S.M. Berhe, 1974: *Structure related to the Red Sea evolution in northern Eritrea*. Tectonic, 13 (6), pp. 1371-1380.
- Druyan, .M. & S. Hastenrath, 1991: *Modelling the differential impact of the 1984 and 1950 sea-surface temperatures on Sahel rainfall*, Int. J. Climateol. 11: pp. 367-380.
- Engelbrecht, F.A., 2000: *Nested climate modeling over Southern Africa with a semi-Lagrangian limited area model*, unpublished MSc. Dissertation, University of Pretoria, Pretoria.
- Engelbrecht, F.A., C.J. deW. Rautenbach, G.L. McGregor & J.J. Katzfey, 2002: *January and July climate simulations over the SADC region using the limited-area model DARLAM*, Water SA Vol. 28 No. 4, pp. 361-373.
- FAO, 1994: *Eritrea – Agricultural sector review and project identification*, 3 volumes Report prepared by FAO/IC under Technical Cooperation Programme project TCP/ERI/2353. Rome.

- FAO, 2002: *Special report FAO/WFP crop and food supply assessment mission to Eritrea*, FAO global information and Early warning system on food and agriculture WFP, Rome.
<http://www.fao.org/WAICENT/faoinfo/economic/qIEWS/english/alertes/sptoc.htm>
- Fischer, G., M. Shah & V. Velthuizen, 2002: *Climate Change and Agricultural vulnerability*. IIASA special report under UN Institutional contract agreement No 1113 as a contribution to the World Summit on Sustainable Development, Johannesburg 2002.
- Folland, C.K., T.N. Palmer & D.E. Parker, 1986: *Sahel Rainfall and world-wide sea temperatures*, Nature 320: 602-607.
- Folland, C.K., T.R. Karl & K.Y.A. Vinnikov, 1990: *Observed Climate Variation and change*, The IPCC Scientific Assessment, Cambridge University Press, Cambridge.
- Fu, Q., P. Yang & W.B. Sun, 1998: An accurate parameterization of the infrared radiative properties of cirrus clouds of climate models, J. Climate, 11: 2937-2947.
- Garbesi, K., K. Karen & R. Van Buskirk, 1996: *Preliminary Wind Energy Resources Assessment for Eritrea*, Energy Research and Training Division, Ministry of Energy, Mines, and Water Resources, Asmara.
<http://www.punchdown.org/rvb/wind/WINDREP796.html>
- Gibson, J.K., P. Kallberg, S. Uppala, A. Hernandez, A. Nomura and E. Serrano, 1997: *ERA description. ECMWF Reanalysis Project Report Series 1*, European Centre for Medium Range Weather Forecasts, Reading, UK, 66 pp.
- Goddard, L., S.J. Zebiak, C.F. Popelewski, R. Basher & M.A. Cane, 2001: *Current approaches to seasonal-to-interannual climate predictions*, Int. J. Climateol. Vol. 21, pp. 1111-1152.
- Gordon, H.B. & B.G. Hunt, 1991: *Droughts, floods, and sea-surface temperature anomalies: a modelling approach*, Int. J. Climateol. Vol. 11, pp. 347-365.
- Government of Eritrea (GoE), 1994: *Macro-policy*, Government of Eritrea, Asmara.
- Government of Eritrea (GoE), 1995: *National Environmental Management Plan for Eritrea*, Environment Eritrea, Druckerei Schwenk & Co. GmbH, Frankfurt.
- Government of Eritrea (GoE), 1998: *National Economic Policy Framework and Program for 1998-200*, Government of Eritrea, Asmara.
- Haltiner, G.J., 1971: *Numerical weather prediction*, Wiley, New York.

- Haltiner, G.J. & R.T. Williams, 1980: *Numerical prediction and dynamical meteorology*, Second Edition, Wiley, New York.
- Henderson-Seller, A. & K. McGuffeie, 1987: *A climate modeling primer*, John Wiley & Sons, Chichester.
- Henderson-Seller, A. & K., McGuffeie, 2001: *Forty years of numerical climate modeling*, Int. J. Climato. 21:1067-1109.
- Hewitson, B.C., 2001: *Global and regional climate modeling: Application to Southern Africa*, WRC Report No. 806/1/01, Cape Town.
- Hewitson, B.C., 2004: Climate – A cause for concern, in Water Wheel, WRC Water bulletin, Vol. 3 No. 3, pp. 22-26.
- Houghton, J.J., L.G.M. Filho, et al., (eds) 1996: *Climate Change 1995: The Science of Climate Change*, Cambridge University Press, Cambridge.
- Hurni, H. & T. Koller, 2002: *Eritrea: Sustainable land management in a Sahelian Country*, Syngenta Foundation for Sustainable Agriculture (SFSA).
<http://www.syngentafoundation.com>
- IPCC. Climate Change, 2001: *The Scientific Basis*, contribution of Working Group I to the Third Assessment Report of the Intergovernmental Panel on Climate Change, Cambridge University Press, Cambridge.
- Jones, R., D. Hudson, S. Wilson, G. Jenkins & J. Mitchell, 2003: *Workbook on generating high resolution climate change scenarios using PRECIS*, Hadley Centre for Climate Prediction and Research, Met Office, Bracknell.
- Kalnay, E. & Coauthors, 1996: *The NCEP/NCAR 40-year Reanalysis Project*, Bull. Am. Met. Soc., 77, 437-471.
- Kalnay, E., S.J. Lord & R.D. McPherson, 1998: *Maturity of Operational Numerical Weather Prediction: Medium Range*, Bulletin of the American Meteorological Society, Vol. 79 No. 12, pp. 2753-2769.
- Karen R., 1998: *An Assessment of the Potential for Utility-Scale Wind Power Generation in Eritrea*, Masters Thesis, Environmental Studies Department, San Jose State University, San Jose.
<http://www.punchdown.org/rvb/wind/karen/kth-TableOfContents.htm>
- Katayama, A., 1974: *A simplified scheme for computing radiative transfer in the troposphere*, Tech. Rep. No. 6 Dept. of Met., UCLA, pp. 77.
- Kayouli, C, T. Tesfai, & A. Tewelde, 2002: *Country Pasture/ Forage Resources Profiles Eritrea*. Halhale Research Center, Halhale.
- Kimura, R., 2002: *Numerical weather prediction*, J. winds Engineering & Industrial Aerodynamics, Vol. 90 pp. 1403-1414.

- Kuo H. L., 1974: *Further studies of the parameterization of the influence of cumulus convection on large-scale flow*, J. Atmos. Sci. 31: 1232-1240
- Krzysztofowicz, R., 2001: *The case probabilistic forecasting in hydrology*, J. of Hydrology, Vol. 249, pp. 2-9.
- Lamb, P.J., 1988: *Large scale tropical Atlantic surface circulation patterns associated with sub-Saharan weather anomalies*, Tellus, 30:240-251.
- Layton, A.T., & W.F. Spitz, 2003: *A semi-Lagrangian double Fourier method for shallow water equations on the sphere*, in press, J. Comput. Phys., Vol. xxx, pp. xxx-xxx.
<http://www.sciencedirect.com>
- Lorenz, E.N., 1963: *Deterministic nonperiodic flow*, J. Atmos. Sci. 20: 130-141.
- Leung, L.R., L.O. Mearns, F. Giorgi & R.L. Wilby, 2003: *Regional climate research: needs and opportunities*, Meeting Summaries, Amer. Meteor. Soc., pp. 89-95.
- MacCracken, M.C. & J. Kutzbach, 1991: *Comparing and contrasting Holocene and Eemian warm periods with greenhouse-gas-induced warming*, in Schlesinger, M.E. (ed), *Greenhouse-Gas-Induced climate change: A critical appraisal of simulations and observations*, Elsevier Scie., Amsterdam, pp. 69-78.
- Martyn, D., 1992: *Climate of the World*, Polish Scientific publishers, Warszawa.
- McGregor, J.L., 1993: *Economic determination of departure points for semi-Lagrangian models*, Mon. Weather Rev. 119: 1057-1074.
- McGregor, J.L., 1995a: *Semi-Lagrangian advection on conformal-cubic grids*, Mon. Weather Rev., 124: 1311-1322.
- McGregor, J.L., 1995b: *Semi-Lagrangian advection on a Cubic Gnomonic projection of the sphere*, in Lin, C., Laprise R. & Ritchie, H. (eds), *Numerical methods in atmospheric and oceanic modeling*, Canadian Meteorological and Oceanographic Soc., Ottawa, pp. 153-169.
- McGregor, J.L., 1997: *Regional climate modeling*, Meteorol. Atmos. Phys. 63:105-117
- McGregor, J.L., K.J. Walsh & J.J. Katzfey, 1993: *Nested modeling for regional climate studies*, in Jakeman, A.J., Beck, M.B. & McAleer, M.J. (eds), *Modeling change in environmental systems*, Wiley, Chichester, pp. 367-386.
- Mcguffie, K. and A. Henderson-Sellers, 2001: *Forty years of numerical climate Modeling*, Int. J. Climatol. Vol. 21: 1067-1109.

- Mitchell, J.F.B., 1991: *The equilibrium response to doubling Atmospheric CO₂*, in Schlesinger, M.E. (ed), *Greenhouse-Gas-Induced climate change: A critical appraisal of simulations and observations*, Elsevier Scie., Amsterdam, pp. 49-61.
- Ministry of Agriculture (MoA), 2002: *The national action programme for Eritrea to combat desertification and mitigate the effects of drought (NAP)*, MoA, Asmara.
- Ministry of Land, Water & Environment (MLWE), 1997a: *Agro-Ecological Zones and Legend*, Unpublished report, MLWE, Asmara.
- Ministry of Land, Water & Environment (MLWE), 1997b: *State of the environment - Eritrea*, MLWE, Asmara.
- Ministry of Land, Water & Environment (MLWE), 2001: *Eritrea's initial national communication*, under UNFCCC, MLWE, Asmara.
- Mohr, P.A., 1961: *The geology of Ethiopia*, Ethiopia Observer, 5(3): 186-193.
- Mohr, P.A., 1970: *The geology of Ethiopia*, Addis Ababa press, Addis Ababa.
- Mohr, P.A., 1987: *Structural style of continental rifting in Ethiopia: Reverse décollements*. Eos 68 (35), 721-730.
- Nicholson, S.E., 1979: *The methodology of historical climate reconstruction and its application to Africa*, J. African history, 20: 31-49.
- Nicholson, S.E., 1981: *Rainfall and atmospheric circulation during drought and wetter periods in West Africa*, Mon. Wea. Rev., 109: 2291-2208.
- Nicholson, S.E., 1983: *Sub-Sahara rainfall in the years 1976-80: evidence of continued drought*, Mon. Wea. Rev., 3: 1646-1654.
- Nicholson, S.E., 1986: *On the causes of African drought*. Final Rep., NSF Contract ATM 8212781, Dept of Geography, Clark University.
- Nicholson, S.E. & H. Flohn, 1980: *African environmental and climatic changes and the general atmospheric circulation in late Pleistocene and Holocene*, Climatic Change 2:313-348.
- Norris, W.B. & K.G. Doty, 1998: *Meteorological Modeling Protocol*, Southern Appalachian Mountains Initiative, University of Alabama, Huntsville.
- Ogbazghi, W., 2001: *The distribution and regeneration of Boswellia papyrifera (Del.) Hochst. In Eritrea*, Tropical Resources Management Papers, Wageningen University, Wageningen.
- Ooyama, K., 1964: *A dynamical model for the study of tropical cyclone development*, Geofis. Int., 4: 187-198.

- Owen, J.A. & C.K. Folland, 1988: *Modelling the influence of sea-surface temperatures on tropical rainfall*, in Gregory, S. (ed), *Recent climatic change: A regional Approach*, Belhaven Press, London, pp. 141-153.
- Perkey D.J., & C.W. Kreitzberg, 1976: *A time dependent lateral boundary scheme for limited-area primitive equation models*, Mon. Wea. Rev. 104: 744-755.
- Rančić, M., R.J. Purser & F. Mesinger, 1995: *A global shallow-water model using an expanded spherical cube: Gnomonic versus conformal coordinates*, Quart. J. Roy. Meteor. Soc. 122: 959-982.
- Rautenbach, C.J. deW., 1999: *Introduction of a hybrid vertical co-ordinate to an Atmospheric General Circulation Model*, Unpublished PhD thesis, University of Pretoria, Pretoria.
- Richardson, L.F., 1922: *Weather prediction by numerical process*, Cambridge University Press, reprinted Dover, 1965.
- Rind, D., 1991: *Climate variability and climate change*, in Schlesinger, M.E. (ed), *Greenhouse-Gas-Induced climate change: A critical appraisal of simulations and observations*, Elsevier Scie., Amsterdam, pp. 69-78.
- Robert, A., 1981: *A semi-Lagrangian, semi-implicit numerical integration scheme for the primitive meteorological equations*, Atmos. Ocean 19: 35-46.
- Ropelewski, C.F. & S. Halpert, 1991: *The Southern Oscillation and northern hemisphere temperature variability*, in Schlesinger, M.E. (ed), *Greenhouse-Gas-Induced climate change: A critical appraisal of simulations and observations*, Elsevier Scie., Amsterdam, pp. 369-376.
- Rossby, C.G., 1939: *Relation between variations in the intensity of the zonal circulation of the atmosphere and the displacements of the semi-permanent centers of action*, J. Marine Res., 2.38-55.
- Sadourny, R., 1972: *Conservative finite-differencing approximation of the primitive equations on quasi-uniform spherical grids*, Mon. Weather Rev., 100: 136-144.
- Schreck III, C.J. & F.H.M. Semazzi, 2003: *An investigation of the variability of the climate of Eastern Africa during the recent decades*, Contribution to Exchange, No. 27.
- Slingo, J.M., 1987: *The development and verification of a cloud prediction scheme for the ECMWF model*, Quart. J. Roy. Meteor. Soc. 106: 899-927.
- Smith, R.N.B., 1990: *A scheme for predicting layer clouds and their water content in a general circulation model*, Quart. J. Roy. Meteor. Soc. 116: 435-460.

- Staniforth, A. & J. Côté, 1991: *Semi-Lagrangian integration schemes for atmospheric models – a review*, Mon. Wea. Rev. 119: 2206-2223.
- Sundquist, H., 1978: *A parameterization scheme for non-convective condensation including prediction of cloud water content*, Quart. J. Roy. Meteor. Soc. 104: 677-690.
- Taylor, K.E., 2000: *Summarizing multiple aspects of model performance in a single diagram*, PCMDI Report No. 55, UCRL, Livermore.
- Trenberth, K.E., G.W. Branstator & P.A. Arkin, 1988: *Origins of the 1988 North American drought*, Science, 242: 1640-1645.
- University of Asmara (AU) & Ministry of Agriculture (MoA), (1998): *Rehabilitation of degraded lands, Eritrea*, Second Edition, Asmara.
- UNFCCC, 2003: *Caring for Climate*, a guide to the climate change convention and the Kyoto Protocol, UNFCCC, Bonn.
- Van Buskirk, R., G. Karina G. & R. Karen, 1997: *Wind resource assessment of Eritrea, Africa: Preliminary results and status*, in Solaris, G. (ed), *Proceedings of the 2nd European & conference on Wind Engineering*, edited by G. Solari, June 1997, Italy.
<http://www.punchdown.org/rvb/wind/ITPAPER2.html>
- Viner, D., M. Hulme & S.C.B. Rapper, 1995: *Climate change scenarios for the assessments of the climate change on regional ecosystems*, J.therm. Biol. Vol.20, No. 1/2., pp. 175-190.
- Walker, J. & P.R. Rowntree, 1977: *The effect of soil moisture on circulation and rainfall in a tropical model*, Quart. J. Roy. Meteor. Soc. 103: 29-46.
- Wilks, D., 1995: *Statistical methods in the Atmospheric Sciences – An introduction*, Academic Press, Inc., San Diego.
- Wilson, S., D., Hassell, D. Hein, R. Jones, & R. Taylor, 2003: *Installing and using the Hadley Centre regional climate modeling System-PRECIS*, version 0.9a, Hadley Centre for Climate Prediction and Research, Met Office, Bracknell.